I&EC research
Industrial & Engineering Chemistry Research

pubs.acs.org/IECR

Review

An Evolving Insight into Metal Organic Framework-Functionalized Membranes for Water and Wastewater Treatment and Resource Recovery

Tin Le,[#] Xi Chen, Hang Dong, William Tarpeh, Adelaida Perea-Cachero, Joaquín Coronas, Stephen M. Martin, Munirah Mohammad, Amir Razmjou, Amirsalar R. Esfahani, Negin Koutahzadeh, Peifu Cheng, Piran R. Kidambi, and Milad Rabbani Esfahani*

Cite This: https://doi.org/10.1021/acs.iecr.1c00543

Read Online

ACCESS | Metrics & More | Article Recommendations

ABSTRACT: Metal organic frameworks (MOFs) represent one of the largest classes of porous crystalline materials. MOFs have been increasingly applied as functionalizing agents for membranes because of their porosity, high surface area, small particle size, aspect ratio control, tuneability, compatibility with a polymeric network, and exuberance of diverse functional groups. In this comprehensive review paper, we discuss achievements, opportunities, and challenges related to the functionalization of different types of membranes using MOFs for water and wastewater treatment and desalination. The current synthesis and fabrication approaches of MOF-functionalized membranes were identified and critically reviewed. The effects of MOFs on membrane performance, including permeation, selectivity, and antifouling, were discussed. Also, the application of MOF-functionalized membranes in aqueous environments for conventional applications such as heavy metal removal and emerging applications such as resource recovery was enunciated. Finally, recommendations and future directions were provided for further improvement in the field of MOF-functionalized membranes for water treatment and reuse.

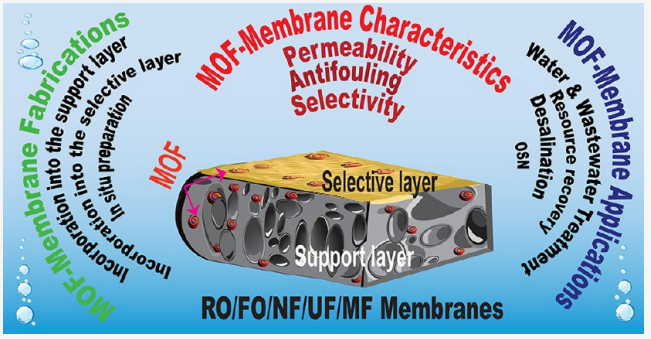

1. INTRODUCTION

Rapid modernization has led to massive population growth, which requires careful, sustainable management of natural resources to ensure continued prosperity in the foreseeable future. Chief among those concerns is the increasing scarcity of freshwater sources; half the world will face water stress by 2030.[1] The problem of water scarcity in the world is only comparable in urgency and magnitude to that of global warming due to greenhouse gases, with no doubt about the narrow link between both. Therefore, there is a need to consider alternative water sources and utilize them through water and wastewater treatment methods.[2] Water quality and process efficiency are the two important factors in developing water and wastewater treatment techniques.[3,4]

Membrane technologies provide efficient separations, and have been widely used in water purification since the 1960s. Reverse osmosis (RO) has become the gold standard for seawater and brackish water desalination, and nanofiltration (NF) membranes have shown acceptable performance for pretreatment of RO and as an independent filtration process for water treatment.[5,6] In membrane separations, chemical potential gradients drive permeant transfer across a semi-permeable membrane, and contaminants are rejected by various mechanisms such as size exclusion, electrostatic repulsion, and other physicochemical properties.[7] Compared to other purification methods, the advantages of membrane filtrations are low energy consumption and operational costs, small footprint, and resilience.[8] However, there is still a need to improve the membrane performance in terms of salt rejection (selectivity), water flux (permeability), and antifouling to achieve more cost- and energy-efficient separation.[9]

One strategy of addressing these issues is to fabricate membranes with surface additives to take advantage of their physical and chemical properties. Several surface modification techniques such as self-assembly, layer-by-layer (LBL) fabrication, physical depositions, and chemical grafting have been used to modify or functionalize membrane surfaces with

Received: February 6, 2021
Revised: April 2, 2021
Accepted: April 6, 2021

different organic and inorganic additives. Membrane surface functionalization using metal oxides (Al_2O_3, TiO_2, SiO_2, ZnO, MgO, Fe_2O_3, and zeolite), metals (Cu, Ag), carbon-based materials, and nanofiber polymers provided tunable physicochemical properties and unique functionalities regarding the membrane selectivity, permeability, and antifouling capability.[10−14] While nanoparticles (NPs) have been widely investigated for membrane surface modifications, lack of tunability, aggregation during the modification process, lack of porosity, poor compatibility with the polymeric network, and leaching out due to the lack of stability were identified as the drawbacks of using nanoparticles (NPs).

Metal organic frameworks (MOFs) are a kind of porous coordination polymers, or combination of organic ligands and metal clusters, which form into a highly crystalline structure. These nanomaterials are generally extremely porous and possess high surface area; the MOF structures can be fine-tuned by further functionalizing or exchanging the constituent materials.[15] In addition, their organic ligands enable MOFs to form robust coordination interactions with polymeric membranes resulting in enhanced stability in the membrane. Because of the advantages of MOFs, MOFs-functionalized membrane materials have been synthesized via various methods, and are widely investigated in treatment of water and wastewater, and resource recovery applications.

In this review, we discuss the three main aspects of membrane functionalization using MOFs, including fabrication techniques, membrane characteristics, and application of MOF-functionalized membranes in water and wastewater treatment. The current fabrication techniques of MOFs and their incorporation into the membrane matrix are discussed, and the corresponding advantages and disadvantages of each one are highlighted. The effects of different MOFs on the morphology, structure, and consequently on membrane performance (selectivity, permeability, and antifouling) are discussed. Finally, the recent advances and applications of MOF-functionalized membranes to meet urgent challenges in water and wastewater treatment, desalination, and resource recovery are discussed.

2. FABRICATION OF MOF-FUNCTIONALIZED MEMBRANES

2.1. Bare MOF Membrane Fabrication via in Situ Preparation (Direct- and Secondary-Growth MOF Membrane Synthesis). In situ preparation methods prepare bare MOF membranes with a continuous and intergrown MOF layer. The continuous layer should be defect-free without cracks and pinholes, and the MOF grains are intergrown with internal chemical bonds. The membrane often contains a porous support layer (e.g., porous alumina) amended with a MOF layer instead of separate nanoparticles. There are two different methods to grow MOFs on porous supports: direct growth and secondary growth. During direct growth fabrication, the support initially contains no MOF crystals. Supports with or without chemically modified surfaces are immersed in the growth solution with metal and ligand precursors, where nucleation, growth, and intergrowth of MOF crystals all happen within this single step. The challenge with this direct growth method is that most MOF crystals may grow in the bulk solution instead of on the support surface because of the weak bonding between the MOF crystals and the support surface. To facilitate dense and continuous membrane fabrication on the support, the secondary growth method may involve a seeding procedure to implant seed MOF crystals onto the substrate, followed by secondary growth of MOF membranes on the seed layer. Both methods were originally developed to prepare MOF membranes for gas separations,[16] because the MOF layer maintained near-optimal selectivity due to the pores of the MOF structures. However, the as-prepared membranes can be used for water and wastewater treatment if the MOF structures are water-stable, such as metal carboxylate frameworks with high-valence metal ions, metal azolate frameworks with nitrogen-donor ligands, and MOFs with modified hydrophobic pore surfaces or blocked metal ions.[17] All these frameworks have strong coordination bonds or significant steric hindrance to minimize the damages on metal−ligand bonds by water hydrolysis. However, long-term stable performance (i.e., hundreds of hours) is still a concern for these membranes, and requires further investigation, especially under extreme pH environments due to the weak mechanical strength of the bare MOF layer.

2.1.1. Direct Growth. Direct growth methods are comparatively simple because nucleation, growth, and intergrowth of MOF crystals occur in a single step. However, they preclude control of the orientation and continuous growth of MOF crystals due to weak bonds between the MOF layer and the support layer. Thus, most direct growth methods require a specific support surface if it is unmodified, or modification of the support surface to enhance the interfacial bonding between the MOF and the support layers.

In situ solvothermal synthesis is a widely applied method for the direct growth of MOF crystals on different supports. The first continuous and well-intergrown MOF membrane was developed using in situ solvothermal synthesis with MOF-5 and porous α-alumina support without surface modification.[18] Briefly, during the synthesis, the organic linker (1,4-benzene dicarboxylic acid) was dissolved in DMF, and the mixture was loaded into a Teflon-lined autoclave. Then a dry α-alumina disc was immersed into the solution for 30 min, followed by addition of dehydrated $Zn(NO_3)_2$. Dehydration was reported as an influential parameter for obtaining continuous membranes. The mixture was then sealed and heated to 105 °C in an autoclave. Membranes with different thicknesses could be obtained by varying synthesis time. After synthesis, samples were then cooled, washed, and dried at 60 °C for 24 h. The final membranes were continuous and well-intergrown between grains, which improved mechanical strength and chemical homogeneity. Note that the α-alumina support surface was not modified, but covalent bonds could be formed between the carboxylic acid groups in the MOF crystals and the hydroxyl groups on the alumina support surface.[16] The reaction temperature could be reduced by replacing the solvent DMF with pure methanol, which interacts weakly with zeolitic imidazolate frameworks (e.g., ZIF-8) and thus can escape from the cavities at room temperature. The reaction time could also be substantially reduced if assisted by microwave-assisted heating, which has been proven effective for enhancing heterogeneous nucleation and growth for many ZIF membranes such as ZIF-8, ZIF-22, and ZIF-90.[19−21] Besides using specific MOF-support pairs that can form covalent bonds, another strategy to enhance the heterogeneous nucleation of MOF crystals on unmodified support surfaces is using supports containing the same metal as the MOF because the metal in the support can intergrow with the MOF. For example, a $Cu_3(BTC)_2$ MOF (HKUST-1) membrane was successfully prepared on an oxidized copper net support by Guo et al.[22]

https://doi.org/10.1021/acs.iecr.1c00543
Ind. Eng. Chem. Res. XXXX, XXX, XXX−XXX

The Cu^{2+} ions in both the copper net and in the reaction solution provided a metal source for crystal growth.[22] A simpler method was reported using the metal on the support as a "single metal source" for both MOF growth and layer support,[23] which resulted in a thin and continuous MOF membrane once the metal source on the support surface was consumed and a layer was formed.

Further improvement on the heterogeneous nucleation and direct growth of the MOF can be achieved by chemically modifying the support layer. One common modification is grafting a self-assembled monolayer (SAM) on the support with desired functional groups. For example, an APTES (3-amino-propyltriethoxysilane)-modified aluminum oxide support can be used to synthesize a ZIF-90 membrane.[21] In this arrangement, APTES serves as a covalent linker between the membrane and the support and promotes heterogeneous nucleation and growth. However, SAM techniques are limited to specific MOFs and suitable surface-functionalized substrates. To create a modification method that can address various support surfaces such as metals and plastics, a free-standing MOF membrane synthesis method can be applied.[24] During this synthesis, a poly(methyl methacrylate)(PMMA) membrane can be spin-coated onto any solid substrate, and then the PMMA can be converted to poly(methacrylic acid)(PMAA) via hydrolysis using concentrated sulfuric acid. The PMMA−PMAA-coated substrate can then be immersed into a MOF precursor solution under high pressure (e.g., autoclave) for a suitable reaction time to obtain a MOF membrane. And finally, a free-standing membrane can be produced by dissolving the PMMA−PMAA layer using chloroform. This method is versatile for different support surfaces but requires multistep synthesis. An in situ one-step method was later reported based on counter-diffusion to prepare well-intergrown ZIF-8 membranes.[25,26] Briefly, a metal precursor solution was soaked in a porous α-alumina support, followed by a rapid solvothermal reaction in a ligand solution. The concentration gradient enabled metal ions to diffuse from the support to the solution, and the ligand to diffuse from the solution to the support. Both species met in a reaction zone near the support surface, and limited the membrane formation to the interface, which simplified fabrication, and resulted in thinner membranes (e.g., 1.5 μm) with improved microstructure. A similar membrane made from the ZIF-8 and α-alumina support was tested for the first time for seawater desalination in 2016 with bioinspired polydopamine modification on the α-alumina surface.[27]

2.1.2. Secondary Growth. While the direct growth method is highly affected by the support surface, secondary growth methods facilitate substrate-insensitive dense and continuous MOF membrane fabrication via a seed-assisted process. These secondary methods require extra complexity (synthesis steps) compared with the direct growth but enable finer control of the final orientation and dense continuous growth of the MOF crystals.

Different seeding techniques have been developed for the secondary growth of MOF membranes. The first dense coating of HKUST-1 MOF on untreated α-alumina was prepared using a dip-coating seeding method.[28] The method achieved much denser and uniformed MOF coating than those prepared via direct growth because direct growth caused more nucleation and crystallization occurring in the solution rather than on the support. During seeding, the untreated α-alumina was dip-coated with a dispersion of HKUST-1 crystals in water, followed by similar hydrothermal synthesis as direct growth. The seeding process promoted preferential crystallization on the support with low concentration mother liquors, but the MOF crystals exhibited no preferred orientation once crystallized, which precludes high selectivity and permeability due to unaligned pore directions. Fabrication of preferentially oriented and well-intergrown MOF films on α-alumina was later achieved using a rubbing seeding method on a modified α-alumina support. The support was first dip-coated with polyethylenimine (PEI) to enhance the attachment of seeds via H-bonding. The MOF crystals were crushed into submicrometer particles and deposited on PEI coated supports by rubbing,[29] resulting in a randomly oriented seed layer but an oriented membrane. The preferred orientation was attributed to faster growth along one direction during the secondary growth on the randomly oriented seeds. The significance of the nanosized MOF seed crystals was also reported for improved secondary growth and the seed crystal size can be controlled using capping reagents.[30] For example, sodium carboxylates (formate, acetate, or oxalate) were used as capping agents to reduce the lanthanide-MOF crystals to approximately 100 nm in diameter. Size control was achieved because the capping reagent and linkers share the same chemical functionality, and the competitive coordination of the capping reagent regulated crystal growth rate and size. In addition to the two most common seeding techniques (dip-coating and rubbing), alternatives such as spin-coating,[31] heating,[32] and most recently electrospinning[33] have been explored. Among them, electrospinning enables seeding on various types of supports and low-cost seeding for large-area supports. Briefly, the seeding solution can be first loaded into a syringe, which is connected to a hose with a capillary tip. A high voltage can then draw the viscous solution from the metallic tip into fibers, and the fibers can be deposited onto a rotating tubular support surface with high uniformity. This method allows precise control of the seed layer thickness and continuous and uniform seeding on the support surface. Besides seeding for secondary growth of bare membranes, electrospinning has also been widely investigated for fabricating composite nanofibrous membranes incorporated with MOFs for heavy metal removal.[34]

Although the direct growth method is challenging for the fabrication of dense MOF membranes, it can be applied as a seeding technique such as reactive seeding and layer-by-layer seeding methods. Reactive seeding methods overcome the major challenge of other methods: introducing direct chemical bonds between the support surface and the MOF layer without introducing extra organic materials, which can be complex and not environmentally friendly. Reactive seeding enhances the binding strength between the MOF crystals and supports by direct reaction between the inorganic support with the organic precursor to growing a seeding layer. For example, aluminum in the α-alumina support served as the aluminum precursor and directly reacted with organic dicarboxylic acids such as 1,4-benzenedicarboxylic acid (H_2BDC), to form a seed layer under mild hydrothermal conditions. Then secondary growth process could be performed using an $Al(NO_3)_3{\cdot}9H_2O$ solution.[35] Using this reactive seeding method, many other MOF membranes have also been prepared such as the ZIF-68 membrane on a ZnO modified α-alumina support.[36] This in situ seeding growth process can be further simplified using a step-by-step growth method or LBL seeding method, also known as liquid-phase epitaxy (LPE).[37] Without hydrothermal

https://doi.org/10.1021/acs.iecr.1c00543
Ind. Eng. Chem. Res. XXXX, XXX, XXX−XXX

conditions, supports such as α-alumina can be sequentially dipped into a ligand solution such as 1,3,5-benzenetricarboxylic acid (H_3BTC), and a metal precursor solution such as $Cu(CH_3COO)_2)\cdot H_2O$. During the first step, H_3BTC molecules are grafted onto the support surface via covalent bonds between the carboxyl groups on H_3BTC and the hydroxyl groups on alumina. Thus, no specific activation process is needed for the support. The ungrafted carboxyl groups will still bind with Cu^{2+}, which in turn connects to more carboxyl groups to enable continuous growth. With several repeat cycles, the seed layer can be dried and ready for secondary growth. The LBL method is more often used for fabricating MOF films but not defect-free membranes;[38] however, it is suitable for seeding during membrane fabrication using secondary growth methods.

Recently, a similar step-by-step growth process was reported to functionalize thin-film composite (TFC) membranes with Ag-MOFs, which was not a bare MOF membrane but shared a similar synthesis procedure.[39,40] Briefly, the TFC membranes were first soaked in silver acetate solution at ambient temperature and then immersed in 2-aminoterephthalic acid/ethanol solution to form Ag-MOFs on the membrane surface. These membranes prevented biofouling by leveraging the antimicrobial activity of silver, and the TFC polymer supports likely had stronger mechanical strength than the bare MOF membranes with nonflexible supports. The synthesis of more MOF-functionalized membranes with similar flexible polymer supports will be discussed in the following sections.

Overall, both direct growth and secondary growth methods are favorable for bare MOF membrane synthesis. These bare membranes have a pure continuous MOF layer, which could provide near-optimal selectivity by leveraging the pore sizes of the MOF crystals. Between the two methods, secondary growth was more complex with a seeding step, but provided better control on the MOF crystal orientation and dense growth, which enabled improved selectivity with aligned pores of MOF crystals. The trade-off of the high selectivity with bare MOF membranes was the stability because of the weak mechanical strength of the MOF structure and the inflexible supports. During water and wastewater treatment, most of the time, membrane stability is prioritized over solute−solute selectivity, as demonstrated by widely applied TFC membranes. Thus, future research should focus on improving the bare membrane stability using flexible supports.

2.2. Immobilization/Incorporation into the Active Layer (Interfacial Polymerization). Current RO and NF membranes are TFC consisting of aromatic polyamide prepared by interfacial polymerization.[41,42] In general, interfacial polymerization occurs through interaction between *m*-phenylenediamine (MPD) and trimesoyl chloride (TMC) on a support layer, during which MPD and TMC are dissolved in water and *n*-hexane, respectively.[43,44] Piperazine (PIP) can be an alternative to MPD, and some additives can be included in MPD or TMC solutions to generate different selective layers.[45,46] Thin-film nanocomposite (TFN) membranes are TFC membranes with embedded fillers (zeolites,[47] oxides,[48] MOFs,[49] graphene oxide,[50] etc.) into their polyamide layer. The fillers can be added either to the aqueous phase or the organic phase, as mentioned above. Hydrophilic fillers are dispersed better in the MPD aqueous solution while hydrophobic fillers are dispersed in the TMC organic solution. The interfacial polymerization exhibits rapid kinetics (usually completed in 1−2 min) and is thermodynamically favorable,[51] which allows a facile and continuous fabrication process. There are several techniques for incorporating MOFs into the selective layer, such as evaporation controlled filler positioning,[52] layer-by-layer depositions of MOF nanoparticles,[53] crystal growth of filler on top of the asymmetric support,[54] dip coating,[55] and deposition of Langmuir−Schaefer films.[56]

Several water-stable MOFs such as ZIF-8,[49,52,53,55,57−69] ZIF-11,[70,71] ZIF-67,[55] ZIF-93,[54] MIL-53(Al),[49,64] MIL-68(Al),[70] MIL-101(Cr),[49,56,70−73] MIL-125,[74] CuBDC,[75] CuBTTri,[76] HKUST-1 (or Cu-BTC),[54,77] UiO-66,[74,78−84] Ag-MOF,[85] Ag-BTC,[86] their functionalized forms,[64,80,81,84,87−93] and combinations with other MOFs[71] and inorganic nanomaterials[68,85] have been studied for functionalization of TFN membranes for applications such as water purification, wastewater treatment, and organic solvent nanofiltration. The common results of the inclusion of MOFs in the selective layer of TFNs were improved water fluxes/permeances without losing separation efficiency. Wang et al.,[57] employed ZIF-8 based TFN membranes for desalination and dye removal from water.[57] Interfacial polymerization was carried out on polysulfone (PSf) UF membranes. Different concentrations of ZIF-8 were used in the aqueous phase (0.05−0.20 w/v%), organic phase (0.05−0.20 w/v%), or both aqueous and organic phases (0.10 w/v%, in each). The membranes prepared by adding the MOF particles in the aqueous phase, organic phase, or both phases were referrered to as PA/ZIF-8(A), PA/ZIF-8(O), and PA/ZIF-8(B), respectively. The PSf membrane was tapped on a glass plate and immersed in the aqueous solution/dispersion for 2 min. Once the excess aqueous phase was removed, the wet membrane was soaked in the organic solution/dispersion for 20 s. The polyamide/ZIF-8 layer was cured at 60 °C. The obtained membrane structure properties (chemical structure, morphology, hydrophilicity) were greatly influenced by the ZIF-8 concentration and the liquid phase (organic or aqueous) where ZIF-8 was dispersed. The fluxes of all the PA/ZIF-8 membranes increased by increasing the ZIF-8 concentration because of the microporous ZIF-8 structure that provided additional pathways in the active layer for water transport. For dye removal, the water flux and rejection of PA/ZIF-8(A) and PA/ZIF-8(O) membranes improved at 0.05−0.15 w/v% MOF concentrations in comparison to the blank membrane, owing to the ZIF-8 properties (hydrophobic porous structure and nanoscale pore size) and the suitable compatibility between polyamide and ZIF-8 nanocrystals. The flux was slightly higher for PA/ZIF-8(O) than for PA/ZIF-8(A) due to the better dispersion of the hydrophobic nanofillers in the organic phase. On the other hand, the membrane prepared by incorporating the MOF crystals in both the aqueous and the organic phase (PA/ZIF-8(B)) overcame the dye removal performance of PA/ZIF-8(A) and PA/ZIF-8(O), for which ZIF-8 was only included in either the aqueous phase or the organic phase, respectively. The water permeance (2.26 L m^{-2} h^{-1} bar^{-1}) as well as the Congo red rejection (99.98%) for PA/ZIF-8(B) was higher than those achieved with PA/ZIF-8(A) (1.7 L m^{-2} h^{-1} bar^{-1} and 99.4%) and PA/ZIF-8(O) (2.0 L m^{-2} h^{-1} bar^{-1} and 98.9%), both prepared with a 0.20 w/v% ZIF-8 concentration (like PA/ZIF-8(B)). This is explained by a combination of the high ZIF-8 loading, the better distribution, and the lower aggregation of ZIF-8 crystals in PA/ZIF-8(B). Gong et al.[88] reported a thin (ca. 20 nm) polyamide-MOF layer on a polydopamine-modified single-wall carbon nanotube (SWCNT) film supported on a poly(ether sulfone) (PES) MF membrane (Figure 1a).[88] The

https://doi.org/10.1021/acs.iecr.1c00543
Ind. Eng. Chem. Res. XXXX, XXX, XXX−XXX

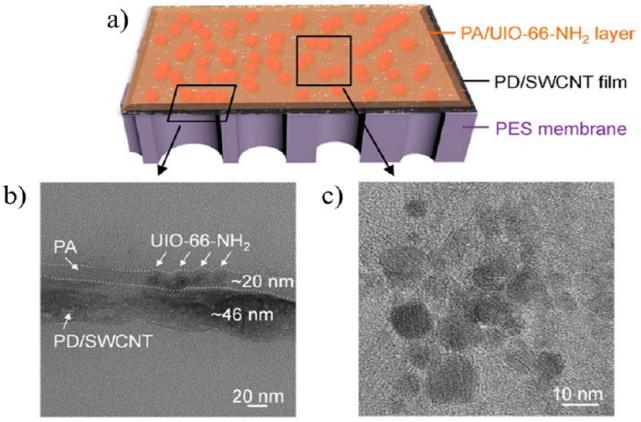

Figure 1. (a) Schematic representation of the polyamide/UiO-66-NH_2 active layer on the PDA-SWCNT film. (b) Cross-section and (c) top-view TEM images of the TFN prepared with a MOF concentration of 0.2 mg mL^{-1}. Reprinted with permission from ref 88. Copyright 2020 Elsevier.

film was prepared by filtering a dispersion containing the modified SWCNTs on the PES MF support. The as-made NH_2-UiO-66 nanocrystals were dispersed in a PIP aqueous solution (0.05−0.4 mg mL^{-1}). The composite support membrane was preloaded with a few drops of the MOF/PIP dispersion. Next, this dispersion was dripped onto the polydopamine (PDA)-SWCNT film for 30 s to cover its surface completely and the excess was removed. Subsequently, the TMC *n*-hexane solution was poured on the film surface and reacted for 30 s. Once the redundant TMC solution was removed, the membrane was immediately immersed in *n*-hexane for 1 min. The MOF loading in the TFN membrane was controlled by varying the nanofiller concentration in the aqueous phase (0.05−0.4 mg mL^{-1}), obtaining a very dense distribution of nanoparticles in the selective layer with high MOF concentration. The ultrathin active layer (Figure 1b) and the high NH_2-UiO-66 loading (Figure 1c) in these membranes resulted in a water permeance of 46 L m^{-2} h^{-1} bar^{-1} and a salt rejection (Na_2SO_4) as high as 97.1%.

When TFN membranes are fabricated by the conventional method, only a small filler amount (up to *ca.* 1.5 atom % of metal-based on XPS analysis) was effectively introduced into the skin polyamide layer, limiting the possible advantages provided by the filler addition.[94] Taking this into consideration, Van Goethem et al.[52] proposed a method called evaporation-controlled filler positioning (EFP) for placing ZIF-8 filler particles at the water/solvent interface in a controlled way before starting the interfacial polymerization process (Figure 2a).[52] Polysulfone support membranes were prepared by immersion precipitation and then impregnated in MPD aqueous solution. The excess solution was removed by a rubber wiper. ZIF-8 was dispersed in *n*-hexane to produce membranes with loadings between 0.005 and 0.4 w/v%. The membranes were then immersed in the resulting solution. Subsequently, *n*-hexane was completely evaporated at ambient conditions so that all ZIF-8 particles were deposited at the interface (Figure 2b). The membranes were covered by a TMC solution in *n*-hexane, and interfacial polymerization was carried out for 1 min. The TMC solution was drained off, and the membrane surface was rinsed with *n*-hexane. The performance of the final TFN membranes was evaluated by filtration of NaCl aqueous solutions. The EFP-TFN membranes showed a ca. 3-fold increase in permeation without compromising salt rejection. Regardless of the particle size of ZIF-8 (75 or 150 nm), the best performance was achieved with a MOF loading as low as 0.005 w/v% (80 times less than for other reported ZIF-8 TFN membranes).[69] Besides, the performance of the EFP-membranes was more reproducible than that of the conventional TFN membranes. The same authors reported that the HCl formation during the interfacial polymerization reaction between an acyl chloride and a diamine (as said above, usually TMC and MPD) could degrade the ZIF-8 and generated Zn^{2+} which increased the water permeance with a small loss of rejection at high concentrations.[95]

Modified MOFs have been frequently incorporated into TFNs in order to improve (1) MOF compatibility with the polymeric matrix in the selective polyamide layer, (2) MOF dispersibility in the organic/aqueous phase during interfacial polymerization, and/or (3) minimize MOF aggregation (e.g., ZIF-8,[96−105] HKUST-1,[106] NH_2-UiO-66[80,107−109]). In 2019, Zhao et al.[108] reported the synthesis of NH_2-UiO-66 nanocrystals modified with polyvinylpyrrolidone (PVP), PVP-UiO-66-NH_2 to avoid the nanofiller aggregation and increase compatibility between the organic and inorganic counterparts.[108] TFNs were prepared by a drop-coating method employing a hydrolyzed polyacrylonitrile (HPAN) membrane as a substrate (Figure 3). The polyacrylonitrile (PAN) membrane was hydrolyzed by immersion in a sodium hydroxide aqueous solution and then in deionized water to achieve the HPAN membrane. PVP-UiO-66-NH_2 nanoparticles were dispersed in deionized water at a concentration ranging from 0.1 to 0.8 wt %. The PVP-UiO-66-NH_2 dispersion and the poly(vinyl alcohol) (PVA) aqueous solution were blended and drop-coated on the HPAN membranes. Next, a glutaraldehyde aqueous solution was added for the cross-linking reaction (80 °C, 30 min). As-fabricated TFNs showed higher hydrophilicity, enhanced filtration properties, and enhanced long-term stability. Water permeance reached a value of 131 L m^{-2} h^{-1} bar^{-1} with an exceptional rejection (>99.9%) for four dyes (congo red, methyl blue, Reactive

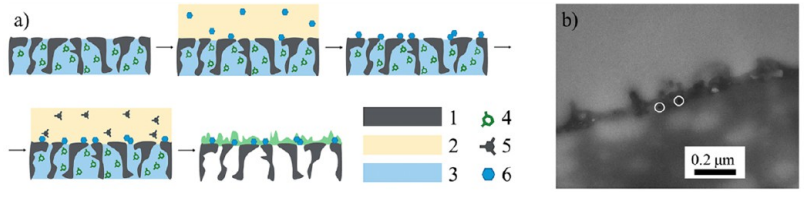

Figure 2. (a) Schematic representation of the evaporation-controlled filler positioning (EFP) (1, support membrane; 2, organic (*n*-hexane) phase; 3, aqueous phase; 4, MPD; 5, TMC; 6, ZIF-8). (b) TEM cross-section image of a EFP-TFN membrane showing the ZIF-8 particles (white circumferences). Adapted with permission from ref 52. Copyright 2016 Royal Society of Chemistry.

https://doi.org/10.1021/acs.iecr.1c00543
Ind. Eng. Chem. Res. XXXX, XXX, XXX−XXX

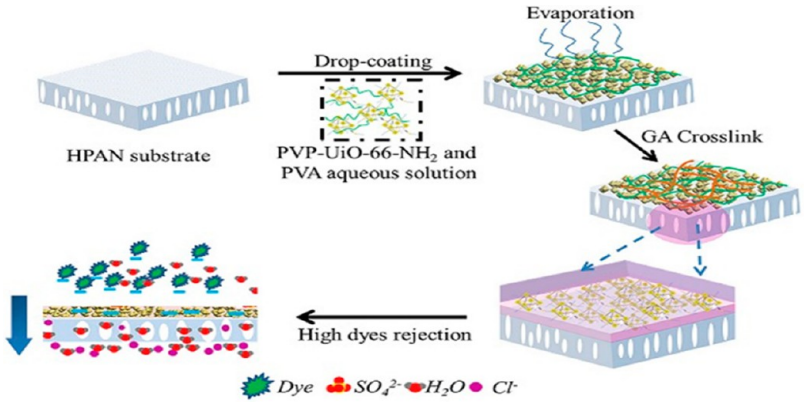

Figure 3. Synthetic procedure for the PVA/PVP-UiO-66-NH_2/PAN membrane. Reprinted from with permission from ref 108. Copyright 2019 Elsevier.

Black 5, and Direct Red 23). However, salt rejections were lower for the TFN membranes than for the TFC one due to the presence of the modified MOF in the selective layer that created additional molecular transport channels for water and salts to permeate.[108] However, aggregation of MOFs limits the loading concentration of MOFs to the membrane matrix and also influences the membrane performance. Therefore, efficient and straightforward methods to avoid the aggregation of MOFs during surface functionalization are still critically needed.

2.3. Immobilization/Incorporation into the Support Layer. It is possible to incorporate MOF particles in the support layer to functionalize membranes for water and wastewater treatments. Blending methods in which the fillers and the organic matrices are mixed to generate mixed matrix membranes (MMMs) are the common techniques. Besides these, phase inversion (the method mainly used for commercially available polymeric membranes) and electrospinning are the most popular approaches. Dope dispersions are a mixture of polymer, nanofillers, solvent, and pore former, and in the case of nanocomposite membranes for water treatment, they usually consist of 17−20 wt % polymer, 0.5−10 wt % nonsolvent, and 0.5−30 wt % nanofiller.[110] The methods to control demixing (solvent/nonsolvent) in phase inversion are immersion precipitation, thermally induced phase separation, evaporation-induced phase separation, and vapor-induced phase separation. To our knowledge, the latter has not been employed for integrating MOFs in membrane supports. Commercial polymeric membranes are usually fabricated by immersion precipitation (or nonsolvent-induced phase separation, NIPS).[111] Immersion precipitation proceeds by casting the MOF-polymer blending on a suitable support (e.g., nonwoven polypropylene) or casting on the glass plate directly and then immersing into a nonsolvent coagulation bath (normally water). Polymer precipitation occurs because of the solvent and nonsolvent exchange.[111,112] The exchange continues until demixing takes place in such a way that the initial homogeneous blending turns into two phases: the polymer-rich phase with embedded MOF particles that gives rise to the membrane structure and the liquid-rich phase that forms the pores.[112,113] The internal structure of the final membranes is asymmetric with a dense skin layer and finger-type pores. Several MOFs including ZIF-8,[114] ZIF-L,[115] MIL-53(Al),[116] MIL-68(Al),[117] HKUST-1,[118,119] HKUST-1@GO,[120] Cu(tpa)@GO,[121] UiO-NH_2,[122] UiO-66@GO,[123] MOF-5,[124] Ag-MOF,[125] Ce-MOF,[126] Zn/Co-MOF-74,[127] TMU-5,[128] etc. have been used for functionalization of polymeric membranes for water and wastewater treatment applications. For instance, Misdan et al.[118] generated a TFC membrane with a polysulfone HKUST-1 MOF-incorporated support by immersion precipitation.[118] The asymmetric MOF-polymer support was prepared by dissolving the polysulfone in *N*-methyl-2-pyrrolidone (NMP) and adding PVP as the pore former. Commercial HKUST-1 (0.25−0.75 wt %) was gradually added to the casting solution. The functionalized membranes showed higher hydrophilicity, water flux, and enhanced antifouling properties while maintaining $MgSO_4$ rejection (97.31%). NaCl rejection was increased by increasing MOF concentration in the support layer (from ca. 20% to ca. 45%) due to the Donnan effect caused by the electrostatic repulsion between the ions and the functional groups of the membrane surface (coming from HKUST-1 and poly-(piperazineamide)).

Composite membranes with graphene oxide (GO) have been effectively applied in water purification.[120] However, the strong interactions between GO nanosheets can cause aggregation and stacking, resulting in low permeation and antifouling efficiency.[129−131] The incorporation of MOFs into the GO structure can modify the GO structure. Ma et al.[123] chose UiO-66 as a porous modifier of GO.[123] They anchored the MOF particles on the surface of GO nanosheets and used the UiO-66@GO composite as a filler in UF membranes for dye removal (methyl orange and Direct Red 80) from water. The MOF@GO composite was prepared via in situ crystallization. The membranes were fabricated by immersion precipitation of PES using PVP as an additive and different amounts (0−3 wt %) of UiO-66@GO. The data showed that the presence of UiO-66 prevented GO stacking and provided unique properties to the composite material. Compared to PES and GO/PES membranes, the water flux of UiO-66@GO/PES (3 wt % filler loading) increased by 351% and 78%, respectively. Moreover, the UiO-66@GO/PES membrane achieved higher hydrophilicity, water purification performance, and antifouling efficiency.

MOFs have also been used for the functionalization of hollow fiber membranes. Spinning is the immersion precipitation technique for the fabrication of hollow fiber membranes. In the spinning method, a single fiber or multiple fibers are produced continuously by extrusion through a spinneret followed by solidification.[110,132] The spinneret contains a hollow needle with a larger outer-diameter channel that extrudes the polymer solution and another channel with a

https://doi.org/10.1021/acs.iecr.1c00543
Ind. Eng. Chem. Res. XXXX, XXX, XXX−XXX

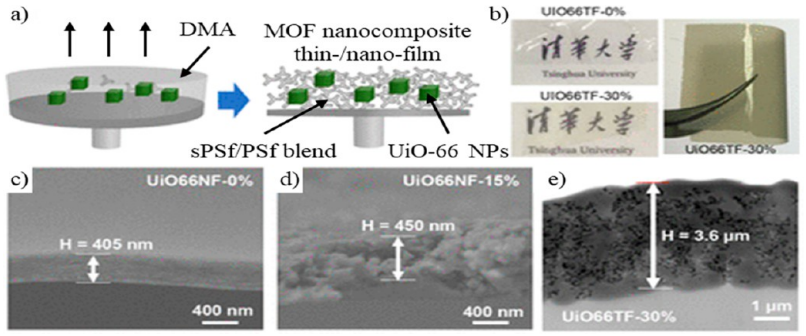

Figure 4. (a) Fabrication strategy of the UiO-66 nanocomposite films. (b) Photographs of polymer and nanocomposite thin films. (c) Cross-sectional TEM image of a pure-polymer nanofilm (UiO66NF-0%). (d) Cross-sectional TEM image of the UiO66NF-15% nanofilm. (e) HRTEM cross-sectional image of the UiO66TF-30% nanofilm. Adapted with permission from ref 141. Copyright 2018 American Chemical Society.

smaller inner-diameter that extrudes the internal coagulant (bore fluid).[110,133−135] Cheng et al.[136] prepared MOF/PVDF hollow fibers with hydrophobic properties for application in direct contact membrane distillation (DCMD) by dry-jet-wet spinning,[136] for which there exists an air gap between the end of the spinneret and the external coagulant bath. Aluminum fumarate MOF particles were dispersed into *N*,*N*-dimethylacetamide (DMA) solvent. PVDF (polymeric matrix) and 1,2-propylene glycol (PG) (nonsolvent) were added to the aluminum fumarate MOF suspension. Water was used as the internal and external coagulant. With a MOF loading of 1 wt %, the effective membrane porosity increased by 52.4%, the water flux was enhanced by 50.5%, and the thermal conductivity was reduced by 38.6%, thus improving the thermal efficiency of DCMD. In addition, the MOF/PVDF composite hollow fiber showed stable flux and high salt rejection (>99.9%) over a 50 h desalination test period. The authors[136] concluded that the incorporation of proper MOF additives could render larger pores and higher porosity, surface roughness, and mechanical stability, enhancing the membrane performance in distillation processes.

In evaporation-induced phase separation (EIPS), also called solution casting or dry cast method, the polymer is dissolved in a mixture of a volatile solvent and a less volatile nonsolvent,[113,137] After MOF addition, the resulting suspension is cast onto a clean plate or support. When the solvent is evaporated, the nonsolvent-rich droplets grow and coalesce to become larger.[137] Thus, the polymeric solution is demixed in two phases (precipitation): the polymer-rich phase, containing the MOF fillers, and the polymer-lean phase.[113,137] Once the nonsolvent enriched droplets are extracted, a skinned membrane with a highly porous structure is formed.[137] Solvents of different boiling points can be used to control the morphology of the final membrane.[113] Despite its simplicity, this method is rarely employed for integrating MOF in water treatment membranes,[138−141] probably due to the great dependence of the rate of solvent evaporation on membrane morphology. Cross-linked membranes based on postsynthetic polymerization of NH_2-UiO-66 nanocrystals and polyurethane oligomer were fabricated by EIPS.[140] First, an isocyanate-terminated polyurethane oligomer was dissolved in anhydrous chloroform. NH_2-UiO-66 nanoparticles were added to obtain membranes with MOF loadings of 50, 60, and 70 wt %. The reaction suspension was cast onto a clean PTFE dish. The cross-linked membranes were peeled off, purified in DMF and chloroform, and finally dried. The as-prepared UiO-66-urea based membrane with the highest loading showed uniform texture and mechanical resistance. It was able to remove the dyes eosin Y and rhodamine B from aqueous solutions as well as completely separate eosin Y/methylene blue, rhodamine B/malachite green, and rhodamine B/methylene blue mixtures in water. This was due to the selective adsorption capacity of the membrane to rhodamine B and eosin Y dyes. Liu et al.[141] prepared UiO-66 nanocomposite thin films with thicknesses ranging from 0.45 (UiO66NFs, Figure 4c,d) to 3.6 μm (UiO66TFs, Figure 4e) using polysulfone as the polymeric matrix and sulfonated polysulfone (sPSf) as an additive.[141] The UiO-66 nanocrystals (5−50 wt %) were dispersed in DMA, and then polysulfone-sPSf polymeric blend was added and dissolved (Figure 4a). The incorporation of sPSf additives along with nanosized fillers yielded high dispersity and interfacial bindings between the MOF and the polymer resulting in mechanically and thermally stable membranes (Figure 4b). The membrane microporosity was enhanced with pore sizes below 1 nm, enabling ion-sieving properties. This rendered increased water permeance (up to 1.41 L m^{-2} h^{-1} bar^{-1}) and separation performance (Na_2SO_4 rejection of 83−96%).

Some polymers (e.g., polypropylene, poly(vinyl alcohol)) cannot be dissolved at room temperature. Therefore, it is necessary to increase the temperature to attain a dispersed solution. In thermally induced phase separation (TIPS), the polymer is dissolved in the solvent at a temperature close to, or higher than, its glass transition temperature.[112] The hot MOF-polymer suspension is then cast onto a plate or substrate. When the temperature is decreased, the demixing/precipitation occurs owing to a reduction in the solubility of the polymer.[112,113] The solvent is removed by means of freeze-drying, extraction, or evaporation.[112,113] These kinds of membranes possess either porous honeycomb-like or spherulitic internal structures depending on the polymer fraction in the casting solution.[112] Despite the notable advantages of this method (high porosity, microstructures with narrow pore size distributions, reproducibility, process simplicity, low density of defects, etc.),[113] there exist few examples of MOF membranes following the TIPS technique. Ren et al.[142] fabricated MIL-PVDF multifunctional UF membranes with an ultrahigh MIL-53(Fe) loading via a blending method of predispersion in acetone and TIPS.[142] MIL-53(Fe) was predispersed in acetone. PVDF was dissolved in DMF and then added to the MOF suspension. Next, acetone was evaporated to keep a high dispersity and proper viscosity and concentration. The resulting solution was cast by hand with a film scraper onto a glass substrate. Finally, DMF was removed by the TIPS

https://doi.org/10.1021/acs.iecr.1c00543
Ind. Eng. Chem. Res. XXXX, XXX, XXX−XXX

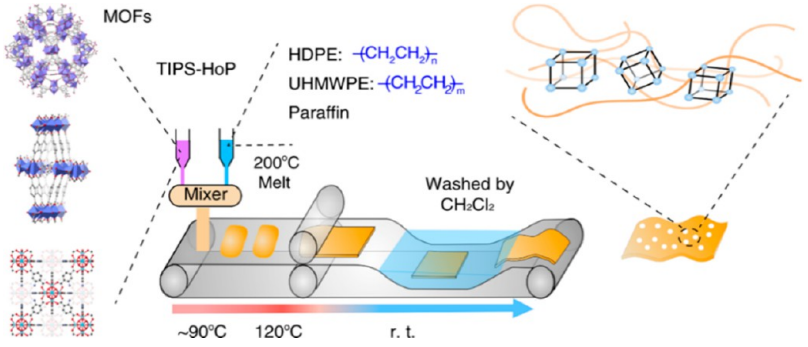

Figure 5. Schematic of the MOF membrane fabrication process using the TIPS-HoP method.[143] Reproduced with permission from ref 143. Copyright 2019 Nature Communications.

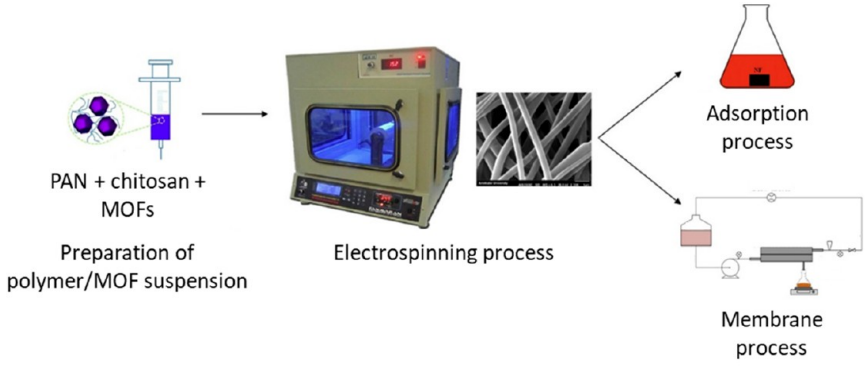

Figure 6. Schematic of the synthesis of nanofibers/MOFs and its application for the removal of metal ions by adsorption and membrane processes. Adapted with permission from ref 147. Copyright 2019 Elsevier.

process. A maximum MOF loading of ca. 61% (based on EDS element composition) was obtained due to the enhanced dispersity and pore size restriction. Hydrophilicity and water flux increased with higher MOF loading in the membranes. Besides, the MIL-PVDF membranes showed an outstanding performance for removing methylene blue from an aqueous solution by adsorption while maintaining high permeability and UF efficiency. This performance was due to the favorable pore size, porosity, roughness, and hydrophilicity of the membranes. A novel strategy called thermally induced phase separation-hot pressing (TIPS-HoP) was reported by Wang et al. (Figure 5).[143] It combines both TIPS and hot pressing methods in order to produce ultrahigh MOF loading membranes with strong thermal and chemical robustness, high flexibility, and acceptable mechanical strength. They prepared composite membranes with 10 distinct MOFs: MIL-100(Cr), Mg-MOF-74, ZIF-8, BIT-72, MOF-801, MOF-5, Zn-BLD, MOF-808, HKUST-1, and NH_2-UiO-66. First, MOF nanocrystals were suspended in the melt of high-density polyethylene (HDPE), ultrahigh-molecular weight polyethylene (UHMWPE), and paraffin at 200 °C. The suspension was then placed onto a belt to be treated with heat (120 °C) and pressure between two rolls (roll-to-roll hot pressing) to form the membrane. After the suspension was cooled to room temperature, paraffin was removed by soaking in dichloromethane. A filler loading up to 86 wt % was attained regardless of the type of incorporated MOF. The composite membranes were applied in organic dye (Congo red, crystal violet, rhodamine B, methylene blue, fuchsine acid and orange G) separation from water. The hierarchical porous structure, large surface area, and tunable pore chemical environment of the membranes contributed to achieve an ultrahigh water permeance (up to 125.7 L m^{-2} h^{-1} bar^{-1}) and an excellent organic dye rejection (>98%) in water treatment.

Electrospinning generates fibrous membranes with diameters ranging from micrometers to nanometers through an electrically charged jet of polymer solution/melt.[112,144,145] The obtained fibers feature high porosity, micro- or nanopore size, interconnected open pore structure and high surface-area-to-volume ratio.[112,145,146] Jamshidifar et al.[147] used electrospinning for incorporating NH_2-UiO-66 fillers into PAN/chitosan nanofibrous membranes for removal of Pb^{2+}, Cd^{2+}, and Cr^{4+} ions from aqueous solutions.[147] The PAN/chitosan/NH_2-UiO-66 fibers were collected on a PVDF nanofibrous sublayer also prepared by electrospinning. MOF particles, synthesized by microwave heating, were added in a 2−15 wt % concentration to the blend solution. The influence of several parameters (MOF concentration, membrane thickness, metal ion concentration, temperature, and filtration time) on heavy metal removal was thoroughly studied. Increasing the membrane thickness, the MOF loading, and the initial concentration of metal ions in aqueous solution rendered an increased metal ion removal and a decreased water flux. Yang et al.,[148] reported a superhydrophobic PVDF nanofibrous membrane prepared with Fe-BTC MOF as a filler onto a nonwoven substrate via electrospinning for desalination by direct membrane distillation (DCMD) (Figure 6).[148] The dope solution was prepared by dissolving PVDF in a DMA/acetone solution and then adding commercial Fe-BTC (1−5 wt %). The MOF-PVDF membranes exhibited a uniform Fe-BTC distribution on the nanofibers. The presence of the MOF helped to increase hydrophobicity, fiber diameter, pore size, and porosity of the membranes. The optimized membrane showed a water flux of 3.26 L m^{-2} h^{-1} and outstanding salt

https://doi.org/10.1021/acs.iecr.1c00543
Ind. Eng. Chem. Res. XXXX, XXX, XXX−XXX

rejection (NaCl) of 99.99%. More examples of electrospun nanofibrous composite membranes incorporating MOFs for water treatment are found in literature.[149−158]

Recently, some novel strategies for integrating MOFs in the support layer were reported.[159−164] For instance, Wang et al.[162] encapsulated ZIF-11 nanocrystals in the nanoporous layer of a HPAN support through a fine-tuning contra-diffusion method to form nanoconfined composite membranes (Figure 7).[162] Initially, PAN membranes were hydrolyzed to attain

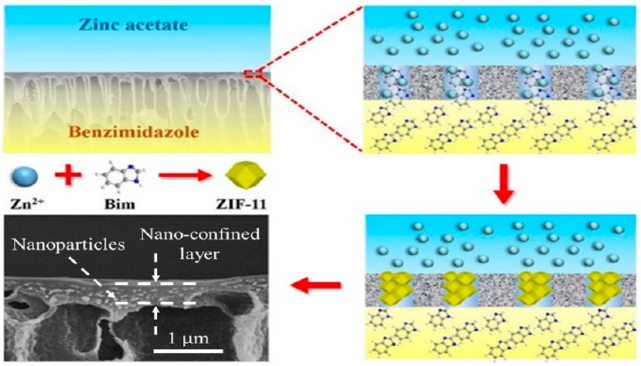

Figure 7. Schematic of the fine-tuning contra-diffusion method to form ZIF-11 nanoconfined composite membranes. On the left bottom: cross-sectional SEM image of ZIF-11/PAN composite membrane. Adapted with permission from ref 162. Copyright 2016 American Chemical Society.

HPAN supports. Metal and ligand sources for MOF synthesis were dissolved separately. The HPAN substrate was fixed horizontally in a homemade U type diffusion cell with the nanoporous layer facing up. The metal ion solution was poured on top of the support surface while the linker solution was added to contact the surface facing down. The resulting nanoconfined composite membranes were applied in methylene blue removal from aqueous solutions. The porous NPs were formed inside the nanoporous skin layer of the HPAN support in such a way that the support nanopores were used as templates to confine the size and distribution of nanofillers. The barrier skin layer of the nanoconfined composite membranes had minimal thickness, reducing the mass transfer resistance of water. This caused the water permeance to increase significantly (46.4 L m^{-2} h^{-1} bar^{-1}), while maintaining the rejection (98.4%). Moreover, the nanoconfined composite membranes were stable for a 60 h test period without performance deterioration. Another alternative technique to include MOFs in membrane substrates is freeze-drying. Multifunctional MOF hollow tubes were fabricated by the freeze-drying process for filtration of air and liquid pollutants.[164] Five distinct MOFs (NH_2-UiO-66, UiO-66, ZIF-8, NH_2-MIL-101(Al), and Zn-MOF-74) were incorporated with tunable loadings (30−70 wt %) in the hollow tubes (4.5−8.0 mm inner diameters) using sodium alginate (SA) as the polymer. MOF particles were first dispersed in SA. The MOF@SA suspension was then poured into a mold with a glass template placed in the middle. The system was frozen in liquid nitrogen so that an ice solid with the mold shape was produced. Next, the template was peeled off and the hollow ice solid was freeze-dried to obtain the hollow tube. All the MOF hollow tubes showed porous textures with low densities (<0.1 g cm^{-3}), homogeneous distribution of nanocrystals, high mechanical robustness, and uniform shape regularity. Nonetheless, the as-prepared MOF-based hollow tubes were unstable in water. After cross-linking with a $CaCl_2 \cdot 2H_2O$ solution, the ZIF-8@SA hollow tube (50 wt % ZIF-8 loading) maintained robustness, morphology, and filtration efficiency. Among the different hollow tubular configurations, the double-layer coaxial hollow tube prepared with ZIF-8 and NH_2-MIL-101(Al) (after cross-linking) exhibited a high removal efficiency (>94%) for mixed-pollutants in aqueous solutions (AsO_4^{3-} and methyl orange). This double-layer coaxial hollow tube thus combined the high filtration efficiency (>90%) of the ZIF-8@SA hollow tube (50 wt % loading) for AsO_4^{3-} and that of the NH_2-MIL-101(Al)@SA hollow tube (50 wt % loadings) for methyl orange. This work demonstrated that the freeze-drying protocol, employing ice as the platform, provides a high degree of processability for MOF composites.

3. CHARACTERISTICS OF MOF-FUNCTIONALIZED MEMBRANES

3.1. Effect of MOFs on Membrane Permeability.

MOFs are promising fillers for the functionalization of thin-film nanocomposite (TFN) membranes due to their high diversity of organic moieties and metal cations that bring diverse functionality and enhanced compatibility with different polymers. MOF functionalizations improve membrane permeability by increasing the membrane surface hydrophilicity, providing extra pathways for water molecules, and optimizing the cross-linking of the polyamide layer. Figure 8 shows the

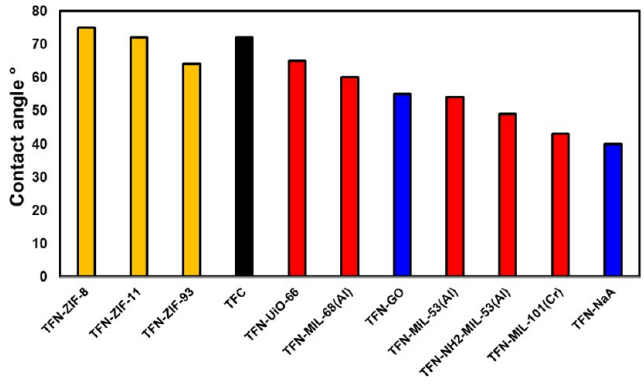

Figure 8. Contact angles of TFC and TFN membranes functionalized by random dispersion of several nanofillers in the polyamide thin film.[47,49,70,71,169] The distinct colors in the graph represent TFNs incorporating different families of materials as fillers: (orange) ZIFs; (black) no fillers (TFC); (red) carboxylate type MOFs; (blue) inorganic materials.

effect of MOFs on the hydrophilicity of different membranes. MIL-101(Cr), a carboxylate type MOF displaying mesoporous cages with diameters of 2.9 and 3.4 nm, featuring 1.2 nm pentagonal and 1.6 nm hexagonal openings,[165] was the first MOF used to functionalize TFN membranes.[49] This MOF not only made a more hydrophilic membrane surface (as observed through the decrease of the water contact angle) but also provided preferential flow pathways (faster than those corresponding to the bare polyamide) for the solvents.[49] However, as compiled in Table 1, hydrophobic MOFs, such as zeolitic imidazolate framework ZIF-8, also increased the water flow through the membrane even though they did not substantially decrease the membrane water contact angle as hydrophilic MOFs do. An explanation of the positive effect of

https://doi.org/10.1021/acs.iecr.1c00543
Ind. Eng. Chem. Res. XXXX, XXX, XXX−XXX

Table 1. Effect of Different MOFs on Water Permeation of the TFC Membrane at Different Water and Wastewater Treatment Applications

type of membrane/fabrication technique	MOF	effect	application	ref
continuous on anodic Al_2O_3	ZIF-8, UiO-66	reversible hydration	selective transport of alkali metal ions	170,171
phase inversion	ZIF-8, MOF-74	increase water flux	UF	127
TFC on continuous layer	ZIF-93, HKUST-1	increase water flux	NF	54,172
TFN	UiO-66	increase water flux and boron removal	RO	82
TFN	MIL-101(Cr)	increase water flux	RO	72
TFN	ZIF-8	increase water flux	RO	69
TFN	ZIF-8	increase water flux	NF	59
TFC on LBL MOF	ZIF-8	increase water flux	NF	53
TFN	ZIF-8/CNT	increase water flux and chlorine stability	RO	68
phase inversion hollow fiber (dry-jet-wet spinning)	Al fumarate	increase mass tranfer and thermal efficiency, long-term stability	MD	136
TFN	CuBDC nanosheet	increase water flux and antifouling	FO	75
TFN	CuBTTri	increase water flux and antibiofouling	RO	76
phase inversion (immersion precipitation)	hydrophilic hollow ZIF-8	increase water flux	UF	114
phase inversion (immersion precipitation)	Ce-MOF	increase water flux, dye removal and antifouling	NF	126
BTFC	ZIF-93, HKUST-1	increase water permeance	NF	54
TFN	ZIF-8	increase water flux and dye rejection	NF	57
TFN	NH_2-UiO-66	increase water flux, ultrathin active layer (20 ± 3 nm)	NF	88
TFN	ZIF-8	increase water flux, ultralow filler loading (0.005 w/v%)	filtration of aqueous NaCl solutions	52
TFN	PVP-UiO-66-NH_2	increase water flux and dye rejection, long-term stability	filtration of salts and dyes	108
TFC	HKUST-1	increase water flux	NF	118
phase inversion (immersion precipitation)	UiO-66@GO	increase water flux and dye rejection	UF	123
phase inversion hollow fiber (dry-jet-wet spinning)	Ag-PEI	increase water flux and antibiofouling	UF	135
phase inversion (EIPS)	NH_2-UiO-66	effective dye removal from water	filtration and separation of dyes in water	140
phase inversion (EIPS)	UiO-66	increase water flux and salt rejection	NF, FO	141
phase inversion (TIPS)	MIL-53(Fe)	increase water flux and methylene blue rejection	UF	142
phase inversion (TIPS-HoP)	MIL-100(Cr), Mg-MOF-74, ZIF-8, BIT-72, MOF-801, MOF-5, Zn-BLD, MOF-808, HKUST-1 and NH_2-UiO-66	increase water flux, ultrahigh filler loading	MF, UF	143
electrospun nanofibrous membrane	NH_2-UiO-66	increase water flux	filtration of metal ions	147
electrospun nanofibrous membrane	Fe-BTC	increase water flux	DCMD	148
nanoconfined composite membrane	ZIF-11	increase water flux, long-term stability, active layer thickness ≈0	NF	162
double-layer coaxial hollow tube	ZIF-8, NH_2-MIL-101(Al)	efficient capture of mixed inorganic−organic contaminants	filtration of single or mixed contaminants in aqueous solutions	164

https://doi.org/10.1021/acs.iecr.1c00543
Ind. Eng. Chem. Res. XXXX, XXX, XXX−XXX

ZIF-8, which is hydrophobic and negatively charged, on permeation might be the impact of ZIF-8 on the cross-linking degree of the polyamide. Two side reactions can occur between diamine and acid chloride during interfacial polymerization.[166] On the one hand, the cross-linking reaction of another diamine molecule with a terminal acid chloride group of TMC through amide linkage (−CO-NH) led to a network chain-branching structure. On the other hand, the hydrolysis of the third or terminal acid chloride group of TMC produced free carboxylic acid groups in the polyamide layer, increasing the hydrophilicity of the membrane matrix. Both types of structures were necessary to attain high-performance desalination membranes.[166] The network chain-branching structure formed via a cross-linking reaction is achieved when the MPD/TMC ratio increases, and it resulted in higher salt rejections with slightly lowered fluxes.[167,168] In contrast, the structure obtained by hydrolysis (with lower MPD/TMC ratios) increased the water flux due to the hydrophilic properties.[168] Thus, it is convenient to keep a 1:1 ratio between cross-linking and hydrolysis reactions to achieve a polyamide layer with equal fractions of network chain-branching and hydrophilic structures, obtaining higher water fluxes with acceptable salt rejections.[166] Due to the membrane monomer bondings with the filler functionalities, less cross-linking is achieved in a TFN membrane, as stated for ZIF-8 as a filler.[69] Low concentration of ZIF-8 (up to 0.05 w/v% in the membrane synthesis suspension) with uniform dispersion accelerated the interfacial polymerization, favoring the presence of the typical nodular polyamide structures, which increased the surface roughness. The electrostatic interaction between the protonated amine monomer and ZIF-8 produced by a high concentration of ZIF-8 (up to 0.5 w/v%) reduced the rate of interfacial polymerization and aggregation of MOF particles. The lower particle aggregation in turn, resulted in reductions in both the surface roughness and the contact angle. This provoked a simultaneous increase of the water flux and a decrease of the Na_2SO_4 rejection.[59] Duan et al.[69] encapsulated ZIF-8 in polyamide film during the interfacial polymerization membrane synthesis and reported a reduction in water contact angle with increasing hydrophobic ZIF-8 loading as nondesirable results.[69] The simultaneous incorporation of hydrophobic ZIF-11 and hydrophilic MIL-101(Cr) MOFs resulted in enhanced membrane permeation.[71]

3.2. Effects of MOFs on Membrane Antifouling Properties. The inclusion of MOF nanoparticles has been shown to alter the surface roughness, electrical charge, hydrophilicity, and antibacterial nature of TFN membranes, all of which greatly impact membrane fouling and biofouling properties.[173,174] The enhanced membrane surface charge and hydrophilicity introduced by the MOFs increase the repulsion of particles from the membrane surface while promoting the hydrophilic−hydrophilic interaction between water molecules and membrane surface, resulting in enhanced antifouling properties. MOFs with antibacterial properties kill the bacteria attached to the membrane surface, effectively mitigating the biofouling.[11,85,174,175]

MOFs, such as UiO-66 and Ag-MOFs, are widely investigated membrane additives for antifouling and antibiofouling due to their hydrophilic and antimicrobial properties, as explained below. The membrane additives increase surface roughness, which increases both water permeability and fouling due to the increased surface area provided by the MOFs. However, Ag-based MOFs counteract fouling and biofouling by utilizing the hydration layer to repel surface contaminants and antimicrobial properties of Ag to kill biocontaminants. Many researchers have utilized UiO-66, which possesses a highly negative surface charge and high water stability.[40,81,85,87,94,122,130,143,176−180] Sun et al.[122] have developed a UF membrane by functionalizing UiO-66 onto PSf membranes at 0.3 wt % loadings. Only low MOF loading was required to have a substantial antifouling effect, whereas an overdosage of MOF causes agglomeration. By adding poly(sulfobetaine methacrylate) (PSBMA), they were able to envelop the MOFs to ensure more even distribution. While the 0.3 wt % MOF membrane had the roughest surface, it also possessed the highest flux recovery ratio (72.5%) due to the enhanced hydration layer.[122] Here flux recovery ratio (FRR) is defined as the percentage of pure water flux after filtration and cleaning to the pure water flux of the pristine membrane. Another common method is to pair UiO-66 with graphene oxide (GO) in order to further improve molecular sieving and ion rejection. Fang et al.[179] synthesized TFN membranes consisting of UiO-66 in GO/PAN membranes. The UiO-66 filtered out organic contaminants and provided additional channels for efficient water permeation. This membrane maintained a flux recovery ratio of 95% after 1000 min cycling, demonstrating acceptable antifouling performance.[179] Heu et al. prepared UiO-66 incorporated into PA membranes to explore photocatalytic effects for antifouling performance. The FRR improved from 49.9% to 79.0% at 10 wt % loading. Under UV irradiation, this increased further to 97.0%, which indicated effective photocatalytic ability.[180] In a similar study, Chang et al.[177] utilized a chitosan coating on top of the MOF/GO layer. This, in combination with the MOF/GO layer, resulted in a significant increase in FRR (from 42.9% to 88.0%).[177] Xiao et al. created different TFN by incorporating UiO-66 and UiO-66-NH_2 onto PA membranes to enhance performance in both aqueous and organic phases. The most effective membranes were synthesized using UiO-66 in the organic phase, which formed the thinnest films and the largest pore sizes. They possessed a biofouling FRR of 98.3%, owing to the hydrophobic surface repelling hydrophilic organic contaminants, as the authors stated.[81]

In comparison to UiO-66, membranes modified by UiO-66-NH_2 provided better rejection for divalent ions while retaining good antifouling properties. In addition, many groups further functionalized these membranes in order to further improve selectivity or antifouling.[87,94,130,143,176,178] Wang et al.[143] loaded UiO-66-NH_2 onto polyethylene (PE) membranes by thermally induced phase separation-hot pressing (TIPS-HoP). These membranes use an adsorption process for separation instead of filtration methods, governed primarily by electrostatic interactions. At 86 wt % loading, the membrane performance was highly stable for Cr removal. The membrane foulants could be removed using a quick $NaNO_3$ wash, resulting in an FRR of 97%.[143] Li et al. controlled the pore size of the membrane by varying the MOF loading. A loading of 0.2 wt % improved water flux by over 500% and increased FRR from 8% to 90%.[176] Zinadini's group[130] added melamine (Mlm) to PES UF membranes in order to improve thermal stability. Increasing the Mlm loading introduced a trade-off between FRR and water flux because the increased surface roughness compromises the enhanced hydrophilicity. The enhanced thermal stability enabled operation at a higher temperature at which fouling is reduced and flux is increased due to decreased feed viscosity.[130] Cao et al.[178] synthesized a

https://doi.org/10.1021/acs.iecr.1c00543
Ind. Eng. Chem. Res. XXXX, XXX, XXX−XXX

self-assembling membrane by adding additional poly(acrylic) acid (PAA) onto a mixed cellulose ester (MCE) membrane to improve the dispersion and strengthen the stability of the membrane. Normally, UiO-66-NH_2 was unstable in a basic environment, leading to flux drop due to the crystal structure degradation. However, this membrane was stable under both acidic conditions and alkaline conditions up to pH 11 due to the addition of PAA. In addition, the MOF loading both increased hydrophilicity of the membrane and electrostatic repulsion, leading to a FRR increase from 40% to 86%.[178] Golpour and Pakizeh prepared a novel NF membrane with a PA-MOF layer and a polyphenylsulfone (PPSU)-GO layer with a 0.05 wt % loading, which resulted in a pure water flux (PWF) improvement of 44% and an increase in FRR of 7.3%. This antifouling performance was attributed to surface hydrophilicity increase caused by MOF functionalization, which counteracted the hydrophobicity of the bare membrane.[87] Gohain et al.,[94] developed a NF membrane consisting of a PSF layer incorporated with mesoporous synthetic hectorite (MSH) and UiO-66-NH_2. This MSH incorporation resulted in a thicker selective layer and increased thermal stability. In addition, rejection for a variety of metal salts was improved at the cost of water flux.[94]

Pejman et al.[175] investigated FO membranes functionalized with zwitterions and Ag-MOFs. The synergistic effects between zwitterions and Ag-MOFs resulted in an increase in the water flux of over 400% as well as over 99% dieoff of *E. coli*, which indicated significant antibiofouling effectiveness.[175] Similarly, Firouzjaei et al.[85] developed a TFN membrane by ultrasonic irradiation utilizing GO and Ag-MOFs for water treatment and antifouling improvement. The additives increased the negative surface charge of the membrane, which enhanced biofouling resistance in addition to the antimicrobial effects of Ag.[85]

Zeolitic imidazolate frameworks (ZIFs) are a group of hydrophobic Zn-based MOFs with applications in oil separation and salt rejection. In particular, the most studied ZIF, ZIF-8, possesses a high amount of micropores for microfiltration effectiveness. Wang et al.[181] reported a microfiltration membrane for oil/water separation composed of a metal−phenolic network and MOF combination with alternating Ti (IV)-tannic acid (TTN) and ZIF-8 layers. The TTN layers enhanced the hydrophilic effect to counteract the hydrophobicity of the ZIF-8 layers. ZIF-8 provided a hierarchical structure for the membrane. Antifouling was significantly improved from 59% to 86% due to a hydration layer block oil adhesion.[181] Zhang et al.[182] have developed PES membranes with incorporated ZIF-8 to introduce a high number of micropores to increase hydrophilicity. However, due to the increased surface roughness, fouling increased. This was mitigated by increasing MOF nanoparticle diameter from 30 to 100 nm to decrease pore density, which resulted in a FRR of 94%.[182] Wang et al.[183] synthesized a FO membrane by in situ growth of ZIF-8 on a polydopamine (PDA)/PS membrane. Although the MOF was hydrophobic, due to its thin layer, water permeated across to the hydrophilic PDA layer, resulting in enhanced water permeation. The presence of ZIF-8 killed almost 99% of bacteria owing to many antibacterial components such as Zn^{2+}, imidazole, and Zn−O bonds.[183]

Cu-based MOFs possess similar antimicrobial effects but allow for tuning of ion selectivity and flux enhancement.[76,184] Lin et al.[185] prepared a PES membrane that used HKUST-1 and poly(PMMA-*co*-MAA) in order to generate nanovoids for increased water permeability. HKUST-1 acted as a sacrificial template, hydrolyzing to produce more and larger pores, while poly(PMMA-*co*-MAA) ensured even distribution of the MOF. Increasing MOF loading resulted in water flux enhancement by almost 300%, but FRR decreased from 61.4% to 33.6%. This trade-off came from the increased pore sizes allowing for more significant blocking of the membrane active area by the foulants..[185] In a similar work, Yang et al.[120] additionally added GO to enhance antifouling. HKUST-1 promoted the dispersion of GO, which lowered surface roughness and increased pores. The FRR increased from 50% to 88%, attributed to surface hydrophilicity, smoother surface, and negative surface charge.[120,185]

Misdan et al.[118] incorporated CuBTC nanoparticles into PSf membranes with a TMC/PIP selective layer. The MOF addition significantly reduced the thickness of the PIP layer due to the additional hydrophilic groups added to the surface, which strongly attracted PIP. The optimal loading was determined to be 0.25 wt % MOF, above which water transport across the membrane was inhibited due to the thickened poly-PIP layer. Owing to the MOFs filling in the ridge-and-valley surface morphology of the membranes, the smoother surface resulted in an FRR increase from 60% to 85%.[118] In a similar study, Dai et al.[75] developed a composite FO membrane incorporating CuBDC into PA sheets. These additives improved the hydrophilicity of the membrane and acted as a molecular sieve for ion rejection. This caused FRR to increase from 69% to 89% due to a combination of the hydration layer repelling foulants and Cu's biocidal properties hindering biofouling.[75] Samantaray et al.[186] explored the use of a multilayered membrane for ion separation in water by RO. The membrane consisted of an antibacterial polymeric active layer, phosphonium-conjugated GO-anchored CuMOF, and a mechanical support. While GO is effective at molecular sieving, its great swelling reduces long-term separation efficiency. The incorporation of MOFs reduced the swelling, allowing the GO layers to maintain their separation ability, while the phosphonium helps to positively charge the membrane to repel positive ions. FRR significantly improved from 70.0% to 98.8%.[186] Shu et al.[187] developed an UF 2-D MMM incorporated with BUT-203/PEI at 73 wt % loading for dye rejection. Water flux significantly increased over 500% without a compromise in the efficiency of salt rejection. Since the hydrophilicity actually decreased due to the addition of hydrophobic groups from BUT-203/PEI, the water flux enhancement was attributed to molecular sieving effects of the pores, which accepted water but rejected dye molecules, leading to the membrane antifouling performance (FRR increased from 67% to 89%).[187] Gholami et al.[128] synthesized UF PES membranes incorporated with TMU-5, a Zn-based MOF, to improve flux and fouling resistance. As MOF loading was increased, the hydrophilicity of the membrane increased due to the addition of hydrophilic hydroxyl groups that moved toward the top layer of the membrane. The flux increased by 36.6% while the FRR increased by 73.3%. This foul resistance was attributed to hydrophilicity, surface smoothness, and low surface energy, with surface smoothness being the most dominant factor.[128] Shukla's group developed a composite membrane consisting of a Zn-MOF incorporated into polyphenylsulfone membranes. The addition of these MOFs at 0.5 wt % increased PWF by almost 100% with an FRR of 92%, a result of the negative surface charge and surface hydrophilicity.[188] Abdi and Nasiri[189] reported functionalization

https://doi.org/10.1021/acs.iecr.1c00543
Ind. Eng. Chem. Res. XXXX, XXX, XXX−XXX

Table 2. Effect of Different MOFs and Methods on Antifouling and Biofouling of the TFC Membrane for Different Water Separation Applications. N/A Indicates Unreported by Paper

MOF (loading)	attachment method	membrane	pristine water flux ($L/m^2 \cdot h$)	pristine flux recovery (%)	MOF water flux ($L/m^2 \cdot h$)	MOF flux recovery (%)	ref
ZIF-8 (N/A)	in situ growth	TTN/ZIF-8/ TTN@PVDF	4095	59.0	6369	86.0	181
UiO-66-PSBMA (0.3 wt %)	phase inversion	PSf	240	64.5	602	72.4	122
UiO-66/UiO-66-NH2(0.2 w/v%)	doping	PA	33.56	93.30	87.86	96.82	81
UiO-66-NH_2 (0.2 g/L)	self-assembly	PAN	373.6	8.0	2107	90.0	176
CuBTC (0.25 wt %)	doping	PSf	25.0	58.0	31.0	85.0	118
Ag-MOFs (0.05 wt %)	doping	zwitterion/DEDA/ PA	3.5	28.0/42.0	16.0	69.0/70.0	175
UiO-66-NH_2 (0.1 wt %)	blending	PES	44.62	59.20	46.54	95.22	194
AlFu (0.75 wt %)	phase inversion	PES	1.4	92.51	7.7	96.88	189
UiO-66 (9.01 wt %)	self-assembly filtration	GO−CS	3.30	42.9	14.62	88.0	177
HKUST-1 (0.3 wt %)	doping	PES	180	61.4	490	33.6	185
GO-Ag-MOF (N/A)	interfacial polymerization	PES	N/A	75.0 95.0	N/A	30.0 72.0	85
UiO-66-NH_2@PAA (1 mL)	vacuum-assisted self-assembly	MCE	11400	40.0	2330	86.0	178
TMU-5 (0.1 wt %)	phase inversion	PES	133.29	25.47	182.02	98.74	128
Cu-iMOF (0.05 g)	hydroxylation	PVA/PVDF	410.00	59.76	627.32	82.89	184
MOF1/MOF2 (0.1 wt %)	interfacial polymerization	PA	30.0	70.0	36.0/41.0	90.0/95.0	191
BUT-230 (N/A)	spin coating	PEI	1483	67.0	8000	89.0	187
MSH@UiO-66-NH_2 (0.01 wt %)	phase inversion	PSf	104.0	90.4	82.0	80.5	94
UiO-66-NH_2 (0.05 wt %)	interfacial polymerization	PA-MOF/PPSU-GO	44.77	90.5	64.40	97.8	87
CAU-1 (1.0 wt %)	phase inversion	PPSU	39.0	89.0	47.9	93.0	190
HKUST-1@GO (0.12 wt %)	phase inversion	CA	98.99	49.78	183.51	88.13	120
ZIF-8 (0.12 wt %/v)	interfacial polymerization	PA	18.0	69.4	28.0	89.3	75
UiO-66 (0.08 $\mu g/m^2$)	phase inversion	GO@PAN	487.4	8.0	93.9	95.0	179
MIL-101-NH_2 (N/A)	doping	PES/CC	24.0	51.9	25.48	59.0	192
CuMOF (0.5 wt %)	doping	P^+GO/RO	24.0	70.0	19.7	98.8	186
ZIF-8 (N/A)	in-situ growth	PDA/PSf	6.2	N/A	9.6	62.5	183
CuBTTri (0.1 wt %)	interfacial polymerization	PES	0.86	30.0	3.38	50.0	76
ZIF-8 (3 wt %)	spin-casting	PES	N/A	N/A	121.5	94.0	182
UiO-66-NH_2 (86 wt %)	TIPS-HoP	PE	∼0	n/a	200.0	97.0	143
UiO-66/GO (10 wt %)	hydrothermal	PA	138.0	49.9	228.0	97.0	180
Ce-MOF (0.5 wt %)	phase inversion	PES	14.69	62.27	21.2	91.55	126
Zn-MOF (0.5 wt %)	phase inversion	PPSU	17.0	45.0	33.0	92.0	188
MIL-88A (Fe) (5 mg)	vacuum filtration	GO	9.4	42.1	99.1	98.8	193

of PES membranes with Al fumarate (AlFu) MOF in order to facilitate enhanced water flux. The water flux of the membrane increased by 450% and the FRR increased from 92.5% to 96.9% because the MOF nanoparticles increased surface hydrophilicity, weakening bovine serum albumin (BSA) contaminant bonds, and increased porosity.[189] Xiao et al.[190] synthesized a MMM from PPSU incorporated with CAU-1, an Al-based MOF. The MOF addition resulted in water flux enhancement at low concentrations (up to 1.0 wt %), but it decreased due to agglomeration at high concentrations. Once loading reached 2.5 wt %, defects in the membrane caused water flux to rise again. The optimal loading point was determined to be 1.0 wt % which provided the highest PWF along with a FRR of 93%.[189,190]

Mansor et al.[191] synthesized a PA membrane incorporated with green (using carboxylmethyl cellulose as organic ligands) binary and ternary MOFs for salt removal. MOF loading at 0.1 wt % enhanced water flux by 20−35% and improved FRR to 95%. This antifouling was attributed to hydrogen bonding on the surface which resisted foulant attachment.[191] Liu's group[192] has developed a novel UF membrane consisting of a PES layer incorporated with MIL-101-NH_2 in conjunction with carbon cloth (CC) for phosphate removal. Since an electric field is applied to the membrane for phosphate removal, CC is needed to provide a conductive material because PES and the MOF are nonconductive. The electric field significantly improved phosphate rejection (nearly 100%) as well as antifouling.[192] Xie et al.[193] used a similar MOF, MIL-88A (Fe), which is Fe-based and is incorporated into GO sheets to impart photo-Fenton catalytic properties. The MOFs added pillar-like structures to the surface, which resulted in increased surface roughness, enhancing surface hydrophilicity

https://doi.org/10.1021/acs.iecr.1c00543
Ind. Eng. Chem. Res. XXXX, XXX, XXX−XXX

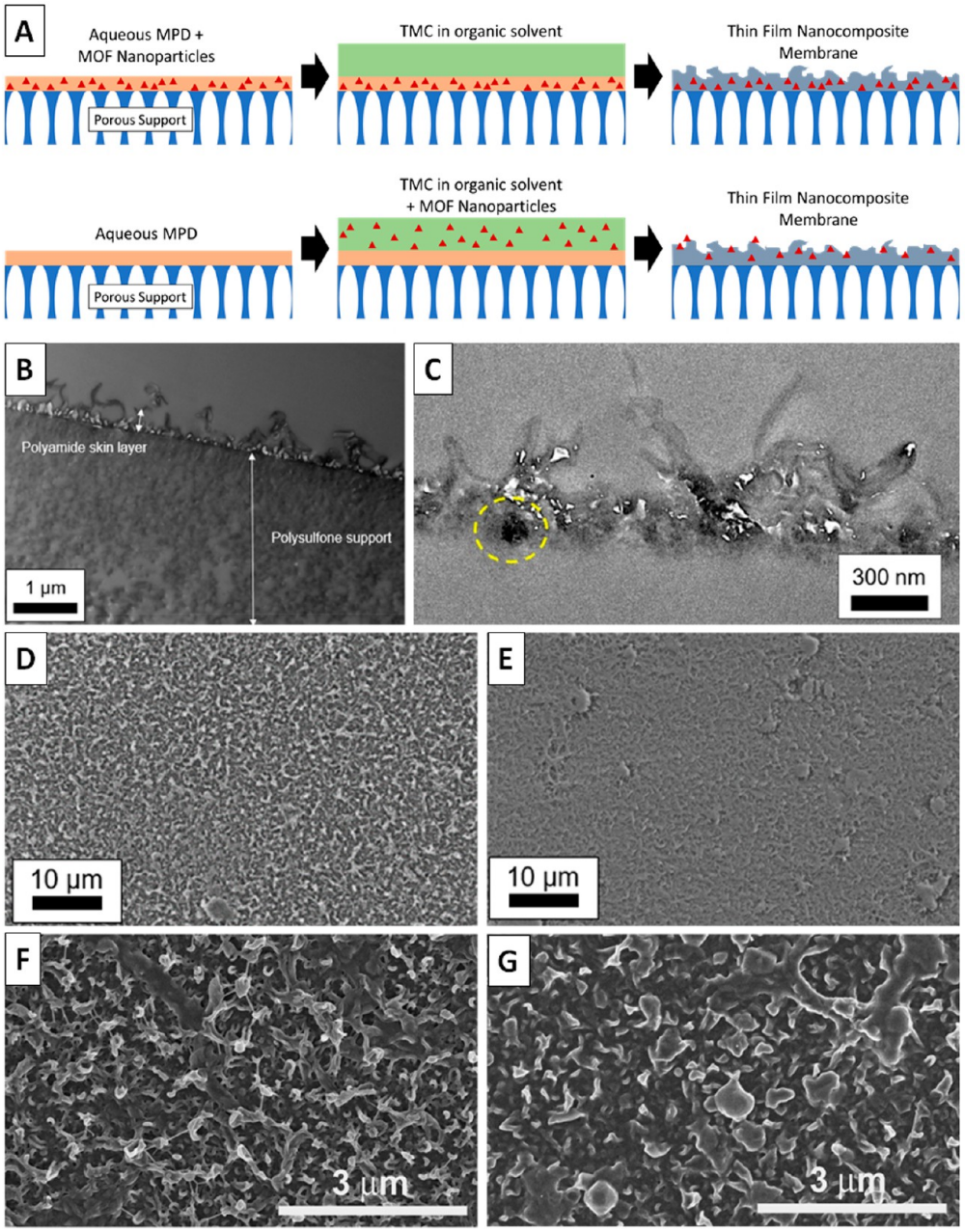

Figure 9. (A) Schematic depicting the formation of MOF-containing interfacially polymerized thin film nanocomposite (TFN) membranes via incorporation from the aqueous phase (top) and the organic phase (bottom); cross-sectional TEM images of (B) a thin film composite (TFC) RO membrane showing the "ridge and valley" structure of the interfacially polymerized polyamide (PA) and (C) TFN membrane containing a PCN-222 MOF nanoparticle incorporated from the aqueous phase(circled in yellow); SEM surface images of (D) a plain PA TFC membrane and (E) a TFN membrane containing aggregates of myristic acid functionalized PCN-222 nanoparticles incorporated from the aqueous phase; SEM images of (F) a plain polyamide membrane and (G) a TFN membrane containing ZIF-8 nanoparticles incorporated from the organic phase.[69,209] Adapted with permission from refs 69 and 209. Copyright 2015 and 2020 Elsevier and American Chemical Society, respectively.

by a great number of additional water channels. By utilizing light and H_2O_2, they were able to significantly degrade dye molecules and regenerate the membrane.[193] Mohammadnezhad et al.[126] developed a novel Ce-MOF/PES MMM for NF dye removal. A loading point of 0.1 wt % was determined to be optimal because higher loading resulted in pore blockage. Dye rejection remained the same regardless of MOF loading. The lowered surface roughness of the membrane improved FRR from 62.3% to 91.6%.[126]

Because of the significant threat of fouling and biofouling to the long-term operation of membranes for water treatment, MOFs represent an opportunity for versatile functionalization which can improve properties such as water flux or targeted rejection in addition to improving antifouling and antibiofouling effectiveness (Table 2). The wide amount of possible metal clusters and organic ligands for synthesis leaves much undiscovered potential for future work.

4. MOF-FUNCTIONALIZED MEMBRANE APPLICATIONS

4.1. Desalination by MOF-Functionalized Membranes. RO and forward osmosis (FO) are osmotic

https://doi.org/10.1021/acs.iecr.1c00543
Ind. Eng. Chem. Res. XXXX, XXX, XXX−XXX

membrane processes that have been applied to desalination applications. RO processes account for the majority of desalination processes,[195] and numerous advances in membrane technology over the past several decades have sought to increase the efficiency and viability of RO processes as a method of providing clean water to water-scarce regions.[196] Forward osmosis (FO) has primarily been studied for applications such as wastewater treatment and remediation.[197] NF membranes have also been used for desalination but are generally only effective at removing large divalent ions, and exhibit poor rejection for monovalent salts (e.g., NaCl). Thin-film composite (TFC) polyamide is one of the most important membrane materials applied in commercial RO processes.[41,198−200] TFN membranes are fabricated by incorporating nanoparticles during the traditional TFC interfacial polymerization process to alter membrane performance and properties[47,201−208] as depicted in Figure 9. The inclusion of these nanoparticles results in the formation of additional pore structures, which can offer preferential water transport pathways within the polyamide matrix.

Recent work has focused on the formation of TFN membranes via the inclusion of MOF nanoparticles.[49,52,74,95] Transport in TFC membranes is generally limited by diffusion, and the overall free volume within the active layer of each TFC determines the permeance of water and solutes present in the feed.[210−213] When MOFs are present within the active layer, their internal pores can act as alternative transport pathways, resulting in rapid transport across the membrane. The rejection and permeation of a MOF-TFN also change significantly depending on the size of the pores in the MOF structure.[214] Studies have shown that increases in overall membrane permeance may occur but are often accompanied by a loss in ion rejection due to pore sizes larger than both water molecules and salt ions.[52,95] The inclusion of MOF nanoparticles has also been shown to alter the surface roughness and hydrophilicity of TFN membranes, impacting membrane permeance as well as resistance to fouling.[67,69]

4.1.1. Reverse Osmosis and Nanofiltration Membranes. *ZIF-8 Based TFN Membranes.* Zeolitic imidazolate frameworks such as ZIF-8 have been studied by a variety of groups for applications in RO and nanofiltration membranes.[53,60,67,69,215,216] The ZIF-8 structure contains 3.4 Å pores that are capable of separating water molecules from hydrated sodium ions based on size differential, as water molecules and hydrated Na^+ ions have diameters of ∼2.75 Å and ∼7.20 Å, respectively. The addition of ZIF-8 can result in improved water flux and biofouling resistance, but the membrane performance depends strongly on ZIF-8 particle size and loading level, membrane fabrication method, functionalization of the ZIF-8 particles, and on the type of porous support membrane used.

Effects of ZIF-8 Loading Level, Nanoparticle Size, and Membrane Fabrication Method. One of the earliest reports of TFN membranes containing ZIF-8 was by Duan et al.[69] in which ∼200 nm ZIF-8 nanoparticles were incorporated into interfacially polymerized polyamide RO membranes via dispersion in the organic solvent phase at loadings of up to 0.40 w/v%,[69] resulting in a 162% increase in water permeability and a salt rejection greater than 98% under brackish water feed conditions (2000 ppm of NaCl). They also observed decreased cross-linking and increased hydrophilicity at the surface of the TFN membrane, indicating that ZIF-8 incorporation can impact the physical properties of the polyamide layer. As stated above, Van Goethe et al.[52] have reported the careful positioning of 75- and 150 nm ZIF-8 nanoparticles at the aqueous/organic interface during interfacial polymerization via a EFP method.[52] The resulting TFN membranes exhibited up to a 220% increase in permeability at relatively low loading levels (0.005 w/v%) without any decrease in salt rejection. Wang et al.[67] studied TFN membranes with ZIF-8 nanoparticles ranging in size from 50 to 400 nm at loading levels up to 0.4 w/v% in which the nanoparticles were incorporated from the aqueous phase.[67] They observed the best performance with the 50 nm particles at a loading of 0.3 w/v% (∼60% increase in permeance with a salt rejection of 99%), which was attributed to the improved dispersion of the smaller nanoparticles in the organic phase prior to polymerization. The authors also reported a decrease in biofouling with the incorporation of the ZIF-8 nanoparticles due to increased hydrophilicity and decreased roughness of the membrane surface. The authors suggest that reduced cross-linking in the PA layer due to the presence of ZIF-8 resulted in an increase in the concentration of hydrophilic carboxylic acid groups at the membrane surface leading to a reduction in contact angle. Lee et al.[60] studied TFN membranes that incorporated ZIF-8 nanoparticles with diameters ranging from 60 to 250 nm in which the nanoparticles were incorporated from the organic-solvent phase. They observed that while increasing ZIF-8 loading resulted in increased permeation, the salt rejection tended to decrease at loading levels greater than ∼0.2 w/v%. In addition, the particle size appeared to impact both the adsorption of particles on the support membrane surface and the final permeation properties of the membranes, with the best performance observed for a 150 nm particle at a 0.2 w/v% loading resulting in a 43% increase in water permeance and a salt rejection of 99.2% under brackish water conditions.

Effects of ZIF-8 Functionalization. Zhang et al.[97] reported the fabrication of TFN membranes containing polydopamine functionalized ZIF-8 nanoparticles with loading levels up to 0.04 wt %. The membranes containing 0.03 wt % of the modified particles exhibited a 43.8% increase in water permeability, which decreased at higher loading levels. The membranes maintained high salt rejection values (98.4% to 99.0%) that decreased slightly with increasing particle loading. The TFN membranes exhibited a significant increase in resistance to fouling with both Gram-negative and Gram-positive bacteria that was attributed to the biocidal nature of the ZIF-8/polydopamine nanoparticles. Zhu et al.[100] reported the formation of TFN membranes containing ∼60 nm polystyrenesulfonate (PSS) modified ZIF-8 nanoparticles.[100] The resulting membranes exhibited up to a 114% increase in permeation flux while maintaining salt rejections of ∼90% for Na_2SO_4 under brackish water feed conditions (1250 ppm).

Effect of Porous Support Type on ZIF-8 TFN-RO Membranes. The majority of RO TFN membranes are synthesized using a hydrophilic porous polysulfone or poly(ether sulfone) porous membrane as support. However, Li et al.[217] have reported a method to produce TFN membranes containing ZIF-8 (as well as several other MOFs) via the in situ synthesis of the MOF on hydrophobic polypropylene support prior to interfacial polymerization to form a selective polyamide active layer.[217] The authors reported a water permeability of 3.22 L m^{-2} h^{-1} bar^{-1} with a salt rejection greater than 99% under brackish water conditions (2000 ppm). This represented a significant increase over the

https://doi.org/10.1021/acs.iecr.1c00543
Ind. Eng. Chem. Res. XXXX, XXX, XXX−XXX

~5% salt rejection exhibited by the control membrane produced on polypropylene support in the absence of ZIF-8.

UiO-66 Based TFN Membranes. UiO-66 is a water-stable zirconium-based MOF having a pore size of ~6 Å. Ma et al.[83] reported the formation of interfacially polymerized RO TFN membranes containing ~500 nm UiO-66 particles at loadings of up to 0.2 wt %.[83] The TFN membranes exhibited a 52% increase in water permeability at a loading level of 0.1 wt % compared with the pristine TFC RO membrane, while exhibiting only a slight decrease in salt rejection to 95.3%. Liu et al.[82] reported the use of RO TFN membranes containing UiO-66 nanoparticles that improve boron rejection—a significant challenge for seawater desalination in certain parts of the world.[82] The membranes exhibited the expected improvement in water flux and salt rejection, and also showed improved boron rejection rates of up to 91% compared to 82% for the pristine TFC RO membrane. As stated above, Gong et al.[88] reported the formation of nanofiltration TFN membranes containing ultrasmall UiO-66-NH_2 nanoparticles on the order of 10−20 nm. These small nanoparticles allowed the creation of thin TFC active layers (~20 nm thick) and resulted in a high permeation flux of 46 L m^{-2} h^{-1}, an increase of 53%, while maintaining a high salt rejection of 97.1% for the divalent salt Na_2SO_4. The membranes exhibited much lower salt rejection for chloride salts (~40% for $MgCl_2$ and $CaCl_2$, and ~5% for NaCl). Zhao et al.[218] reported a spray-assisted deposition technique used to form TFN RO membranes containing ~100 nm UiO-66-NH_2 nanoparticles for a range of loading levels.[218] These membranes exhibited up to a 72% increase in membrane water permeability under brackish water feed conditions while exhibiting slight decreases in rejection as loading level increases.

Effect of MOF Particle Aspect Ratio and Pore Functionalization in a TFN Membrane. The aspect ratio of nanoparticles can also influence the desalination performance of TFN-RO membranes. Bonnett et al.[209] reported the fabrication of RO TFN membranes containing high aspect ratio nanoparticles of the zirconium-based MOF PCN-222.[209] PCN-222 contained two types of linear channels with pore sizes of 3.7 and 1.3 nm and were prepared as nanorods with a length of ~300 nm and a diameter of ~100 nm. The effective size of the PCN-222 pores was decreased through the incorporation of myristic acid at several different loading levels. The resulting membranes exhibited a 95% increase in water permeability accompanied by a slight decrease in salt rejection (from 97.5% to 96.0%) under brackish water conditions (2000 ppm of NaCl).

Desalination Using Hybrid MOF Nanofiltration Membranes. There have been several examples of hybrid membranes that combine MOF particles with other nanomaterials such as carbon nanotubes or graphene. Wang et al.[219] reported the formation of ZIF-8/graphene oxide (GO)-based TFC membranes.[219] The hybrid membranes exhibited improved nanofiltration permeance and resistance to biofouling while maintaining the ability to reject divalent salts. Lee et al.[215] reported on the creation of TFN membranes incorporating ZIF-8 nanoparticles/carbon nanotube (CNT) hybrids at loading levels up to 0.8 w/v%.[215] The hybrid materials consist of CNTs decorated with a nearly continuous layer of MOF nanoparticles. As before, the optimum observed loading level was 0.2 w/v%, with a 38% increase in permeability and a salt rejection of 99.2%. At higher loadings, both permeance and salt rejection decreased due to significant particle aggregation.

4.1.2. Forward Osmosis (FO). FO is a membrane separation technique that employs TFC osmotic membranes similar to those used in RO and nanofiltration. FO utilizes a draw solution with higher concentration than the feedstream to create a transmembrane osmotic pressure difference, that drives water transport across the osmotic membrane. Conventional FO membranes can suffer from low water flux, significant internal concentration polarization, and reverse solute flux (RSF), in which the draw solute leaks across the membrane into the feed solution. There are several examples in the literature of the incorporation of ZIF-8 and UiO-66 nanoparticles into interfacially polymerized FO membranes resulting in increased water permeance.[83,96,220,221] Beh et al.[96] produced TFN FO membranes containing ZIF-8 nanoparticles or polystyrenesulfonate (PSS)-coated ZIF-8 nanoparticles via interfacial polymerization.[96] The authors observed poor performance in the membranes containing uncoated ZIF-8 particles but reported an increase in water flux of 116% from a synthetic oil emulsion for the membranes containing PSS-coated particles. This increase was, however, accompanied by an undesirable increase in RSF. The ZIF-8 containing membranes also exhibited decreased swelling, indicating that the ZIF-8 particles improved the physical stability of the membranes.

Ma et al.[220] reported the formation of interfacially polymerized FO TFC membranes on phase inversion cast polysulfone supports containing ~500 nm UiO-66 MOF nanoparticles with loadings up to 12.9 wt %.[220] The authors observed an increase of up to 50% in water permeance at a loading of 6.5 wt % while observing a slight decrease in salt rejection. It is important to note that in this case, the authors are modifying the underlying support membrane rather than the interfacially polymerized active layer. Ma et al.[83] also prepared interfacially polymerized TFN RO membranes containing UiO-66 as discussed above.[83] When tested under FO conditions, the 0.1 wt % UiO-66 loaded TFN membranes exhibited up to a 30% increase in water flux. Wang et al.[221] reported on a technique to form FO TFN membranes via the deposition of ~145 nm UiO-66 particles at the substrate interface prior to interfacial polymerization.[221] The resulting membranes exhibited up to a 140% increase in water permeability combined with improved salt selectivity. The increased water permeability is attributed to increased surface hydrophilicity and roughness, as well as the formation of water channels in the membrane structure.

Kim et al.[222] prepared cellulose acetate (CA)-based membranes containing ZIF-302 (with a pore size of 7.9 Å) at loadings of up to 15 wt % for osmotically driven processes.[222] In contrast to the interfacially polymerized membranes described above, the CA/ZIF-302 membranes were prepared via a phase inversion casting technique to produce an asymmetric membrane with the CIF-302 particles dispersed throughout. The authors observed improved FO water permeances with increasing MOF content, but decreasing salt selectivity above a loading of 5 wt %. The authors also reported that the inclusion of ZIF-302 particles led to improved resistance to alginate fouling.

4.2. MOF-Functionalized Adsorptive Membranes for Heavy Metals Removal. Another emerging application of MOF-functionalized membranes is the adsorptive removal of heavy metal ions (Table 3). Heavy metal ions in water bodies

https://doi.org/10.1021/acs.iecr.1c00543
Ind. Eng. Chem. Res. XXXX, XXX, XXX−XXX

Table 3. Performance of Selected MOF-Functionalized Membranes for the Removal of Different Ions from Water or Wastewater Streams. "N/A" Indicates Not Reported in the Original Source

metal in MOF	ion	membrane	fabrication	feed concn (ppm)	removal efficiencies (%)	capacity (mg/g)	ref
Zr	Cd (II)	MOF-808/PAN	nanofiber synthesized via coelectrospining	30 ppb	~60%	225.05	149
Zr	Cd (II)	UiO-66-NH_2/PAN/chitosan	electrospinning	100 ppm	89%	415.6	147
Zr	Zn (II)	MOF-808/PAN	nano	30 ppb	~70%	287.06	149
Zr	Cr (VI)	UiO-66-NH_2/cellulose nanofibers	surface coating	~5.5 ppm	78.2%	N/A	228
Zn	Cr (VI)	ZIF-8, ZIF-67 with silk nanofiber	electrospinning	7.4 mg/L = 7.4 ppm	99%	7.4 (uptake of MOF)	229
Zr	Cr (VI)	UiO-66-NH_2/PAN/chitosan	electrospinning	100 ppm	85.5%	372.6	147
Sb, La, Sr	Pb (II)	Sr-TBC, La-TBC, Sb-TBC, with PVA	electrospinning	100 ppm	92.3% (La), 58.9% (Sr), 50.7% (Sb)	91, 124, 194	156
Zr	Pb (II)	UiO-66-NH_2/PAN/chitosan	electrospinning	100 ppm	94%	441.2	147
Zn	As (V)	ZIF-8, ZIF-67/silk nanofiber	electrospinning	5.5 mg/L = 5.5 ppm	92%	50 (uptake of MOF)	229
Zr	Hg (II)	MOF-808/PAN	electrospinning	50 ppb	34%		230
Zr	Tb (III)	UiO-66-$(COOH)_2$/PAN	colloid-electrospinning	350 mg/L = 350 ppm	N/A	214.1	231
Zr	Eu (III)	UiO-66-$(COOH)_2$/PAN	colloid-electrospinning	350 mg/L = 350 ppm	N/A	191.9	231

pose long-term risks to the environment and human health.[223,224] While the direct use of bare (also termed bulk) MOF membranes to adsorb metal ions exhibits great removal efficiencies, it requires large amounts of MOFs and is not cost-effective, particularly at industrial scales.[17,225] To overcome these limitations, MOFs are often immobilized on porous substrates to form adsorptive membrane materials. In water-environment applications, various substrate materials have been tested for MOFs,[164,226,227] but electrospun nanofibrous membranes incorporated with MOFs are the most widely investigated for adsorption of heavy metal ions due to the large surface-to-volume ratio, high porosity, high flux and adsorption efficiency, and low cost of the substrate. When the effective pores of the synthesized membrane are relatively large (micrometers), embedded MOFs function as the adsorption sites for ions. In contrast, the membrane selects ions based on the size-exclusion mechanism when the pores are relatively small.[17] Recent studies have incorporated many MOFs (primarily Zr- and Zn-based) on various polymeric nanofibers, and demonstrated effective aqueous adsorption of a wide range of ions. Polyacrylonitrile (PAN) membranes with Zr-based MOF-808 exhibited high adsorption capacities to Cd^{2+} and Zn^{2+} of 225.1 and 287.1 mg/g, respectively, and removed 60–70% of the pure Cd^{2+} and Zn^{2+} ions.[149] UiO-66-NH_2/cellulose, UiO-66-NH_2/PAN/chitosan, and ZIF-67/silk nanofibers demonstrated effective Cr^{6+} adsorption, with the latter giving a removal efficiency of 99%.[147,228,229] A removal efficiency of 92% As^{5+} was attained by a silk nanofibrous membrane with ZIF-8,[229] and Pb^{2+} was reported to be adsorbed by UiO-66-NH_2/PAN/chitosan (89.6 mg/g capacity) and La-based MOF/plan poly(vinyl alcohol) membrane (92% removal).[147,156] The MOF-808/PAN membrane adsorbed Hg^{2+}, with a removal efficiency of 34%.[230] UiO-66-$(COOH)_2$/PAN was also used in separating rare earth heavy metals Tb^{3+} and Eu^{3+}, presenting high capacities of 214 and 191 mg/g, respectively.[231] The reusability of these membranes is usually tested by three to four cycles over the time order of hours. For example, a recent bench-scale test using MOF-functionalized membranes to adsorb Cd^{2+} regenerated the membrane with nitric acid, and the permeate recovery dropped only 5% compared to initial performance after four adsorption–desorption cycles.[149]

While many studies have interrogated the thermodynamics of adsorption by measuring adsorption capacity at equilibrium, a few studies have also investigated adsorption kinetics. Adsorption of heavy metal ions on MOF-808 and UiO-66-$(COOH)_2$ incorporated in different nanofibrous membranes correlates best with the pseudo-second order model, indicating that physical sorption happens without covalent bonding, making the reversal desorption facile.[149,231,232] The calculated rate constant was relatively high, and the adsorption saturation was as fast as 10 min for removing Cd^{2+} and Zn^{2+} using MOF-808/PAN membranes and followed the Langmuir isotherm model.[149,231] The preparation of MOFs requires an activation process to recover the loss of porosity due to the residual solvent in the MOFs during synthesis. Different activation methods exist, including heating, drying, and hydractivation.[225,227] The choice of activation method influences the adsorption behavior of the membranes incorporated with the MOFs. A recent study indicated that while activation is important, a certain portion of residual solvent is necessary to maintain the pore integrity and mechanical robustness.[149] The hydractivation strategy activates MOFs via a water exchange process and vacuum drying, and is reported to improve adsorption capacities of Cd^{2+} and Zn^{2+} using the MOF-PAN membranes compared with other conventional activation techniques.[149,225]

Adsorption of heavy metal ions using MOF-functionalized membranes is influenced by various operating conditions. Because adsorption is primarily carried out by pressure-driven filtration, the pressure difference across the membrane plays an important role in the membrane adsorption. While raising the applied pressure increases the water flux, it also accelerates the saturation of the active MOF adsorption sites, and reduces the substrate porosity due to compaction. Concentration of the feed stream is another important parameter and impacts the

https://doi.org/10.1021/acs.iecr.1c00543
Ind. Eng. Chem. Res. XXXX, XXX, XXX–XXX

suitability for MOF-functionalized membranes for waters with varying metal concentrations. Lowering the concentrations delays the saturation of the MOF adsorbent sites, which enlarges the feed volume that can be treated. Coexisting cations in the solution significantly affect the membrane performance, which is an important concern for treating various feed waters. Overall, the presence of other cations reduces the adsorption efficiencies of the target ions because the membrane exhibits different selectivities to different ions.[149,230,231] It is suggested that selectivities of these membranes to different ions can be elucidated as the interplay of adsorbate electronegativity and ionic radius: ions with stronger electronegativity and larger size tend to exhibit lower removal efficiency.[34,149,230] In a recent study on MOF-808 embedded nanofibrous polyacrylonitrile (PAN) membranes, heavy metal ions (Zn^{2+}, Cd^{2+}, Pb^{2+}, and Hg^{2+}) preferentially adsorbed compared with common coexisting ions in wastewater (Na^{+}, Mg^{2+}, and Ca^{2+}). This can be explained by the greater electronegativities of heavy metal ions, which leads to stronger binding to the anionic adsorption sites.[230] However, the electronegativities cannot completely explain different selectivities to pure heavy metal ions, and the steric effect of ions is postulated to be important; that is, ions with large sizes shield the adsorption sites, thus lowering the removal efficiencies.[230] Changing solution pH influences protonation/deprotonation of ligands in MOFs, affecting active sites of adsorbents and, hence, changes adsorption capacity of the membrane for different metal ions.[233] The thickness of the membrane active layer should be balanced between the adsorption and permeation required for a given application. Thicker membranes enable higher loading of MOFs, and hence greater capacity, whereas the increased transfer resistance also lowers the water flux.[6,230]

Water stability is another major concern for applying MOF-functionalized membranes to remove heavy metal ions.[234,235] Previous studies reported that UiO-66-NH2 incorporated PAN/chitosan and UiO-66-(COOH)2 incorporated PAN nanofibrous membranes were chemically stable at pH 2−7 in aqueous solutions.[149,231,233] Further work is needed to investigate the water stabilities of a wider range of MOFs incorporated in membranes. The long-term mechanical robustness of the composite membrane should also be studied to inform long-term, full-scale water treatment. Because the active MOFs sites determine the capacity of the membrane, developing advanced morphological properties of the substrate membranes that increase the porosity and enable more exposed active MOF sites can significantly improve the adsorption performance. While current lab-scale studies usually study heavy metal ion adsorption on the time order of hours and test very limited regeneration cycles (<10), evaluations of reusability of MOF-functionalized membranes in long-term experiments are necessary for advancing the technology to practical applications. Impacts of coexisting ions on membrane adsorption have been studied using synthetic solutions, but the experimental concentrations of different ions are usually set as identical (from 30 ppb to 350 ppm in the literature reviewed), which is not representative for most real waters (e.g., municipal or industrial wastewater, drinking water influent). Future systematic investigations of the effects of coexisting ion concentrations and physicochemical properties that represent real wastewater on the capacity, selectivity, and reusability of the membrane are critically needed. Improving the adsorption selectivity to specific ions is also an important future direction.

4.3. MOF-Functionalized Membranes for Nitrogen and Phosphorus Recovery. Nutrient recovery from wastewater involves the selective separation of nitrogen and phosphorus-containing solutes such as urea, ammonia, nitrate ions, and phosphate ions from wastewater streams. Both nitrogen and phosphorus are key nutrients for plant growth, and excess quantities released in both agricultural and urban wastewater can have negative impacts on the environment and human health. For example, excess phosphate can result in eutrophication that leads to algal blooms that can be toxic as well as lead to the formation of "dead zones" such as those that form each year in the Gulf of Mexico due to agricultural runoff.[236−239] Nutrient recovery has been identified as one of the key challenges in the 21st century for environmental protection, forming a circular economy, and reducing energy consumption. Several membrane-based processes have been proposed for nutrient recovery applications, including membrane distillation, electrodialysis, microbial fuel cells, microbial electrolysis cells, and membrane bioreactors.[240−242] While MOF-based membranes have been studied in detail for other aspects of the wastewater treatment process, more investigations that pertain specifically to nutrient recovery are needed.[17,243]

There have been several reports on the use of MOFs for ammonia adsorption applications in the gas phase, but none from aqueous solutions.[244−246] In contrast, there have been several reports on the adsorption of phosphate ions from aqueous solutions. Zhang et al.[247] reported on the use of the lanthanum based La-MOF-500 (with a 1,3,5-BTC linker) for the adsorption of phosphates from an aqueous solution with high adsorption capacity.[247] Similarly, He et al.[248] have reported on the formation of Ce-MOF/Ce(III) composite particles that adsorb phosphate over a wide pH range with high adsorption capacity.[248] Lastly, Nehra et al.[249] reported on the use of MIL-100(Fe) to adsorb phosphate from aqueous solutions. These examples indicate significant potential for MOF-based phosphate recovery, but none of them relies on a membrane-based separation. In contrast, Liu et al.[192] reported the removal of phosphate via a combined ultrafiltration and capacitative deionization (UF/CDI) process, where the UF membrane was modified through the addition of NH_2-MIL-101(Al) particles.[192] The high phosphate adsorption affinity of the MOF particles within the UF membrane increases water purity on the permeate side of the membrane. Further research is needed in the area of MOF-based membranes for nutrient recovery applications.

Beyond ammonia and phosphate, the nanometer-scale tuning afforded by MOF-based membranes could be used to design solute-selective membrane separation processes. For example, concentrating nitrate from polluted waters (e.g., agricultural runoff, brine from ion exchange or RO) could generate nitrate fertilizers. These separation processes could also be combined with catalytic unit processes to form reactive separations that concentrate nitrate and then convert it to dinitrogen for removal or ammonia for recovery. Similarly, MOF-based membranes targeted at urea as a solute could recover it from nitrogen-rich waste streams for use as a fertilizer, chemical precursors, and component of diesel exhaust fluid.[250] Forward osmosis can achieve up to 20% recovery, which requires further concentration via membrane distillation; in contrast, a MOF-based membrane could potentially achieve higher recovery in a single step using ligand exchange. Similarly, ligand exchange has been used to selectively recover

https://doi.org/10.1021/acs.iecr.1c00543
Ind. Eng. Chem. Res. XXXX, XXX, XXX−XXX

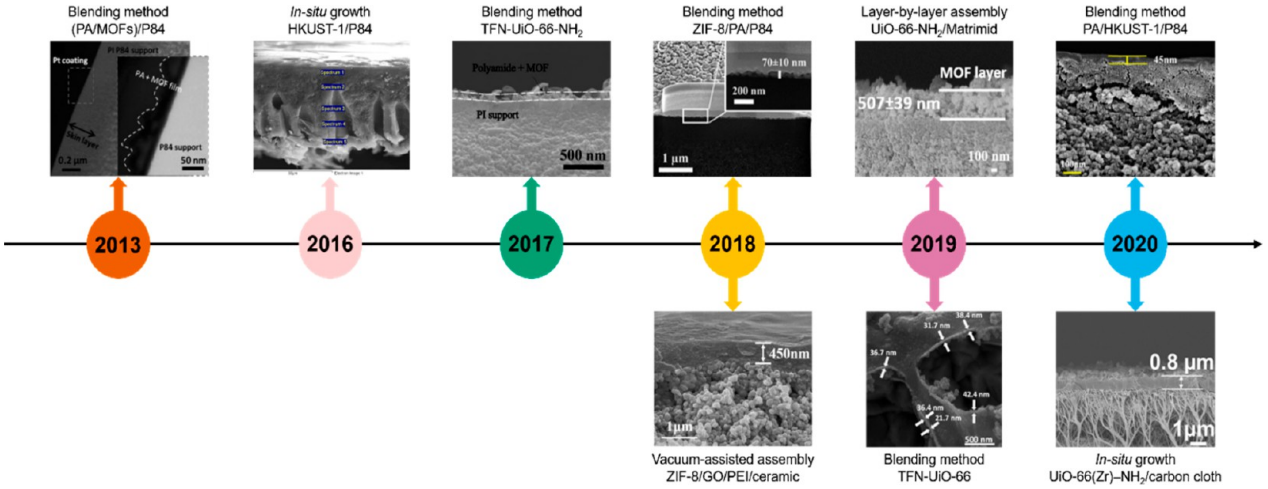

Figure 10. Timeline for the recent progress in the field of ultrathin MOF membranes for organic solvent nanofiltration. Figures reproduced with permission from references as follows: (PA/MOFs)/P84, (2013, American Chemical Society),[49] The MOF-functionalized membranes of HKUST-1/P84 (2016, Elsevier),[264] TFN-UiO-66-NH_2 (2017, AIChE),[109] ZIF-8/PA/P84 (2018, Elsevier),[55] ZIF-8/GO/PEI/ceramic (2018, Elsevier),[265] UiO-66-NH_2/Matrimid (2019, American Chemical Society),[266] TFN-UiO-66 (2019, Elsevier),[66] PA/HKUST-1/P84 (2020, Elsevier),[267] and UiO-66(Zr)-NH_2/carbon cloth (2020, Elsevier).[268] Detailed works are discussed in this section regarding OSN applications.

ammonia by loading transition metals (Cu and Zn) onto commercial ion exchange resins, which could also be further improved by MOF-based membranes.[251] Thus, there are several opportunities for MOF-based membranes to address critical resource recovery needs through the highly selective transport of environmentally relevant solutes.

4.4. Trace Organic Chemicals. Trace organic chemicals (TOCs) cover a broad range of compounds present as pollutants in water and wastewater streams. Important TOCs include endocrine-disrupting compounds (EDCs), pharmaceutical active compounds (PhACs, such as sulfamethoxazole and ibuprofen), personal care products (PCPs, e.g., surfactants), natural organic matter (NOM, e.g. humic and alginic acid), agricultural compounds (e.g., pesticides), industrial compounds (e.g., polyaromatic hydrocarbons), and chlorinated phenols. Many of these compounds can have negative impacts on the environment and human health at very low concentrations.[252−255] Efforts to remove TOCs from water using membranes have focused on adsorption,[252,255] nanofiltration,[253] and the use of biological remediation techniques such as membrane bioreactors.[254]

To date, efforts focused on the use of MOF-functionalized membranes for TOC removal are still relatively limited. Several recent studies reported the use of MOF-based materials for the analysis of TOCs, such as estrogens via sorption in a mixed matrix membrane,[256] PAH,[257] and phthalate esters[258] via solid-phase microextraction. There are also several examples of the use of MOF-based membranes for larger-scale removal of TOCs from water. Ragab et al.[259] employed a PTFE microfiltration membrane modified with ZIF-8 to adsorb progesterone from water.[259] The addition of ZIF-8 resulted in a 40% increase in membrane adsorption capacity, attributed to the increased specific surface area and hydrogen-bonding, combined with a doubled water permeability. Basu et al.[260] reported the preparation of ZIF-8 containing polyamide thin-film composite membranes for the rejection of PhACs.[260] Their study indicated that the addition of ZIF-8 particles resulted in increased permeation but decreased rejection of acetaminophen compared to the plain polyamide control membrane.

4.5. MOF-Functionalized Organic Solvent Nanofiltration. Organic solvent nanofiltration (OSN), also called solvent resistant nanofiltration (SRNF), is an emerging energy-efficient, membrane-based technology for retaining high value solute products or recovering organic solvents in the pharmaceutical/chemical industry.[261−263] Significant progress has been achieved in the field of OSN in the last two decades (Figure 10).[261−263] However, membranes for OSN still face challenges such as the long-term resistance in various organic solvents under harsh acid/basic conditions[261,263] and the relatively low organic solvent permeance.[261] Because of their high porosity, excellent structural stability, and chemical robustness (in organic solvents), MOF-based membranes have been considered to be a promising platform for OSN (Figure 11).[261−263] Furthermore, the versatile structure and tunable pore size of MOFs can act as size-selective filters for various OSN to enhance the solvent permeance while maintaining high solute rejection.[261,262] Highly performing OSN systems have indeed been realized, especially with

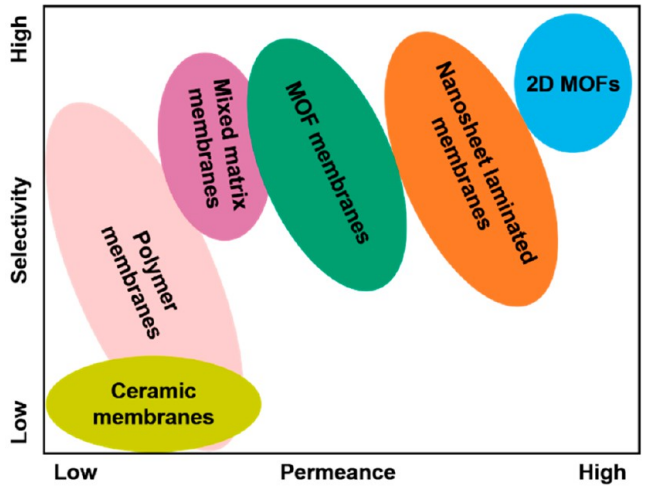

Figure 11. Comparison diagram of the permeance/selectivity performance of different porous membranes.

https://doi.org/10.1021/acs.iecr.1c00543
Ind. Eng. Chem. Res. XXXX, XXX, XXX−XXX

Table 4. Summary of MOF Membranes for Organic Solvent Nanofiltration (OSN) Performance

membrane	solvent	permeance ($L \cdot m^{-2} \cdot h^{-1} \cdot bar^{-1}$)	marker	marker MW ($g \cdot mol^{-1}$)	rejection (%)	ref
HKUST-1/P84	acetone	15	styrene oligomers	236−1800	90 (1800 g mol^{-1})	270
(PDMS/MOFs)/PI	isopropyl alcohol	0.6	rose bengal	1017	98	269
(PA/MOFs)/P84	methanol	3.9	styrene oligomers	236−1200	96 (236 g mol^{-1})	49
HKUST-1/P84	acetone	66	styrene oligomers	236−1800	90 (794 g mol^{-1})	264
HKUST-1/P84	acetone	54	styrene oligomers	236−1700	37 (1700 g mol-1)	271
MIL-53(Al)/PMIA	ethanol	0.7	brilliant blue G	854	94	273
TFN-ZIF-11	methanol	6.2	sunset yellow	452	90	70
TFN-UiO-66-NH_2	methanol	20	tetracycline	444	99	109
TFN-MIL101-ZIF11	methanol	6.3	sunset yellow	452	93	71
ZIF-8/PA/P84	methanol	8.7	sunset yellow	452	90	55
ZIF-8/GO/PEI/ceramic	methanol	6.1	methyl blue	800	99	265
ZIF-96 (simulation)	n-hexane	379	paracetamol	151	100	279
ZIF-25 (simulation)	methanol	357	paracetamol	151	100	279
UiO-66-NH_2/Matrimid	ethanol	0.88	rose bengal	1017	96.3	266
UiO-66-NH_2/Matrimid	dimethylformamide	4.58	rose bengal	1017	93.1	266
ZIF-8/PES	ethanol	2.5	rose bengal	1017	86	272
TFN-UiO-66	methanol	11	sunset yellow	452	97.9	66
PA/HKUST-1/P84	methanol	9.59	brilliant blue G	858	98.8	267
UiO-66(Zr)-NH_2/carbon cloth	dichloromethane	0.17	methylene blue	319	99.9	268
UiO-66(Zr)-NH_2/carbon cloth	methanol	0.24	Nile red	318	99.88	268

ultrathin (<1 μm) defect-free MOF membranes (Figure 10). Here, we review recent progress of MOF-based membranes for OSN (Table 4). We summarize the different synthesis approaches of untrathin MOF-based OSN membranes and discuss the underlying mechanisms (Figure 12).

4.5.1. Ultrathin MOF-Based OSN Membranes (<1 μm). Sorribas et al.[49] first used MOFs as fillers in TFN membranes and created the ultrathin MOF-based OSN membranes (as thin as 54 ± 10 nm) by embedding hydrophilic or hydrophobic MOF nanoparticles (ZIF-8, MIL-53(Al), NH_2-MIL-53(Al), and MIL-101(Cr)) into a thin polyamide (PA) film on top of cross-linked polyimide (P84) porous supports. The obtained membranes showed dramatically increased methanol permeability (3.9 L m^{-2} h^{-1} bar^{-1}) compared to the pristine membranes with no MOFs (1.5 L m^{-2} h^{-1} bar^{-1}) due to the enhanced porosity by MOFs, and maintained a high rejection (>96%) to styrene oligomers (molecular weight, MW, 236 g mol^{-1}).[49]

Campbell et al.[264] fabricated hybrid polymer/MOF membranes by chemically modifying polyimide P84 polymer support to introduce nucleation sites, followed by synthesizing HKUST-1 within the pores of polyimide P84 via in situ growth (ISG). The HKUST-1/P84 membrane (HKUST-1 layer <1 μm) allowed for much faster permeance of acetone (66 L m^{-2} h^{-1} bar^{-1}) than the pristine membrane without chemical modification (15 L m^{-2} h^{-1} bar^{-1}), and offered a higher rejection (90%) to styrene oligomers (MW = 794 g mol^{-1}) than the same membrane without chemical modification (~70%), indicating that chemical modification of P84 not only decreased the density of the hybrid membrane but also prevented the defects generated during the uncontrolled growth of MOFs without chemical modification.[264]

Guo et al.[109] synthesized Zr-MOF (UiO-66-NH_2) particles and surface-modified them with long alkyl chains, followed by incorporating the surface-modified UiO-66-NH_2 into the thin polyamide layer (50−120 nm) on polyimide supports to prepare TFN-UiO-66-NH_2 membranes. As a result, the optimized membrane containing 0.15% (w/v) MOF nanoparticles showed fast methanol permeability of 20 L m^{-2} h^{-1} bar^{-1} (~two times as much as the permeance of TFC membrane) with a high tetracycline (MW = 444 g mol^{-1}) rejection of ~99%.[109]

Sarango et al.[55] developed a simple method by dip-coating MOF (ZIF-8 or ZIF-67) suspensions on top of polyimide supports, followed by interfacial polymerization to form MOF/PA/PI membranes. The optimized ZIF-8/PA/PI membrane with one layer of ZIF-8 (thickness of 70 ± 10 nm) showed an increased methanol permeability from 5.8 (pristine TFC membrane) to 8.7 L m^{-2} h^{-1} bar^{-1} with a high rejection (90%) to sunset yellow dye (MW = 452 g mol^{-1}), indicating that the addition of ZIF-8 brought additional transport pathways for methanol, but the pathways for sunset yellow dye remained unchanged.[55]

Yang et al.[265] developed ZIF-8/GO/PEI/ceramic membranes by codepositing ZIF-8@GO composites with polyethylenimine (PEI) matrix on the surface of the tubular ceramic substrate via a vacuum-assisted assembly method. Under the optimum condition (GO concentration, 0.2 g L^{-1}; PEI concentration, 0.02 wt %; ZIF-8@GO concentration, 0.005 wt %), the membrane (with the thickness of ZIF-8/GO/PEI composite, ~420 nm) allowed for methanol permeability of 6.1 L m^{-2} h^{-1} bar^{-1} with methyl blue dye (MW = 800 g mol^{-1}) rejection higher than 99%. The high methanol permeance was caused by the good dispersion of ZIF-8 nanoparticles in the PEI matrix due to templating effect of GO sheets and vacuum-assisted assembly, which offered more well-defined pathways for methanol transfer.[265] Ma et al.[266] developed UiO-66-NH_2/Matrimid membranes by fabricating a continuous polycrystalline UiO-66-NH_2 (via in situ solvothermal synthesis) thin film on a cross-linked polymeric membrane matrix using layer-by-layer assembly. The obtained UiO-66-NH_2/Matrimid membrane (with the thickness of the MOF layer, ~601 nm) showed a 96.3% rejection of rose bengal (MW = 1017 g mol^{-1}) with moderate permeability of ethanol, ~0.88 L m^{-2} h^{-1} bar^{-1}, as well as a high rejection (93.1%) of rose bengal with fast permeance of dimethylforma-

https://doi.org/10.1021/acs.iecr.1c00543
Ind. Eng. Chem. Res. XXXX, XXX, XXX−XXX

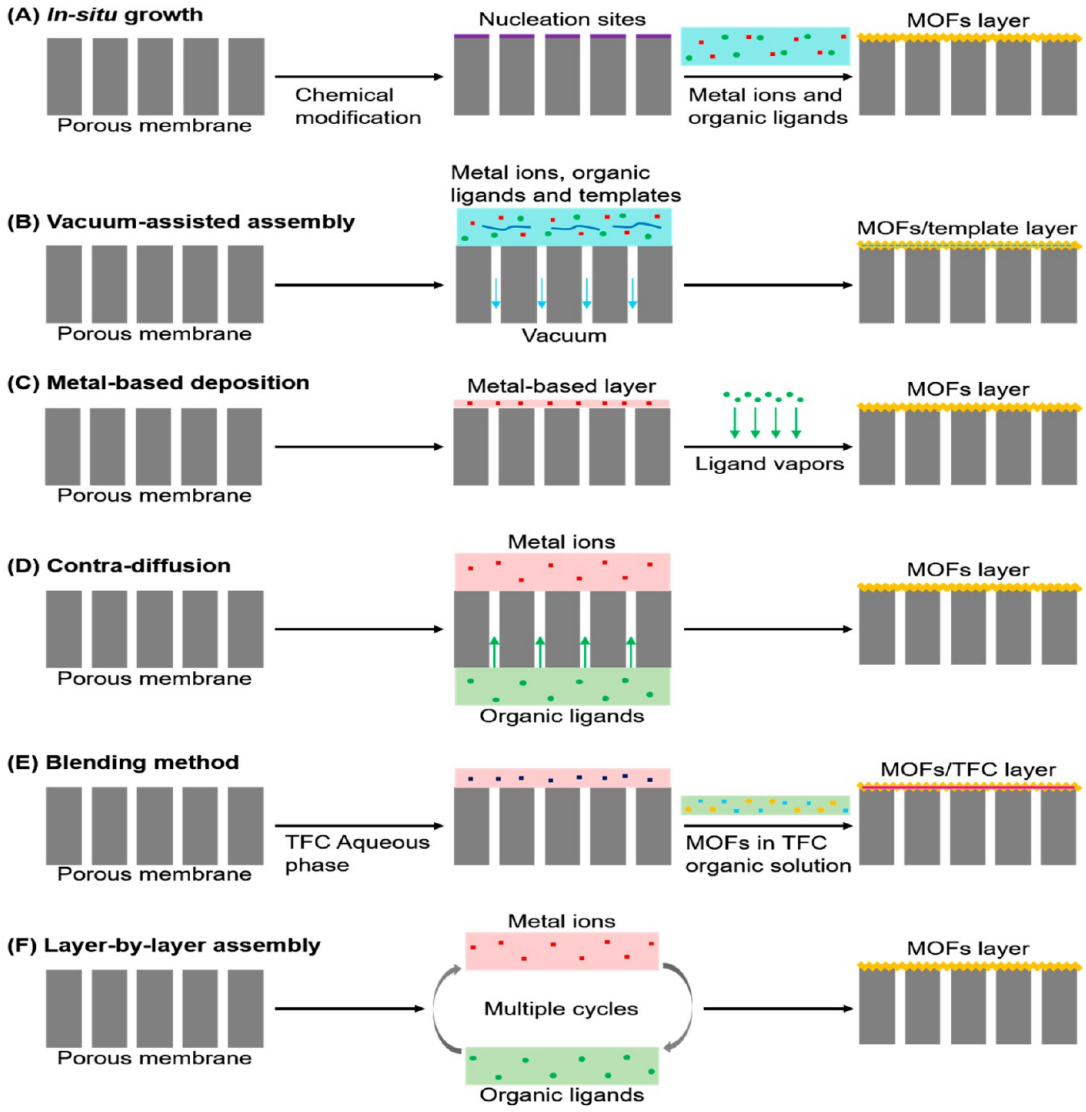

Figure 12. Schematics of fabrication strategies of ultrathin MOF-based membranes for organic solvent nanofiltration: (A) in situ growth,[264,268] (B) vacuum-assisted assembly,[265] (C) metal-based deposition,[19,267,274,275] (D) contra-diffusion,[162,276,277] (E) blending method,[49,55,66,70,71,109] and (F) layer-by-layer assembly.[266] Reproduced with permission from ref 261. Copyright 2019 Royal Society of Chemistry.

mide, ~4.58 L m^{-2} h^{-1} bar^{-1}. The high rose bengal rejection could be attributed to the size exclusion from the well-integrated UiO-66-NH_2 thin layer and the electrostatic repulsion between rose bengal and the MOF membrane.[266]

Paseta et al.[66] used a greener solvent, dimethyl sulfoxide (DMSO), to replace the traditional dimethylformamide (DMF) for dissolving the polymer and activating the TFC membrane, and prepared TFN membranes using MOFs (ZIF-8, ZIF-93, and UiO-66) as fillers. The fabricated TFN-UiO-66 membrane (with the UiO-66 thickness, ~35 nm) exhibited high methanol permeability of 11 L m^{-2} h^{-1} bar^{-1} with a high rejection of 97.9% to sunset yellow (MW = 452 g mol^{-1}).[66] The high methanol permeance resulted from the high MOF porosity, the ultrathin MOF thickness, and the hydrophilic/hydrophobic−hydrophobic interaction between the membrane and the solvent.

Paseta et al. reported a bilayered TFC (BTFC) membrane placing a continuous layer of MOF (HKUST-1 or ZIF-93) in between the support and the PA skin layer. These membranes were applied to the nanofiltration of diclofenac and naproxen aqueous solutions obtaining a respective maximum water permeability of 33.1 and 24.9 L m^{-2} h^{-1} bar^{-1} with a rejection of ≥98% when HKUST-1 was used.[54] The concept was extended by the same group, focusing on MOF ZIF-93, to hollow fiber membranes with improved results as compared to conventional TFC membranes in dye removal from water.[172] Following the same direction, Chen et al.[267] synthesized a HKUST-1 interlayer on a cross-linked polyimide ultrafiltration membrane via metal-based deposition, followed by depositing the TFC nanofiltration layer (interfacial polymerization with PIP and TMC) on the membrane surface to fabricate the OSN membrane. The optimized PA/HKUST-1/cross-linked P84 membrane (the thickness of HKUST-1 interlayer ~40 nm) showed an increased methanol permeability of 9.59 L m^{-2} h^{-1} bar^{-1} compared to that of the TFC membrane (4.75 L m^{-2} h^{-1} bar^{-1}) due to the thinner interlayer, while maintaining a high rejection of 98.8% compared to TFC (95.9%) to Brilliant Blue G 250 dye (MW = 858 g mol^{-1}) which may be mainly assigned to the more negative charge on the membrane surface.[267]

https://doi.org/10.1021/acs.iecr.1c00543
Ind. Eng. Chem. Res. XXXX, XXX, XXX−XXX

Cai et al.[268] first introduced carboxyl groups onto the surface of the flexible carbon cloth by acid treatment, followed by fabricating a continuous polycrystalline UiO-66(Zr)-NH_2 membrane (thickness of 800 nm) on the acidified carbon cloth substrate via in situ solvothermal growth. The obtained UiO-66(Zr)-NH_2/carbon cloth membrane showed a moderate dichloromethane permeability of 0.17 L m^{-2} h^{-1} bar^{-1} with a high rejection of ~99.9% to methylene blue (MW = 319 g mol^{-1}) as well as a moderate methanol permeability of 0.24 L m^{-2} h^{-1} bar^{-1} with a high rejection of ~99.88% to Nile red (MW = 318 g mol^{-1}).[268]

4.5.2. MOF-Based OSN Membranes (Thickness > 1 μm). Basu et al.[269] synthesized chemical-modified MOF particles [$Cu_3(BTC)_2$, MIL-47, MIL-53(Al), and ZIF-8] using *N*-methyl-*N*-(trimethylsilyl)-trifluoroacetamide (MSTFA), and incorporated them as the fillers into a PDMS solution, followed by coating the PDMS solution on top of the polyimide support to fabricate PDMS/MOFs)/PI membranes. The obtained (PDMS/MOFs)/PI membranes (thickness of PDMS/MOFs, ~30−35 μm) showed isopropyl alcohol permeances of 0.5−0.6 L m^{-2} h^{-1} bar^{-1} with increased rose bengal (MW = 1017 g mol^{-1}) rejections of 95%−98% compare to the unfilled membrane (87%) due to the better compatibility between MSTFA modified fillers and the polymer membrane, and the reduced polymer swelling.[269]

Campbell et al.[270] developed an in situ growth (ISG) approach to preparing hybrid polymer/MOF (HKUST-1/P84) membranes for OSN. The fabricated membrane (thickness of hybrid membrane, ~65 μm) showed an acetone permeance of 15 L m^{-2} h^{-1} bar^{-1}, while offering a higher rejection (90%) to styrene oligomers (MW = 1800 g mol^{-1}) due to increased membrane density compared to the mixed matrix membrane (70%).[270] They also fabricated MOF TFC membranes (MOF-TFCs) by synthesizing HKUST-1 on a P84 polymer ultrafiltration membrane with the interfacial synthesis method.[271] The MOF-TFC membrane (thickness of hybrid membrane, ~101 μm) showed higher acetone permeability (54 L m^{-2} h^{-1} bar^{-1}) than HKUST-1/P84 membrane prepared by ISG (16.1 L m^{-2} h^{-1} bar^{-1}), while offering a slightly lower rejection (37%) to styrene oligomers (MW = 1700 g·mol^{-1}) than the HKUST-1/P84 membrane prepared by ISG (42%).[271]

Li et al.[272] fabricated continuous ZIF-8 membranes on porous a polymeric PES support via a simple interfacial synthesis approach (one synthesis cycle). The synthesized ZIF-8/PES membrane showed moderate ethanol permeability of 2.5 L m^{-2} h^{-1} bar^{-1}, while offering a high rejection of 86% to rose bengal (MW = 1017 g mol^{-1}).[272]

Echaide-Górriz et al.[71] combined two MOFs (MIL-101(Cr) and ZIF-11) together and incorporated them in the formation of the TFC layer to produce the TFN-MIL101-ZIF11 membrane. This approach led to a membrane with an intermediate permeance-selectivity performance between that of TFN-MIL-101 and TFN-ZIF-11 membranes and showed a methanol permeability of ~6.3 L m^{-2} h^{-1} bar^{-1} and high rejection of ~93% to sunset yellow (MW = 452 g mol^{-1}) after DMF filtration post-treatment.[71] The authors also synthesized TFN-MOF membranes with MIL-101(Cr), MIL-68(Al), and ZIF-11 using a blending method in which MOFs were dispersed in the organic solution for TFC growth.[70] The optimized TFN-ZIF-11 membrane after DMF filtration post-treatment shows a methanol permeability of 6.2 L m^{-2} h^{-1} bar^{-1} and a high rejection above 90% to sunset yellow.[70]

Zhu et al.[273] used commercial aromatic poly(*m*-phenyleneisophthalamide) (PMIA) and MIL-53(Al) MOF, respectively, as the polymer matrix and the additive filler to fabricate mixed matrix membranes (MMMs) via the phase inversion method. The fabricated MIL-53(Al)/PMIA membrane showed increased ethanol permeability of 0.7 L m^{-2} h^{-1} bar^{-1} compared to that of the pristine membrane without MOF (0.2 L m^{-2} h^{-1} bar^{-1}), while maintaining a high rejection of 94% to brilliant blue G (MW = 854 g·mol^{-1}).[273]

4.5.3. Synthesis Approaches of Ultrathin MOF-Based OSN Membranes. Two competitive nucleation processes happen during the synthesis of a MOF-based OSN membrane: homogeneous nucleation, which exists in the mixed bulk MOF solution, and heterogeneous nucleation which takes place on the surface of the porous membrane substrate.[261] Homogeneous nucleation is typically more uniform. However, heterogeneous nucleation, which relies heavily on the surface property of the porous substrate, tends to form MOF islands with intracrystalline cracks and intercrystalline cracks on the surface.[261,278] Hence, the key point for depositing a uniform continuous MOF layer on the surface of the porous substrate is to improve the heterogeneous nucleation process.[261,262] Several synthesis approaches, such as in situ growth,[264,268] vacuum-assisted assembly,[265] metal-based deposition,[19,267,274,275] contra-diffusion,[162,276,277] blending method,[49,55,66,70,71,109] and layer-by-layer assembly,[266] have been developed, and we summarize them as follows.

(A) *in situ* growth:[264,268] The substrate is pretreated with functional molecules to generate heterogeneous nucleation sites and then immersed into the mixed bulk MOF solution containing metal ions and organic ligands.

(B) vacuum-assisted assembly:[265] The porous substrate is immersed into the mixture of bulk MOF solution and template suspension, and then vacuumed from the substrate side to deposit the MOF/template layer on the substrate surface.

(C) metal-based deposition:[19,267,274,275] The metal-based precursor (metal ions,[19] metal-oxo clusters,[274] or metal-based gel coatings[275]) for MOF is first anchored on the substrate surface, followed by injecting organic ligand vapor precursor.

(D) contra-diffusion:[162,276,277] The two precursors are separated by the porous substrate (barrier) and can only meet through the channels; once they meet each other, MOF starts to crystallize and eventually forms an ultrathin continuous defect-free MOF layer.

(E) blending method:[49,55,66,70,71,109] The aqueous solution for TFC is first deposited on the substrate surface, followed by coating the MOF ink (MOF solutions in organic solution for TFC) to form a MOF/TFC layer on the substrate surface.

(F) layer-by-layer assembly:[266] The target substrate is immersed into the precursor solutions in alternating sequence, followed by repeating the process for certain cycles, which would be able to precisely control the thickness of the synthesized film in nanoscale.

4.6. MOF-Membranes for Lithium Resource Recovery.

Over the past decade, lithium consumption has steadily increased due to its heightened importance in many applications such as ceramic, glass, polymer, and lubricant manufacturing; and especially in the well-known battery technologies. According to a recent review by Li et al.,[280]

https://doi.org/10.1021/acs.iecr.1c00543
Ind. Eng. Chem. Res. XXXX, XXX, XXX−XXX

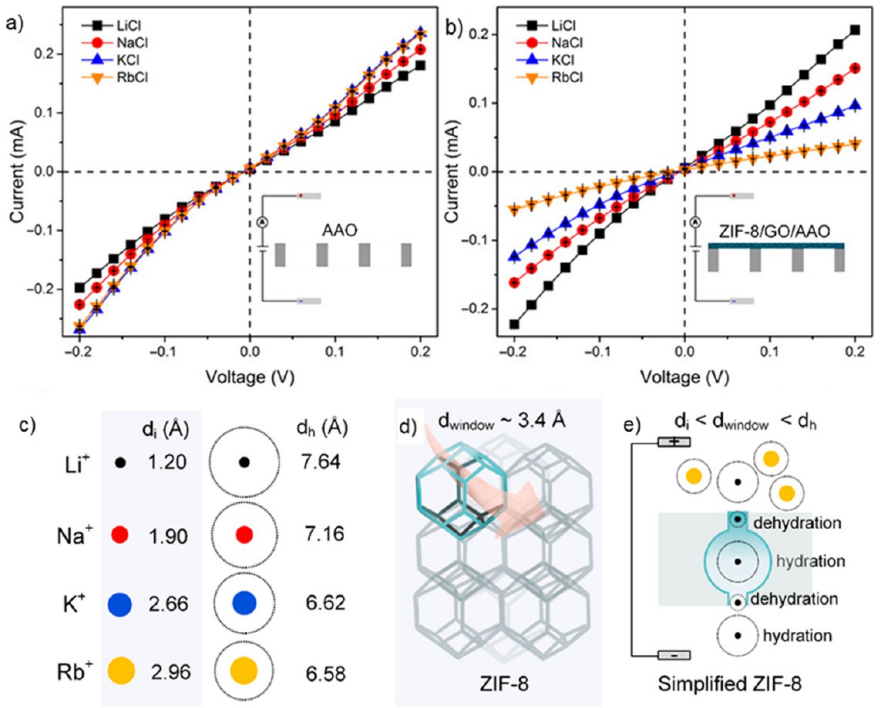

Figure 13. (a) The $I-V$ curve of LiCl, NaCl, KCl, and RbCl solutions through AAO support and (b) the $I-V$ curve of LiCl, NaCl, KCl, and RbCl solutions through ZIF-8/GO/AAO membrane. Reprinted from ref 171. Copyright The Authors, some rights reserved; exclusive licensee American Association for the Advancement of Science. Distributed under a Creative Commons Attribution NonCommercial License 4.0 (CC BY-NC) http://creativecommons.org/licenses/by-nc/4.0/. (c) Illustration of ionic diameter (d_i) and hydrated ionic diameter (d_h) for Li^+, Na^+, K^+ and Rb^+ with its respective values in Å as reported in ref 171; illustration of ZIF-8 membrane crystal structure with pore window size (d_{window}) ≈ 3.4 Å; and (e) illustration of ion partial dehydration and hydration sequence as proposed ion transport in MOF membranes in which $d_i < d_{window} < d_h$. Adapted from ref 171. Copyright The Authors, some rights reserved; exclusive licensee American Association for the Advancement of Science. Distributed under a Creative Commons Attribution NonCommercial License 4.0 (CC BY-NC) http://creativecommons.org/licenses/by-nc/4.0/.

lithium consumption worldwide had risen by 6% annually during the period of 2010−2016, and it is predicted to reach around 95 000 tons in the year 2025.[280] Among the available resources, lithium recovery from salt-lake brine attracts more industrial interest due to the lower cost and higher availability compared to solid resources.[280] Li et al.[280] has also extensively reviewed membrane technologies and processes for lithium recovery from salt lake brine. They concluded that while it is crucial to separate lithium ions (Li^+) from magnesium ions (Mg^{2+}) in the solution for recovery by Li_2CO_3 precipitation, the Li^+ separation from other interfering monovalent ions such as sodium (Na^+) and potassium (K^+) ions remains a difficult challenge due to the similarity in valency and ionic diameter.

In addition, Razmjou et al.[281] critically reviewed recent works on Li^+ selective membranes with emphasis on the vital membrane design principles, including (1) the effect of nanochannel size, (2) the effect of nanochannel chemistry, (3) the effect of morphology, and (4) the effect of driving force. In this section, we focus on the development of MOF-based membranes for lithium recovery due to the highly tunable characteristics of MOFs in modifying the pore window diameter (d_{window}), pore chemistry, the MOF morphology, and heterostructure design. Also, the stability and viability of the membrane fabrication method are also discussed in this section.

4.6.1. Tunable Pore Size. One of the earliest forms of MOFs with Li^+ selectivity was reported by Jung et al.[282] in 2008 using metal−organic polyhedral (MOP)-18. In their work, the 5 nm overall size of MOP-18 was synthesized with a cavity diameter (d_{cavity}) of 13.8 Å, accessible through a d_{window} of 3.8 and 6.6 Å.[282] The MOP-18 particle, which was decorated with a long alkyl chain, was then incorporated into a bilipid layer membrane, mimicking the biological ion pump on a cellular membrane as illustrated in Figure 13. The ion transport activity of MOP-18 is selective toward Li^+ transport ($Li^+ \gg Na^+ > K^+ > Rb^+ > Cs^+$), which suggested that the ion transport is mostly governed by cations-channel binding compared to the cation dehydration process.[282] The biomimetic membrane shows a Li^+/K^+ selectivity of 1.7.[282] Nonetheless, the poor physical and chemical stability of the membrane was not suitable for industrial application.[281] It was also suggested that the ion transport in MOP-18 utilized both pore window sizes (d_{window}) of 3.8 and 6.6 Å.[282] Hence, this might pose a problem when separating similar-sized cations smaller than 6.6 Å.

To address this issue, Zhang et al.[171] has demonstrated that choosing MOFs with an appropriate pore-limiting diameter is key to a good separation between monovalent alkali metal ions. In their work, a highly crystalline ZIF-8 membrane was synthesized on a ZIF-8/GO-seeded AAO (anodized alumina oxide) membrane with an average thickness of 446 ± 74 nm.[171] For this membrane, the ion transport activity was measured with an $I-V$ curve. To measure the ion transport activity, electrical potential (V) is applied across ion-selective membrane, in which the resulting measurement of current (I) in the $I-V$ curve indicates the rate of ion transport across the membrane. On the basis of the $I-V$ curve, the ion transport activity was in the order $Li^+ > Na^+ > K^+ > Rb^+$ (Figure 13b) with a Li^+/K^+ selectivity of 2.18 and a Li^+/Rb^+ selectivity of

https://doi.org/10.1021/acs.iecr.1c00543
Ind. Eng. Chem. Res. XXXX, XXX, XXX−XXX

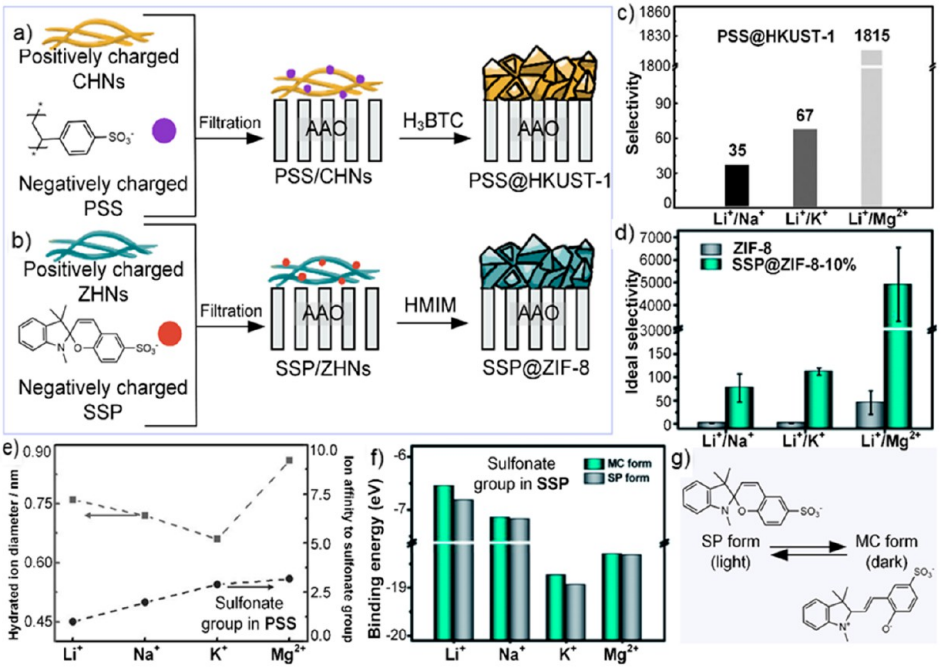

Figure 14. Schematic illustration of the fabrication process of (a) PSS@HKUST-1 and (b) SSP@ZIF-8 membranes on AAO substrate. Notation: CHN, copper hydroxide nanostrands; PSS, polystyrene sulfonate; AAO, anodic alumina oxide; H_3BTC, trimesic acid; ZHN, zinc hydroxide nanostrands; PSS, polystyrene sulfonate; AAO, anodic alumina oxide; HMIM-2, methylimidazole. Adapted with permission from ref 285 (Copyright 2016 John Wiley and Sons) and ref 286 (Copyright 2013 The Royal Society of Chemistry), respectively. (c) Binary selectivity of Li^+/Na^+, Li^+/K^+, and Li^+/Mg^{2+} of PSS@HKUST-1. Reprinted in part with permissions from ref 285. Copyright 2016 John Wiley and Sons. (d) Ideal selectivity of Li^+/Na^+, Li^+/K^+, and Li^+/Mg^{2+} of ZIF-8 and SSP@ZIF-8−10%. Reprinted in part with permissions from ref 286. Copyright 2013 The Royal Society of Chemistry. (e) Hydrated ion diameter and ion affinity to sulfonate group in PSS of Li^+, Na^+, K^+, and Mg^{2+}. Reprinted in part with permissions from ref 285. Copyright 2016 John Wiley and Sons. (f) Calculated binding energies of Li^+, Na^+, K^+, and Mg^{2+} in SP and MC form of SSP sulfonate group in which the chemical structure is shown in panel g. Reprinted in part with permissions from ref 286. Copyright 2013 The Royal Society of Chemistry.

4.67. This observation was attributed to the partial dehydration effects of the hydrated ions in confined nanochannels, which required the ions to lose their hydration shell to be transported through the pore channels of ZIF-8, similar to those mechanisms found in the biological ion channel pump.[171,283] The d_{window} of ZIF-8 (3.4 Å) allowed fully dehydrated ions with size diameter in the following order d_{Li+}(1.20 Å) < d_{Na+}(1.90 Å) < d_{K+}(2.66 Å) < d_{Rb+}(2.96 Å) to transport across ZIF-8 membrane. This explanation is illustrated in Figure 13c,d. The authors reported that Li^+ selectivity was not observed with AAO membrane (Li^+/Rb^+ = 0.6) (Figure 13a) without the nanochannel confinement effect provided by ZIF-8.

To further confirm the role of d_{window} of MOF in ion selectivity, Zhang et al.[171] also fabricated UiO-66 channels with a d_{window} of 6 Å, which is a larger size than the d_{window} of ZIF-8. As expected, the ion selectivity of Li^+/K^+ and Li^+/Rb^+ dropped to 1.58 and 1.82, respectively, confirming that the ion selectivity of MOF membranes decreases with increasing d_{window} up to 1 nm.[171] The work on the ZIF-8 membrane fabrication on the AAO support was extended to flexible polymeric membranes such as the PP and PVDF membrane by Mohammad et al.[284] using a metal-phenolic network such as tannic acid and iron (TA-Fe^{III}) complexes to aid MOF heterogeneous nucleation and growth. The resulting PP/TA-Fe^{III}/ZIF-8 shows clear divalent ions separation from monovalent ions with a selectivity ratio of 3.87 (Li^+/Mg^{2+}), 4.00 (Na^+/Mg^{2+}), and 4.49 (K^+/Mg^{2+}) for lithium resource recovery application.[284] Most inorganic supports such as AAO are brittle and fragile for robust large-scale application in industry; therefore, the fabrication of MOF on a flexible polymeric membrane poses more interest for industrial application due to the inherent mechanical and chemical stability of the support.[284]

4.6.2. Tunable Chemistry. Besides pore window size, the MOF pore chemistry can be tuned to alter the membrane-solute interactions in order to achieve solute-specific selectivity. For example, Guo et al.[285] has utilized polystyrene sulfonate (PSS) to introduce negative charges into the HKUST-1 MOF membrane (denoted as the PSS@HKUST-1 membrane), fabricated on solid-state AAO support, to increase the selectivity of Li^+ ions[285] (Figure 14a).

The linear polymer PSS contains abundant sulfonate groups (approximately four sulfonate groups/nm) to direct the recognition of alkaline and alkaline-earth metal ions.[285] As a result, the PSS@HKUST-1 exhibited Li^+ conductivity of 5.53 × 10^{-4} S/cm at 25 °C which is five orders higher magnitude than with HKUST-1 without PSS using the *I*−*V* curve method, and a Li^+ flux of 6.75 mol m^{-2} h^{-1} in a nanofiltration system, both of which are significantly higher in magnitude than with HKUST-1 without PSS.[285] Note that although HKUST-1 possessed a larger d_{window} of 9 Å, the affinity differences of Li^+, Na^+, K^+, and Mg^{2+} to the incorporated PSS played a tremendous role in achieving a binary selectivity of 35 (Li^+/Na^+), 67 (Li^+/K^+), and 1815 (Li^+/Mg^{2+}), as presented in Figure 14c.[285] Particularly, it is suggested that Li^+ has the lowest binding energy to the sulfonate group (0.21 eV) (Figure 14e), thus allowing the ion transport by "hopping" from one

https://doi.org/10.1021/acs.iecr.1c00543
Ind. Eng. Chem. Res. XXXX, XXX, XXX−XXX

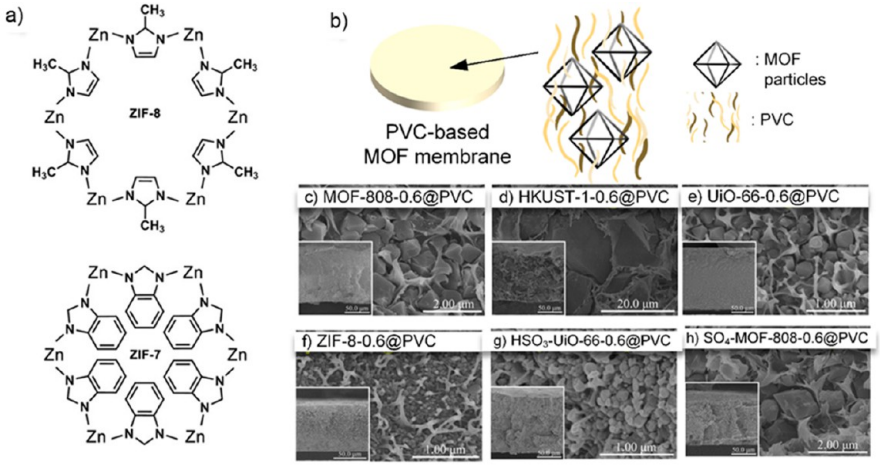

Figure 15. (a) Pore window structure comparison of six-ring ZIF-8 and ZIF-7 with pore window size of 3.4 and 2.9 Å, respectively. Reprinted with permission from ref 171. Copyright The Authors, some rights reserved; exclusive licensee American Association for the Advancement of Science. Distributed under a Creative Commons Attribution NonCommercial License 4.0 (CC BY-NC) http://creativecommons.org/licenses/by-nc/4.0/. (b) Schematic illustration of PVC-based MOF membrane. Adapted with permission from ref 296. Copyright 2020 Elsevier. Cross-sectional scanning electron micrograph (SEM) image of MOF@PVC membrane, particularly (c) MOF-808-0.6@PVC, (d) HKUST-1-0.6@PVC, (e) UiO-66-0.6@PVC, (f) ZIF-8-0.6@PVC, (g) HSO_3-UiO-66-0.6@PVC, and (h) SO_4-MOF-808-0.6@PVC. The images c–h are reprinted with permission from ref 296. Copyright 2020 Elsevier. The value 0.6 represents the weight ratio of MOFs over PVC.

sulfonate group to another *via* a Grotthuss-like mechanism.[285,287−291]

A similar method was employed by Liang et al.[286] in producing Li^+ selective MOF membranes with an added advantage of light-controlled transport. In their work, a negatively charged photochromic compound, sulfonated spiropyran (SSP), was encapsulated into the ZIF-8 membrane on the AAO substrate[286] (Figure 14b), essentially converting the neutral ZIF-8 to possess negatively charged pores. The SSP@ZIF-8-10%/AAO membrane specifically achieved a Li^+ conductivity of 1.6×10^{-4} S/cm and an ideal selectivity of 77 (Li^+/Na^+), 112 (Li^+/K^+), 4913 (Li^+/Mg^{2+}) at 25 °C and dark conditions, using an electrodialysis.[286] The ideal selectivity is based on single ion conductivity measurements across the membrane. Without SSP molecules, the ZIF-8/AAO membrane exhibited a lower ideal selectivity of 1.3 (Li^+/K^+), 1.4 (Li^+/Na^+), and 45.6 (Li^+/Mg^{2+}), which showed that utilizing both d_{window} and pore chemistry together could improve the MOF separation capability (Figure 14d). In dark conditions, the SSP sulfonate group changed from the SP form to the merocyanine (MC) form, as illustrated in Figure 14g. Compared to the SP form, the MC form had more binding sites and lower binding affinity to the ions, as evident from the binding energy calculation (Figure 14f). This subsequently contributed to relatively faster Li^+ transport than in the SSP structure.[286] The controllable ion separation in the MOF membranes allows for different ion separation stages in the same module or the use of a capture and release of ions technique in water treatment.

4.6.3. Interaction of Ion and Water Molecules with MOF Pore Size and Chemistry. Depending on the nanochannel diameter and its surface charge, the behavior mechanism of Li^+ transport can vary. In a recent study by Razmjou et al.,[292] molecular dynamic (MD) simulations on two-dimensional (2D) vermiculate (VCT) based membranes revealed that in nanochannels with a pore size less than 1 nm, the Li^+ transports along the channel by "hopping" alternately between the two walls of the channels. However, with spacing above 1 nm, the Li^+ only hops on one side of the channel wall.[292] This phenomenon can be attributed to the effect of the spontaneous symmetry breaking of charge-regulated surfaces,[293] which mainly occurs when two surfaces of equal charge are within close proximity. In this case, the surface charge densities can change as Li^+ adsorbed on the VCT from the solution and subsequently affects the interaction of the Li^+ already on the surface or attached to the functional group, prompting the ion "hopping" from one wall to another in close quarters.[292] These findings highlighted the mechanism of Li^+ transport that can be achieved in tunable pore size and chemistry of MOF membranes[294,295] which has a great potential to be used as lithium selective membranes.

Ultimately, it would be critical to consider the effect of MOF characteristics (pore size and pore chemistry) on ion and water transport mechanisms. Revisiting the ZIF-8 membrane fabricated by Zhang et al.[171] explained earlier, the interaction of ions and water molecules with ZIF-8 framework were mainly governed by van der Waals forces and Columbic interactions.[171,281] In this case, the dehydration effect in confined space attributed to the small d_{window} has more influence on Li^+ selectivity compared to the neutral pore chemistry of ZIF-8. In the same study, Zhang et al.[171] also reported fabricating a ZIF-7 nanochannel with a d_{window} of 2.9 Å which is of smaller size compared to ZIF-8 (3.4 Å) (Figure 15a).[171] Counterintuitively, there were no Li^+ conductivity and selectivity reported with the smaller d_{window}, as the confined space in ZIF-7 was superhydrophobic.[171] The induced hydrophobicity by the phenyl group of ZIF-7 hindered any water or ion transport altogether.[171] Therefore, both pore size and pore chemistry need to be considered equally upon selecting the type of MOF materials for ion separation.

A recent study by Zhang et al.[296] further elucidates this matter as they studied six different MOFs particles (ZIF-8, UiO-66, HSO_3-UiO-66, HKUST-1, MOF-808, and SO_4-MOF-808) which were then embedded into a polyvinyl chloride (PVC) membrane as a MMM (Figure 15b–h). We note that the authors utilized MOF particles which were synthesized with sulfonate molecules attached to the ligand of the MOF structure, instead of encapsulating external molecules to

https://doi.org/10.1021/acs.iecr.1c00543
Ind. Eng. Chem. Res. XXXX, XXX, XXX−XXX

integrate charges in neutral MOFs as demonstrated by Guo et al.[285] and Liang et al.[286] The measured pore size of the MOF and its selectivity are presented in Table 5. Specifically, HSO_3-

Table 5. Comparison of Synthesized MOF@PVC with Respect to Measured Pore Size (Å), and Ion Separation Ratio of Li^+/Na^+, Li^+/K^+, and Li^+/Mg^{2+} as Reported by Zhang et al.[296] [a]

MOF@PVC	measured pore size (Å)	Li^+/Na^+	Li^+/K^+	Li^+/Mg^{2+}	ref
MOF-808	12.9	0.76	0.60	0.79	296
HKUST-1	8.2	0.80	0.64	1.27	
UiO-66	6.0	0.84	0.71	1.30	
ZIF-8	4.7	1.34	1.18	2.02	
HSO_3-UiO-66	5.5	0.93	0.80	4.79	
SO_4-MOF-808	12.0	0.88	0.70	1.06	

[a]Studied MOFs are MOF-808, HKUST-1, UiO-66, and ZIF-8; compared with MOF included with sulfonate groups which are HSO_3-UiO-66 and SO_4-MOF-808. Table values were obtained from 296. Copyright 2020 Elsevier.

UiO-66@PVC showed selectivity of Li^+/Mg^+ (4.79), although it had a larger pore size compared to ZIF-8@PVC (Li^+/Mg^+ = 2.02), mainly due to the strong interaction between sulfonate groups and Mg^{2+}. Meanwhile, in this case, ZIF-8 still showed superior Li^+/Na^+ and Li^+/K^+ selectivity due to its smaller pore size despite having a neutral charge.[296] These results further confirm that in the MOF membrane with larger pore size, the monovalent and divalent separation needs to rely on the pore chemistry, while for monovalent ion separations (e.g., Li^+/Na^+) the effect of pore size remains dominant.

By far, sulfonate groups have been one of the most widely studied functional groups to fabricate MOF membranes with selective transport of cations, mainly in improving Li^+ selectivity over divalent ions such as Mg^{2+} due to higher binding affinity of Mg^{2+} to sulfonate groups. In theory, this will result in higher permeation of Li^+ compared to Mg^{2+}. However, this may not always be the case. For example, Xu et al.[297] fabricated leaf-like UiO-66-SO_3H membranes on AAO support with 25% of 2-$NaSO_3$-H_2BDC to H_2BDC (denoted as U-SM(25)) (Figure 16c). The authors reported electrical-driven single component permeation in the order of $K^+ > Na^+ > Li^+ > Mg^{2+}$ which precisely depends on the order of hydrated ionic diameter, with the ideal selectivity of 5091 (K^+/Mg^{2+}), 2449 (Na^+/Mg^{2+}), and 776 (Li^+/Mg^{2+}) (Figure 16b).[297] However, in binary solutions, the selectivity is reported to be 5.31 (K^+/Mg^{2+}), 170 (Na^+/Mg^{2+}), and 1.88 (Li^+/Mg^{2+}) (Figure 16d).[297] The decrease in selectivity performance in K^+/Mg^{2+} and especially Li^+/Mg^{2+} was due to more Mg^{2+} permeation compared to K^+ and Li^+, which contradicted the previous understanding of ion transport via size and surface charge selectivity.

Therefore, this finding suggests that not only ion−water and ion−surface interactions are responsible for the observed ion transport, but also the ion−ion competitive interaction in the nanochannels has a substantial influence.[297] There are still limited studies that report the binary selectivity of mixed ions in MOF membranes, as opposed to its ideal selectivity using single ion permeation only. The author claimed that the specific reason for this discrepancy is still unclear.[297] Hence,

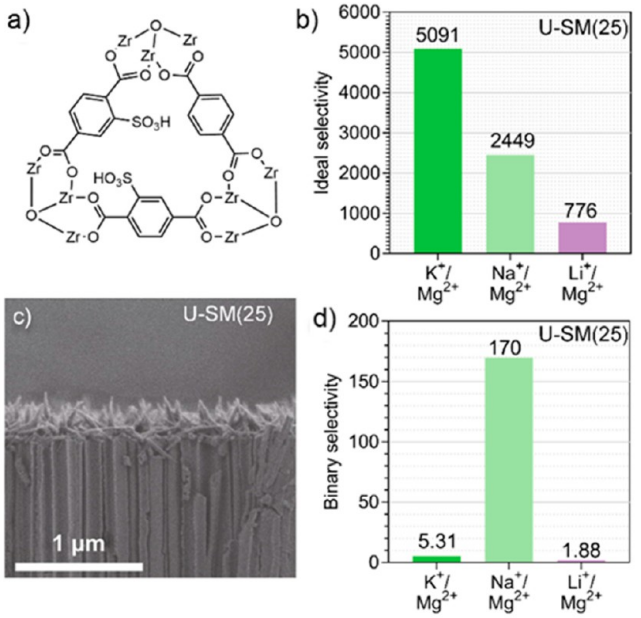

Figure 16. (a) The triangular pore window structure of UiO-66 decorated with HSO_3 functional group used for the fabrication of U-SM, (b) ideal selectivity of K^+/Mg^{2+}, Na^+/Mg^{2+}, and Li^+/Mg^{2+} of U-SM(25), (c) cross-sectional SEM image of leaf-like U-SM(25); and (d) the binary selectivity of K^+/Mg^{2+}, Na^+/Mg^{2+}, and Li^+/Mg^{2+} of U-SM(25) in mixed-salt solution. Figure 16b−d are reprinted in part from ref 297. Copyright 2020 The Authors.

more work needs to be done to understand the ion−ion interaction and its performance in mixed-solution separations.

A recent study by Cha-umpong et al.[298] explained how ion−ion interaction with the membrane surface can affect the nanochannel structure, subsequently affecting ion permeation.[299] Particularly in GO membranes, the interaction of hydrated cations in the interlayer spacing can create a high charge density, which results in stronger interactions with functional groups on the membrane surface, subsequently lowering the interlayer spacing.[298,299] It was found that with the presence of single Na^+, Ca^{2+}, and Mg^{2+}, the interlayer spacing of GO was 9.3, 8.5, and 8.92 Å, respectively.[298] This indicated that the attraction of divalent ions with the membrane surface was stronger than monovalent ions, with Ca^{2+} having a stronger attraction compared to Mg^{2+}.[298] When the cations appeared simultaneously, the interlayer spacings with the presence of $Na^+ + Ca^{2+}$, $Na^+ + Mg^{2+}$, and $Na^+ + Ca^{2+} + Mg^{2+}$ were 8.71, 9.38, and 9.24 Å, respectively.[298] It is important to highlight that the narrow interlayer spacing with the presence of divalent ions can reduce the available passage for the permeation of smaller monovalent ions such as Na^+.[298]

These explanations could be extended to explain the discrepancy in the performance of single salt separation and binary separation in MOF membranes as well. It is possible that in a mixed solution, the Mg^{2+} ions, which were attracted to the sulfonate group, change the surface charge density and effectiveness of the UiO-66-SO_3H, obstructing the transport rate of monovalent ions. The decrease of the UiO-66 cavity size is already observed when $-SO_3H$ groups are introduced, as evidenced by the reduction in pore volume.[297] Besides that, the possibility of pinhole defects or cracks could not be ignored when the contrast between the ideal and binary selectivity of the MOF membrane was reported, as discussed

https://doi.org/10.1021/acs.iecr.1c00543
Ind. Eng. Chem. Res. XXXX, XXX, XXX−XXX

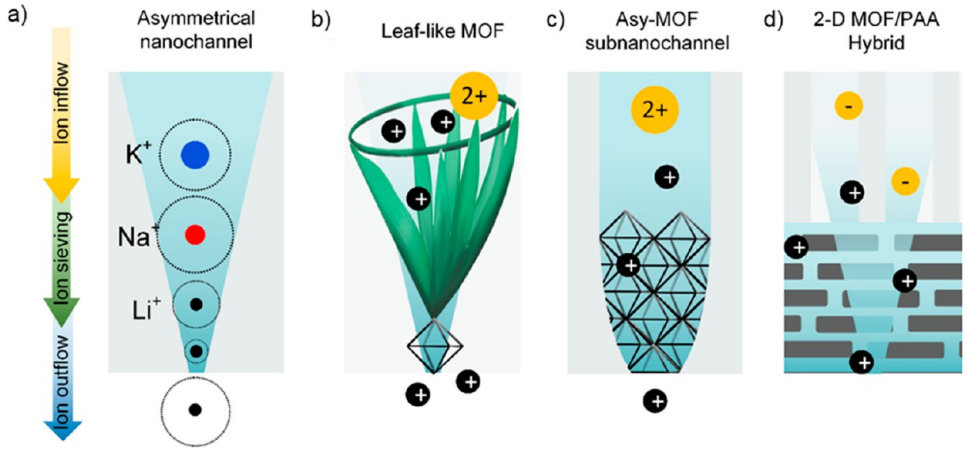

Figure 17. Illustrations of (a) selective filtration of alkali ions according to d_i (adapted in part with permission from ref 303; copyright 2020 Elsevier), (b) asymmetrical leaf-like MOF grown from MOF crystals membrane (adapted with permission from ref 302; copyright 2019 John Wiley and Sons), (c) asymmetrical-MOF subnanochannel from ion-tracked PET membrane (adapted in part from ref. 305; copyright 2020, Jun et al., under exclusive license to Springer Nature Limited), and (d) 2-D MOF/PAA hybrid membrane (adapted in part with permissions from ref 306; copyright 2019 John Wiley and Sons).

by Razmjou et al.[300] regarding the influence of morphological defects in Li^+ separation,[300] similar to those found in rGO membranes.[301]

It is also worth discussing the earlier work by the same author, Xu et al.,[302] in which the similar leaf-like MOF membrane functionalized with amine group instead of the sulfonate group is utilized. In this case, the membrane which was fabricated using UiO-66-NH_2 on AAO showed the ideal selectivity of Na^+/Mg^{2+} and Li^+/Mg^{2+} to be >200 and >60, respectively.[302] Although the differences of the functional groups and their impact on the selectivity were not addressed specifically by the author, it was clear that using a negatively charged sulfonate group would yield higher ideal selectivity for monovalent against divalent ions compared to using positively charged amine groups.

4.6.4. Tunable MOF Membrane Morphology and Heterostructure Design. Besides tuning the intrinsic MOF pore size and surface chemistry, MOFs are also versatile in terms of manipulating the membrane morphology either using (1) the bottom-up approach, in which the membrane is directly synthesized from precursor solution; or (2) the top-down approach in which MOF is synthesized separately and then later assembled into a membrane. The effect of membrane nanochannel morphology in terms of symmetrical and asymmetrical nanochannel to the transportation rate and selectivity of Li^+ was discussed thoroughly in a review by Razmjou et al.[281] In a recent MD simulation study of this effect in GO-based materials,[303] the asymmetrical degree in morphology was found to be the most critical factor to increase Li^+ selectivity compared to pore size and chemistry.

In asymmetrical nanochannels akin to those found in biological protein nanochannels, the hydrated ions gradually lose their hydration shells along the nanochannel, whereas in symmetrical synthetic channels, there is a large dehydration energy penalty when an ion enters the channel.[281,283,304] These are illustrated in Figure 17a. In this subsection, we explore the strategy to modify MOF membrane morphology and its heterostructure design for ion transport.

Bottom-up Approach. Two exemplary works by Xu et al.[297,302] with unique leaf-like morphology of MOF crystal structure which was previously discussed, show a unique way in which MOF can be synthesized to a unique morphology. In their work, UiO-66-X (X-functional group) seeds were used as a nucleation and growth point for UiO-66-X leaves, which created nanosized interstitial pores (Figure 17b). These created a funnel-like characteristic, with nanosized surface pores followed by subnanometer inherent pores, which enabled fast permeation of cations.[302] As discussed in the previous section, this membrane achieved acceptable Na^+/Mg^{2+} and Li^+/Mg^{2+} selectivity in UiO-66-NH_2 membranes.[302] According to the authors, the selective performance was attributed to the density of the leaf-like MOFs which produced smaller interstitial pores, favoring ion separation via size selectivity.[302] Although the author did not consider the effect of asymmetrical morphology of the membrane to ion separation, this method has the potential to customize asymmetrical MOF with nanosubnanometer channels.

Another way to create this asymmetrical effect is to incorporate MOFs into conical shaped ion-tracked channels in PET membranes as demonstrated by the works of Wang and colleagues (illustrated in Figure 17c).[171,305,307] In particular, the asymmetrical UiO-66-$(COOH)_2$ subnanometer channel (SNC) was fabricated by utilizing bullet-shaped nanochannels with tip and base diameters of 59.2 ± 17.0 nm and 363.3 ± 54.8 nm, respectively, in which it was filled with UiO-66-$(COOH)_2$ with a triangular d_{window} of ~6 Å.[305] This design resulted in ion current rectification (ICR) in which the K^+/Mg^{2+}, Na^+/Mg^{2+}, and Li^+/Mg^{2+} selectivities when current is applied from base to tip are 4948.0, 3230.2, and 1590.1, respectively, whereas the reverse current direction resulted in the corresponding selectivities of 366.4, 235.4, and 159.3, respectively.[305] Attributing the performance to the repeated dehydration and rehydration steps and high energy barrier for divalent ions to pass through, the Asy-MOF-SNC approach can be utilized further for the application for Li^+ recovery. Nonetheless, it is acknowledged that the separation of K^+ and Na^+ from Li^+ remains difficult in this design.

MOF membrane asymmetrical properties are not only limited to nanochannel geometry design; but also can be applied to the surface charge distribution and concentration.[306] In the application of energy generation, Wang et al.[306] fabricated bioinspired 2D Cu-TCPP(Fe) on porous anodic

https://doi.org/10.1021/acs.iecr.1c00543
Ind. Eng. Chem. Res. XXXX, XXX, XXX−XXX

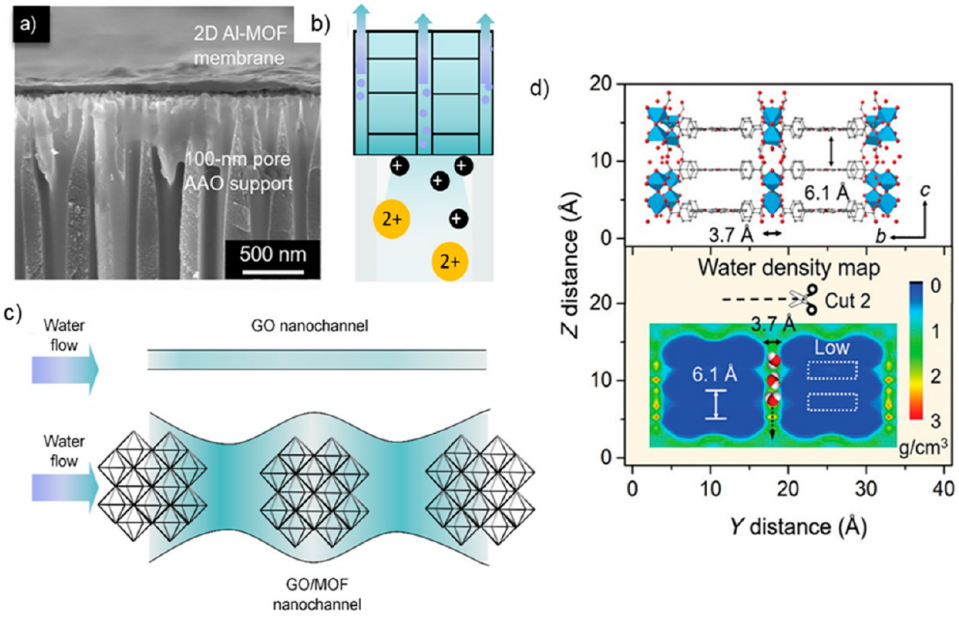

Figure 18. (a) SEM image of 2D Al-MOF on AAO support. Reprinted from ref 294. Copyright The Authors, some rights reserved; exclusive licensee American Association for the Advancement of Science. Distributed under a Creative Commons Attribution NonCommercial License 4.0 (CC BY-NC) http://creativecommons.org/licenses/by-nc/4.0/. (b) Simplified illustration of asymmetrical heterostructure design of MOF membrane, with arrows indicating water transport without ions passing through; (c) illustration of GO nanochannel and GO/MOF nanochannel, in which the latter shows asymmetrical design akin to biological channel. Adapted in part with permission from ref 308. Copyright 2019 Elsevier. (d) Side view (*z*-axis vs *y*-axis) of 2D Al-MOF with water density map showing formation of water channel with the size of 3.7 Å. Reprinted from ref 294. Copyright The Authors, some rights reserved; exclusive licensee American Association for the Advancement of Science. Distributed under a Creative Commons Attribution NonCommercial License 4.0 (CC BY-NC) http://creativecommons.org/licenses/by-nc/4.0/.

aluminum (PAA) via in situ growth (Figure 17d) to investigate the asymmetrical ion transport property and salinity-gradient based energy conversion.[306] They found that the asymmetrical design of Cu-TCPP(Fe)/PAA resulted in a high ICR ratio in a wide pH range favoring the transport of cations over anions. Owing to the asymmetrical design, ion accumulation occurs inside the 2-D MOF channels, causing the electrical double layer to overlap; thus, resulting in an increase in the ion conductivity.[306] This work demonstrated how MOFs can pose as versatile membrane material to create asymmetrical membrane morphology.

Top-down Approach. Novel 2-D nanosheets such as GO[298,299,303] and VCT[292] assembled to support substrates has been a predominant method to produce ion sieve membranes. Instead of directly synthesizing MOF onto support substrates, a top-down approach in which MOF was fabricated first then assembled into a membrane can offer more control in the synthesis method without the need to consider the stability of the support substrate in the MOF synthesis condition.

Recently, it was also shown that water-stable 2D aluminum tetra-(4-carboxyphenyl) porphyrin framework (termed Al-MOF) nanosheets could be assembled onto an AAO via vacuum filtration (Figure 11a).[294] The 2D monolayer and ultrathin membrane could offer a high rejection rate of Na^+, K^+, Mg^{2+}, Ca^{2+}, Al^{3+}, and Co^{2+} ions (~100%) with high water permeability (water permeability, 0.03 L m^{-2} h^{-1} bar^{-1})[294] due to the presence of small water nanochannels (3.7 Å width); smaller than hydrated ion diameters (Figure 18b). While this membrane was an excellent ion sieve for desalination purposes, the potential for Li^+ recovery was low as it exhibited high rejection rates of both monovalent and divalent ions. Separation in 2D materials is based on the interlayer spacing among the nanosheets, the water-stable Al-MOFs were found more resistant to intractable interlayer swelling compared with other 2D materials. Thus, the water transport in Al-MOF nanosheets had a tendency to only occur in the vertically aligned channels, which were formed intrinsically with the size 3.7 Å width along the *z*-axis (Figure 18d).[294] If the interlayer spacing between the 2D nanosheets could be controlled, this Al-MOF may have the potential to selectively separate Li^+ from other ions.

Sui et al.[308] found a unique way to engineer the interlayer spacing of 2D nanosheets by using MOF particles as filler materials or "spacers" in between the layers using the typical filtration method. Specifically, they have shown that water transport in nanochannels between GO nanosheets intercalated with a high amount of MOF spacers is much faster than the water transport in pure GO nanochannels.[308] This work offered flexibility in utilizing MOF nanoparticles in accelerating water transport across 2D membranes for applications of water purification and treatment. Although it was not addressed by the authors, the GO nanochannels altered by intercalated MOFs actually have a potential to create asymmetrical nanochannels with an alternating contrasted and expanded cavity within the channels, thus mimicking biological ion channel design as illustrated in Figure 18c. This strategy is definitely viable to be explored further for the recovery of valuable metal ions such as Li^+, Pb^{2+}, Ni^{2+}, Cu^{2+}, Cr^{3+}, Mn^{2+}, and Fe^3.

4.7. Other Related Works. The inclusion of polymers in the MOF composite film has seen applications in lithium recovery by electrochemical adsorption. This was demonstrated by Wang et al.[309] using polypyrrole (PPy)-threaded HKUST-1 on stainless steel mesh, with a Li^+ adsorption capacity of 37.55 mg/g with an adsorption equilibrium time of

https://doi.org/10.1021/acs.iecr.1c00543
Ind. Eng. Chem. Res. XXXX, XXX, XXX−XXX

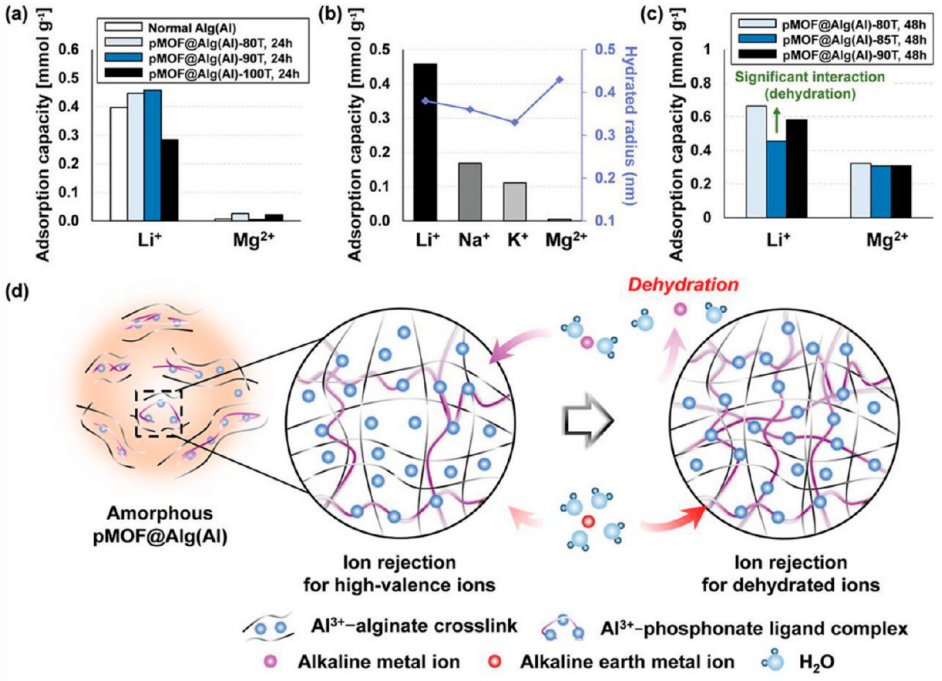

Figure 19. (a) Adsorption capacities of normal Alg(Al), pMOF@Alg(Al)-80T, pMOF@Alg(Al)-90T, and pMOF@Alg(Al)-100T reacted for 24 h on Li^+ and Mg^{2+} ions; (b) adsorption capacities of pMOF@Alg(Al)-90T reacted for 24 h on alkaline and alkaline earth metal ions and hydrated radii of alkaline and alkaline earth metal ions; (c) adsorption capacities of normal Alg(Al), pMOF@Alg(Al)-80T, pMOF@Alg(Al)-90T, and pMOF@Alg(Al)-100T reacted for 48 h on Li^+ and Mg^{2+} ions. (d) Conceptual illustration of the tunable ion sieving behavior on the basis of amorphous structures composed of Al^{3+}−alginate cross-links and Al^{3+}−phosphonate organic ligand complexes in pMOF@Alg(Al). Reprinted in part with permissions from ref 310. Copyright 2019 John Wiley and Sons.

less than 25 min.[309] In this case, the role of PPy is to improve MOF electrochemical performance resulting in ideal selectivity of 35.85 (Li^+/K^+), 19.14 (Li^+/Na^+), and 170.4 (Li^+/Mg^{2+}).[309] However, the authors did not attribute the high selectivity of Li^+ with the pore size of HKUST-1 as the mechanism needed to be studied further.[309] Another group also exploited the tunable sieving of ions in MOFs via the adsorption process in which phosphonate-MOF (p-MOF) was synthesized and incorporated into alginate hydrogels. However, instead of relying on the crystalline pore size of MOF, Park et al.[310] were able to tune the MOF pore size by modulating the intertwinement degree of the amorphous structure of MOF in order to selectively separate ions with different valences (Figure 19d).

In their work, p-MOF in Al^{3+} based alginate hydrogels (p-MOF@Alg(Al)) were amorphized using a partial hydrolysis process in different reaction temperatures of 80, 90, and 100 °C for 24 h. The adsorption results, presented in Figure 19a, show that high Li^+ adsorption was achieved as the temperature increases up to 90 °C.[310] It was shown that the trend of ion adsorption capacity was decreasing with the increasing hydration radius of the ion (Figure 19b). This finding suggests a new technique to control MOF pore size by amorphization instead of choosing MOF based on its rigid pore size. Although these adsorption studies by Wang et al.[309] and Park et al.[310] are not technically in the form of an MOF membrane, the synthesis method and the understanding of how MOF interacts with ions are worth investigation.

5. PERSPECTIVE AND FUTURE DIRECTION

Together with microfiltration and ultrafiltration, RO and NF processes constitute the largest demand for membranes. TFC membranes are widely employed in RO and NF applications, exhibiting high water flux while maintaining high solute rejection. The functionalization and modification of TFC membranes using MOF to create TFN membranes is a promising technique to provide next-generation membranes with enhanced selectivity, permeability, and antifouling properties. There are still limitations that should be studied for further improvement on MOF-functionalized membranes for water and wastewater treatment applications:

- Since MOFs are relatively expensive compared to polymers, the mechanism of MOF filler incorporation into the TFN membrane must be fully understood to minimize the amount of MOF used for functionalization. This may imply particle size and aspect ratio control of MOFs as well as minimization of agglomeration. In addition to the cost, the optimal amount of MOFs should be selected for proper and homogeneous dispersion in the membrane to maximize MOFs effect. Efficient and straightforward methods to avoid MOF aggregation are critically needed.
- MOFs must demonstrate high water stability under different working conditions as those predominating in water and wastewater treatments with membranes. The MOF stability in water has been an ongoing issue that is hindering its large-scale application in liquid phase application.
- Studies related to the long-term stability of MOF-functionalized membranes in harsh environments, where the MOF stability could be highly affected by high temperature, acidic and alkali conditions, etc., are still scarce. Research on this field is thus required for better understanding the behavior of MOF TFN membranes in

https://doi.org/10.1021/acs.iecr.1c00543
Ind. Eng. Chem. Res. XXXX, XXX, XXX−XXX

the representative conditions for certain water and wastewater treatments.

- While the skin layer of the conventional TFC membrane is reported to be as thin as 10−20 nm, the MOFs have to be nanosized and incorporated into the TFN membranes without increasing the skin layer thickness.
- Theoretical studies are needed to understand transport across TFN membranes, particularly when hydrophilic and hydrophobic MOFs can both enhance the water permeance when embedded in polyamide. There is a lack of computational modeling for MOF-functionalized membranes for water and wastewater treatment applications. Almost all of the current computational modeling related to the MOF-functionalized membranes are for the gas separation, for which the results cannot be applied for the aquatic environments.
- The preparation procedures must be tuned to create the optimum surface properties. It has been shown that depending on the dispersion medium, the MOF can relocate to the bottom or the top of the polyamide membrane, affecting, with the same loading, the hydrophilicity and roughness of the membrane.
- Pure MOF membranes are prone to defects from the synthesis method and/or chemical attacks on the MOF-ligand bonds from brine solutions, which could affect the overall selectivity of the membrane. The use of a robust polymeric membrane possesses more interest for industrial application due to the inherent mechanical and chemical stability of the support.
- Most of the MOF functionalization effort has been dedicated to flat-sheet membranes, while more future efforts should be focused on hollow fiber membranes which present clear advantages in terms of process intensification.
- While MOF-based membranes have been studied in detail for other aspects of the wastewater treatment process, more investigations are necessary to understand their performance pertaining specifically to nutrient recovery. To bring MOF-functionalized membranes to industrial applications, it is necessary to overcome the limitations of MOF-functionalized membranes and reduce their fabrication costs to compete with TFC membranes, particularly in recovery-oriented applications, and expand the applications of TFC down to those of commercial membranes, thus making them competitive enough to replace conventional TFC membranes in water and wastewater treatment applications.

AUTHOR INFORMATION

Corresponding Author

Milad Rabbani Esfahani − *Department of Chemical and Biological Engineering, The University of Alabama, Tuscaloosa, Alabama 35487, United States;* orcid.org/0000-0001-6530-4310; Email: mesfahani@eng.ua.edu

Authors

Tin Le − *Department of Chemical and Biological Engineering, The University of Alabama, Tuscaloosa, Alabama 35487, United States*

Xi Chen − *Department of Chemical Engineering, Stanford University, Stanford, California 94305-6104, United States*

Hang Dong − *Department of Chemical Engineering, Stanford University, Stanford, California 94305-6104, United States*

William Tarpeh − *Department of Chemical Engineering, Stanford University, Stanford, California 94305-6104, United States;* orcid.org/0000-0002-2950-526X

Adelaida Perea-Cachero − *Instituto de Nanociencia y Materiales de Aragón (INMA), CSIC-Universidad de Zaragoza, Zaragoza 50018, Spain; Chemical and Environmental Engineering Department, Universidad de Zaragoza, Zaragoza 50018, Spain*

Joaquín Coronas − *Instituto de Nanociencia y Materiales de Aragón (INMA), CSIC-Universidad de Zaragoza, Zaragoza 50018, Spain; Chemical and Environmental Engineering Department, Universidad de Zaragoza, Zaragoza 50018, Spain;* orcid.org/0000-0003-1512-4500

Stephen M. Martin − *Department of Chemical Engineering, Virginia Tech, Blacksburg, Virginia 24061, United States;* orcid.org/0000-0002-8557-7866

Munirah Mohammad − *Centre for Technology in Water and Wastewater, University of Technology Sydney, Sydney, New South Wales 2007, Australia*

Amir Razmjou − *Centre for Technology in Water and Wastewater, University of Technology Sydney, Sydney, New South Wales 2007, Australia; UNESCO Centre for Membrane Science and Technology, School of Chemical Engineering, University of New South Wales, Sydney, New South Wales 2052, Australia;* orcid.org/0000-0002-3554-5129

Amirsalar R. Esfahani − *Department of Mechanical Engineering, The University of Alabama, Tuscaloosa, Alabama 35487, United States; George W. Woodruff School of Mechanical Engineering, Georgia Institute of Technology, Atlanta, Georgia 30332-0002, United States*

Negin Koutahzadeh − *Environmental Health & Safety, The University of Alabama, Tuscaloosa, Alabama 35487, United States*

Peifu Cheng − *Department of Chemical and Biomolecular Engineering, Vanderbilt University, Nashville, Tennessee 37212, United States;* orcid.org/0000-0001-6010-6411

Piran R. Kidambi − *Department of Chemical and Biomolecular Engineering, Vanderbilt University, Nashville, Tennessee 37212, United States;* orcid.org/0000-0003-1546-5014

Complete contact information is available at: https://pubs.acs.org/10.1021/acs.iecr.1c00543

Author Contributions

#All the authors had equal contribution as the first author.

Notes

The authors declare no competing financial interest.

ACKNOWLEDGMENTS

The authors would like to acknowledge the financial support of the National Science Foundation (NSF) under Grant No. 1941700 and NSF Career No. 1944134 and to the Department of the Interior (DOI), Bureau of Reclamation (BR) under Agreement No. R19AC00087. The authors would like to acknowledge the financial support of the United States Geological Survey (USGS) under Sponsor No. 20-WRC-207214 and to the Environmental Protection Agency (EPA) under Award No. 84014501. The financial Spanish Research Projects MAT2016-77290-R (MINECO/AEI, FEDER/UE), PID2019-104009RB-I00 (MICINN/AEI, FEDER/UE), and T43-20R (the Aragón Government and the ESF) are gratefully

acknowledged. The authors also gratefully acknowledge the use of the resources of the Alabama Water Institute and the Department of Chemical and Biological Engineering at The University of Alabama. Any opinions, findings, conclusions, and/or recommendations expressed in this material are those of the authors(s) and do not necessarily reflect the views of the supporting agencies.

REFERENCES

(1) *Global Water Security: Intelligence Community Assessment*; Defense Intelligence Agency, 2012.
(2) Shannon, M. A.; Bohn, P. W.; Elimelech, M.; Georgiadis, J. G.; Marinas, B. J.; Mayes, A. M. Science and Technology for Water Purification in the Coming Decades. *Nanoscience and Technology* **2009**, 337−346.
(3) Ashbolt, N. J. Microbial contamination of drinking water and disease outcomes in developing regions. *Toxicology* **2004**, *198* (1−3), 229−38.
(4) Alipoori, S.; Rouhi, H.; Linn, E.; Stumpfl, H.; Mokarizadeh, H.; Esfahani, M. R.; Koh, A.; Weinman, S. T.; Wujcik, E. K. Polymer-Based Devices and Remediation Strategies for Emerging Contaminants in Water. *ACS Applied Polymer Materials* **2021**, *3*, 549.
(5) Uemura, T.; Kotera, K.; Henmi, M.; Tomioka, H. Membrane technology in seawater desalination: History, recent developments and future prospects. *Desalin. Water Treat.* **2011**, *33* (1−3), 283−288.
(6) Baker, R. W. *Membrane technology and applications*; John Wiley & Sons, 2012.
(7) Strathmann, H. Membrane Separation Processes: Current Relevance and future opportunities. *AIChE J.* **2001**, *47* (5), 1077−1087.
(8) Rezakazemi, M.; Khajeh, A.; Mesbah, M. Membrane filtration of wastewater from gas and oil production. *Environ. Chem. Lett.* **2018**, *16* (2), 367−388.
(9) Esfahani, M. R.; Aktij, S. A.; Dabaghian, Z.; Firouzjaei, M. D.; Rahimpour, A.; Eke, J.; Escobar, I. C.; Abolhassani, M.; Greenlee, L. F.; Esfahani, A. R.; et al. Nanocomposite membranes for water separation and purification: Fabrication, modification, and applications. *Sep. Purif. Technol.* **2019**, *213*, 465−499.
(10) Esfahani, M. R.; Tyler, J. L.; Stretz, H. A.; Wells, M. J. Effects of a dual nanofiller, nano-TiO2 and MWCNT, for polysulfone-based nanocomposite membranes for water purification. *Desalination* **2015**, *372*, 47−56.
(11) Firouzjaei, M. D.; Seyedpour, S. F.; Aktij, S. A.; Giagnorio, M.; Bazrafshan, N.; Mollahosseini, A.; Samadi, F.; Ahmadalipour, S.; Firouzjaei, F. D.; Esfahani, M. R.; Tiraferri, A.; Elliott, M.; Sangermano, M.; Abdelrasoul, A.; McCutcheon, J. R.; Sadrzadeh, M.; Esfahani, A. R.; Rahimpour, A. Recent advances in functionalized polymer membranes for biofouling control and mitigation in forward osmosis. *J. Membr. Sci.* **2020**, *596*, 117604.
(12) Esfahani, M. R.; Koutahzadeh, N.; Esfahani, A. R.; Firouzjaei, M. D.; Anderson, B.; Peck, L. A novel gold nanocomposite membrane with enhanced permeation, rejection and self-cleaning ability. *J. Membr. Sci.* **2019**, *573*, 309−319.
(13) Koutahzadeh, N.; Esfahani, M. R.; Bailey, F.; Taylor, A.; Esfahani, A. R. Enhanced performance of polyhedral oligomeric silsesquioxanes/polysulfone nanocomposite membrane with improved permeability and antifouling properties for water treatment. *J. Environ. Chem. Eng.* **2018**, *6* (5), 5683−5692.
(14) Koutahzadeh, N.; Esfahani, M. R.; Stretz, H. A.; Arce, P. E. Investigation of UV/H2O2 pretreatment effects on humic acid fouling on polysulfone/titanium dioxide—And polysulfone/multiwall carbon nanotube—Nanocomposite ultrafiltration membranes. *Environ. Prog. Sustainable Energy* **2017**, *36* (1), 27−37.
(15) Lee, J.; Farha, O. K.; Roberts, J.; Scheidt, K. A.; Nguyen, S. T.; Hupp, J. T. Metal-organic framework materials as catalysts. *Chem. Soc. Rev.* **2009**, *38* (5), 1450−9.
(16) Qiu, S.; Xue, M.; Zhu, G. Metal-organic framework membranes: from synthesis to separation application. *Chem. Soc. Rev.* **2014**, *43* (16), 6116−6140.
(17) Li, J.; Wang, H.; Yuan, X.; Zhang, J.; Chew, J. W. Metal-organic framework membranes for wastewater treatment and water regeneration. *Coord. Chem. Rev.* **2020**, *404*, 213116.
(18) Liu, Y.; Ng, Z.; Khan, E. A.; Jeong, H. K.; Ching, C. b.; Lai, Z. *Microporous Mesoporous Mater.* **2009**, *118* (1−3), 296−301.
(19) Kwon, H. T.; Jeong, H.-K. In situ synthesis of thin zeolitic-imidazolate framework ZIF-8 membranes exhibiting exceptionally high propylene/propane separation. *J. Am. Chem. Soc.* **2013**, *135* (29), 10763−10768.
(20) Huang, A.; Bux, H.; Steinbach, F.; Caro, J. Molecular-sieve membrane with hydrogen permselectivity: ZIF-22 in LTA topology prepared with 3-aminopropyltriethoxysilane as covalent linker. *Angew. Chem.* **2010**, *122* (29), 5078−5081.
(21) Huang, A.; Dou, W.; Caro, J. r. Steam-stable zeolitic imidazolate framework ZIF-90 membrane with hydrogen selectivity through covalent functionalization. *J. Am. Chem. Soc.* **2010**, *132* (44), 15562−15564.
(22) Guo, H.; Zhu, G.; Hewitt, I. J.; Qiu, S. Twin copper source" growth of metal- organic framework membrane: Cu3 (BTC) 2 with high permeability and selectivity for recycling H2. *J. Am. Chem. Soc.* **2009**, *131* (5), 1646−1647.
(23) Kang, Z.; Xue, M.; Fan, L.; Ding, J.; Guo, L.; Gao, L.; Qiu, S. Single nickel source" in situ fabrication of a stable homochiral MOF membrane with chiral resolution properties. *Chem. Commun.* **2013**, *49* (90), 10569−10571.
(24) Ben, T.; Lu, C.; Pei, C.; Xu, S.; Qiu, S. Polymer-Supported and Free-Standing Metal-Organic Framework Membrane. *Chem. - Eur. J.* **2012**, *18* (33), 10250−10253.
(25) Xie, Z.; Yang, J.; Wang, J.; Bai, J.; Yin, H.; Yuan, B.; Lu, J.; Zhang, Y.; Zhou, L.; Duan, C. Deposition of chemically modified α-Al 2 O 3 particles for high performance ZIF-8 membrane on a macroporous tube. *Chem. Commun.* **2012**, *48* (48), 5977−5979.
(26) Hara, N.; Yoshimune, M.; Negishi, H.; Haraya, K.; Hara, S.; Yamaguchi, T. Diffusive separation of propylene/propane with ZIF-8 membranes. *J. Membr. Sci.* **2014**, *450*, 215−223.
(27) Zhu, Y.; Gupta, K. M.; Liu, Q.; Jiang, J.; Caro, J.; Huang, A. Synthesis and seawater desalination of molecular sieving zeolitic imidazolate framework membranes. *Desalination* **2016**, *385*, 75−82.
(28) Gascon, J.; Aguado, S.; Kapteijn, F. Manufacture of dense coatings of Cu3 (BTC) 2 (HKUST-1) on α-alumina. *Microporous Mesoporous Mater.* **2008**, *113* (1−3), 132−138.
(29) Lee, J. S.; Kim, J. H.; Lee, Y. J.; Jeong, N. C.; Yoon, K. B. Manual assembly of microcrystal monolayers on substrates. *Angew. Chem., Int. Ed.* **2007**, *46* (17), 3087−3090.
(30) Guo, H.; Zhu, Y.; Qiu, S.; Lercher, J. A.; Zhang, H. Coordination Modulation Induced Synthesis of Nanoscale Eu1-xTbx-Metal-Organic Frameworks for Luminescent Thin Films. *Adv. Mater.* **2010**, *22* (37), 4190−4192.
(31) Wee, L. H.; Tosheva, L.; Itani, L.; Valtchev, V.; Doyle, A. M. Steam-assisted synthesis of zeolite films from spin-coated zeolite precursor coatings. *J. Mater. Chem.* **2008**, *18* (30), 3563−3567.
(32) Yin, X.; Zhu, G. S.; Yang, W.; Li, Y.; Zhu, G. Q.; Xu, R.; Sun, J.; Qiu, S.; Xu, R. R. Stainless-Steel-Net-Supported Zeolite NaA Membrane with High Permeance and High Permselectivity of Oxygen over Nitrogen. *Adv. Mater.* **2005**, *17* (16), 2006−2010.
(33) Fan, L.; Xue, M.; Kang, Z.; Li, H.; Qiu, S. Electrospinning technology applied in zeolitic imidazolate framework membrane synthesis. *J. Mater. Chem.* **2012**, *22* (48), 25272−25276.
(34) Efome, J. E.; Rana, D.; Matsuura, T.; Lan, C. Q. Metal-organic frameworks supported on nanofibers to remove heavy metals. *J. Mater. Chem. A* **2018**, *6* (10), 4550−4555.
(35) Hu, Y.; Dong, X.; Nan, J.; Jin, W.; Ren, X.; Xu, N.; Lee, Y. M. Metal-organic framework membranes fabricated via reactive seeding. *Chem. Commun.* **2011**, *47* (2), 737−739.

https://doi.org/10.1021/acs.iecr.1c00543
Ind. Eng. Chem. Res. XXXX, XXX, XXX−XXX

(36) Kasik, A.; James, J.; Lin, Y. S. Synthesis of ZIF-68 membrane on a ZnO modified α-alumina support by a modified reactive seeding method. *Ind. Eng. Chem. Res.* **2016**, *55* (10), 2831−2839.
(37) Nan, J.; Dong, X.; Wang, W.; Jin, W.; Xu, N. Step-by-step seeding procedure for preparing HKUST-1 membrane on porous α-alumina support. *Langmuir* **2011**, *27* (8), 4309−4312.
(38) Shekhah, O.; Wang, H.; Kowarik, S.; Schreiber, F.; Paulus, M.; Tolan, M.; Sternemann, C.; Evers, F.; Zacher, D.; Fischer, R. A.; Woll, C. Step-by-step route for the synthesis of metal- organic frameworks. *J. Am. Chem. Soc.* **2007**, *129* (49), 15118−15119.
(39) Seyedpour, S. F.; Rahimpour, A.; Najafpour, G. Facile in-situ assembly of silver-based MOFs to surface functionalization of TFC membrane: A novel approach toward long-lasting biofouling mitigation. *J. Membr. Sci.* **2019**, *573*, 257−269.
(40) Pejman, M.; Dadashi Firouzjaei, M.; Aghapour Aktij, S.; Das, P.; Zolghadr, E.; Jafarian, H.; Arabi Shamsabadi, A.; Elliott, M.; Sadrzadeh, M.; Sangermano, M.; Rahimpour, A.; Tiraferri, A. In Situ Ag-MOF Growth on Pre-Grafted Zwitterions Imparts Outstanding Antifouling Properties to Forward Osmosis Membranes. *ACS Appl. Mater. Interfaces* **2020**, *12* (32), 36287−36300.
(41) Cadotte, J. E.; King, R. S.; Majerle, R. J.; Petersen, R. J. Interfacial Synthesis in the Preparation of Reverse Osmosis Membranes. *J. Macromol. Sci., Chem.* **1981**, *15* (5), 727−755.
(42) Hermans, S.; Marien, H.; Van Goethem, C.; Vankelecom, I. F. J. Recent developments in thin film (nano)composite membranes for solvent resistant nanofiltration. *Curr. Opin. Chem. Eng.* **2015**, *8*, 45−54.
(43) Freger, V. Nanoscale heterogeneity of polyamide membranes formed by interfacial polymerization. *Langmuir* **2003**, *19* (11), 4791−4797.
(44) Karan, S.; Jiang, Z. W.; Livingston, A. G. Sub-10 nm polyamide nanofilms with ultrafast solvent transport for molecular separation. *Science* **2015**, *348* (6241), 1347−1351.
(45) Kong, C. L.; Shintani, T.; Kamada, T.; Freger, V.; Tsuru, T. Co-solvent-mediated synthesis of thin polyamide membranes. *J. Membr. Sci.* **2011**, *384* (1−2), 10−16.
(46) Zhang, Z.; Kang, G. D.; Yu, H. J.; Jin, Y.; Cao, Y. M. From reverse osmosis to nanofiltration: Precise control of the pore size and charge of polyamide membranes via interfacial polymerization. *Desalination* **2019**, *466*, 16−23.
(47) Jeong, B. H.; Hoek, E. M. V.; Yan, Y. S.; Subramani, A.; Huang, X. F.; Hurwitz, G.; Ghosh, A. K.; Jawor, A. Interfacial polymerization of thin film nanocomposites: A new concept for reverse osmosis membranes. *J. Membr. Sci.* **2007**, *294* (1−2), 1−7.
(48) Peyravi, M.; Jahanshahi, M.; Rahimpour, A.; Javadi, A.; Hajavi, S. Novel thin film nanocomposite membranes incorporated with functionalized TiO2 nanoparticles for organic solvent nanofiltration. *Chem. Eng. J.* **2014**, *241*, 155−166.
(49) Sorribas, S.; Gorgojo, P.; Tellez, C.; Coronas, J.; Livingston, A. G. High Flux Thin Film Nanocomposite Membranes Based on Metal-Organic Frameworks for Organic Solvent Nanofiltration. *J. Am. Chem. Soc.* **2013**, *135* (40), 15201−15208.
(50) Shao, L.; Cheng, X. Q.; Wang, Z. X.; Ma, J.; Guo, Z. H. Tuning the performance of polypyrrole-based solvent-resistant composite nanofiltration membranes by optimizing polymerization conditions and incorporating graphene oxide. *J. Membr. Sci.* **2014**, *452*, 82−89.
(51) Freger, V. Kinetics of film formation by interfacial polycondensation. *Langmuir* **2005**, *21* (5), 1884−1894.
(52) Van Goethem, C.; Verbeke, R.; Hermans, S.; Bernstein, R.; Vankelecom, I. F. J. Controlled positioning of MOFs in interfacially polymerized thin-film nanocomposites. *J. Mater. Chem. A* **2016**, *4* (42), 16368−16376.
(53) Wang, L. Y.; Fang, M. Q.; Liu, J.; He, J.; Li, J. D.; Lei, J. D. Layer-by-Layer Fabrication of High-Performance Polyamide/ZIF-8 Nanocomposite Membrane for Nanofiltration Applications. *ACS Appl. Mater. Interfaces* **2015**, *7* (43), 24082−24093.
(54) Paseta, L.; Antoran, D.; Coronas, J.; Tellez, C. 110th Anniversary: Polyamide/Metal-Organic Framework Bilayered Thin Film Composite Membranes for the Removal of Pharmaceutical Compounds from Water. *Ind. Eng. Chem. Res.* **2019**, *58* (10), 4222−4230.
(55) Sarango, L.; Paseta, L.; Navarro, M.; Zornoza, B.; Coronas, J. Controlled deposition of MOFs by dip-coating in thin film nanocomposite membranes for organic solvent nanofiltration. *J. Ind. Eng. Chem.* **2018**, *59*, 8−16.
(56) Navarro, M.; Benito, J.; Paseta, L.; Gascon, I.; Coronas, J.; Tellez, C. Thin-Film Nanocomposite Membrane with the Minimum Amount of MOF by the Langmuir-Schaefer Technique for Nanofiltration. *ACS Appl. Mater. Interfaces* **2018**, *10* (1), 1278−1287.
(57) Wang, L. Y.; Fang, M. Q.; Liu, J.; He, J.; Deng, L. H.; Lib, J. D.; Lei, J. D. The influence of dispersed phases on polyamide/ZIF-8 nanofiltration membranes for dye removal from water. *RSC Adv.* **2015**, *5* (63), 50942−50954.
(58) Aljundi, I. H. Desalination characteristics of TFN-RO membrane incorporated with ZIF-8 nanoparticles. *Desalination* **2017**, *420*, 12−20.
(59) Xiao, F.; Wang, B.; Hu, X. Y.; Nair, S.; Chen, Y. B. Thin film nanocomposite membrane containing zeolitic imidazolate framework-8 via interfacial polymerization for highly permeable nanofiltration. *J. Taiwan Inst. Chem. Eng.* **2018**, *83*, 159−167.
(60) Lee, T. H.; Oh, J. Y.; Hong, S. P.; Lee, J. M.; Roh, S. M.; Kim, S. H.; Park, H. B. ZIF-8 particle size effects on reverse osmosis performance of polyamide thin-film nanocomposite membranes: Importance of particle deposition. *J. Membr. Sci.* **2019**, *570*, 23−33.
(61) Zhang, D. P.; Yao, Z. C.; Zhang, H.; Zhu, G. R.; Liu, L.; Gao, C. J. A novel strategy to fabricate thin film nanocomposite reverse osmosis membranes with enhanced desalination performance. *Desalination and Water Treatment* **2019**, *145*, 70−82.
(62) Lee, T. H.; Park, I.; Oh, J. Y.; Jang, J. K.; Park, H. B. Facile Preparation of Polyamide Thin-Film Nanocomposite Membranes Using Spray-Assisted Nanofiller Predeposition. *Ind. Eng. Chem. Res.* **2019**, *58* (10), 4248−4256.
(63) Zhai, Z.; Zhao, N.; Dong, W. J.; Li, P.; Sun, H. X.; Niu, Q. J. In Situ Assembly of a Zeolite Imidazolate Framework Hybrid Thin-Film Nanocomposite Membrane with Enhanced Desalination Performance Induced by Noria Polyethyleneimine Codeposition. *ACS Appl. Mater. Interfaces* **2019**, *11* (13), 12871−12879.
(64) Zhao, Y. Y.; Liu, Y. L.; Wang, X. M.; Huang, X.; Xie, Y. F. F. Impacts of Metal-Organic Frameworks on Structure and Performance of Polyamide Thin-Film Nanocomposite Membranes. *ACS Appl. Mater. Interfaces* **2019**, *11* (14), 13724−13734.
(65) Shafiei, M.; Hajian, M. Poly(vinyl butyral)/zeolitic imidazole framework-8/poly(vinyl alcohol) thin-film nanocomposite nanofiltration membrane: synthesis and characterization. *Iran. Polym. J.* **2019**, *28* (8), 659−672.
(66) Paseta, L.; Navarro, M.; Coronas, J.; Téllez, C. Greener processes in the preparation of thin film nanocomposite membranes with diverse metal-organic frameworks for organic solvent nanofiltration. *J. Ind. Eng. Chem.* **2019**, *77*, 344−354.
(67) Wang, F. H.; Zheng, T.; Xiong, R. H.; Wang, P. P.; Ma, J. Strong improvement of reverse osmosis polyamide membrane performance by addition of ZIF-8 nanoparticles: Effect of particle size and dispersion in selective layer. *Chemosphere* **2019**, *233*, 524−531.
(68) Lee, T. H.; Roh, J. S.; Yoo, S. Y.; Roh, J. M.; Choi, T. H.; Park, H. B. High-Performance Polyamide Thin-Film Nanocomposite Membranes Containing ZIF-8/CNT Hybrid Nanofillers for Reverse Osmosis Desalination. *Ind. Eng. Chem. Res.* **2020**, *59* (12), 5324−5332.
(69) Duan, J. T.; Pan, Y. C.; Pacheco, F.; Litwiller, E.; Lai, Z. P.; Pinnau, I. High-performance polyamide thin-film-nanocomposite reverse osmosis membranes containing hydrophobic zeolitic imidazolate framework-8. *J. Membr. Sci.* **2015**, *476*, 303−310.
(70) Echaide-Górriz, C.; Sorribas, S.; Téllez, C.; Coronas, J. MOF nanoparticles of MIL-68(Al), MIL-101(Cr) and ZIF-11 for thin film nanocomposite organic solvent nanofiltration membranes. *RSC Adv.* **2016**, *6* (93), 90417−90426.

https://doi.org/10.1021/acs.iecr.1c00543
Ind. Eng. Chem. Res. XXXX, XXX, XXX−XXX

(71) Echaide-Górriz, C.; Navarro, M.; Téllez, C.; Coronas, J. Simultaneous use of MOFs MIL-101(Cr) and ZIF-11 in thin film nanocomposite membranes for organic solvent nanofiltration. *Dalton Transactions* **2017**, *46* (19), 6244−6252.
(72) Xu, Y.; Gao, X. L.; Wang, X. J.; Wang, Q.; Ji, Z. Y.; Wang, X. Y.; Wu, T.; Gao, C. J. Highly and Stably Water Permeable Thin Film Nanocomposite Membranes Doped with MIL-101 (Cr) Nanoparticles for Reverse Osmosis Application. *Materials* **2016**, *9* (11), 870.
(73) Butler, E. L.; Petit, C.; Livingston, A. G. Poly(piperazine trimesamide) thin film nanocomposite membrane formation based on MIL-101: Filler aggregation and interfacial polymerization dynamics. *J. Membr. Sci.* **2020**, *596*, 117482.
(74) Kadhom, M.; Hu, W. M.; Deng, B. L. Thin Film Nanocomposite Membrane Filled with Metal-Organic Frameworks UiO-66 and MIL-125 Nanoparticles for Water Desalination. *Membranes* **2017**, *7* (2), 31.
(75) Dai, R. B.; Zhang, X. R.; Liu, M. X.; Wu, Z. C.; Wang, Z. W. Porous metal organic framework CuBDC nanosheet incorporated thin-film nanocomposite membrane for high-performance forward osmosis. *J. Membr. Sci.* **2019**, *573*, 46−54.
(76) Wen, Y.; Chen, Y. Q.; Wu, Z. C.; Liu, M. X.; Wang, Z. W. Thin-film nanocomposite membranes incorporated with water stable metal-organic framework CuBTTri for mitigating biofouling. *J. Membr. Sci.* **2019**, *582*, 289−297.
(77) Dumee, L. F.; Maina, J. W.; Merenda, A.; Reis, R.; He, L.; Kong, L. X. Hybrid thin film nano-composite membrane reactors for simultaneous separation and degradation of pesticides. *J. Membr. Sci.* **2017**, *528*, 217−224.
(78) He, Y. R.; Tang, Y. P.; Ma, D. C.; Chung, T. S. UiO-66 incorporated thin-film nanocomposite membranes for efficient selenium and arsenic removal. *J. Membr. Sci.* **2017**, *541*, 262−270.
(79) Ji, C. H.; Xue, S. M.; Tang, Y. J.; Ma, X. H.; Xu, Z. L. Polyamide Membranes with Net-Like Nanostructures Induced by Different Charged MOFs for Elevated Nanofiltration. *Acs Applied Polymer Materials* **2020**, *2* (2), 585−593.
(80) Liu, H. R.; Zhang, M.; Zhao, H.; Jiang, Y. J.; Liu, G. H.; Gao, J. Enhanced dispersibility of metal-organic frameworks (MOFs) in the organic phase via surface modification for TFN nanofiltration membrane preparation. *RSC Adv.* **2020**, *10* (7), 4045−4057.
(81) Xiao, F.; Hu, X. Y.; Chen, Y. B.; Zhang, Y. F. Porous Zr-Based Metal-Organic Frameworks (Zr-MOFs)-Incorporated Thin-Film Nanocomposite Membrane toward Enhanced Desalination Performance. *ACS Appl. Mater. Interfaces* **2019**, *11* (50), 47390−47403.
(82) Liu, L. F.; Xie, X.; Qi, S. R.; Li, R. H.; Zhang, X.; Song, X. X.; Gao, C. J. Thin film nanocomposite reverse osmosis membrane incorporated with UiO-66 nanoparticles for enhanced boron removal. *J. Membr. Sci.* **2019**, *580*, 101−109.
(83) Ma, D.; Peh, S. B.; Han, G.; Chen, S. B. Thin-Film Nanocomposite (TFN) Membranes Incorporated with Super-Hydrophilic Metal-Organic Framework (MOF) UiO-66: Toward Enhancement of Water Flux and Salt Rejection. *ACS Appl. Mater. Interfaces* **2017**, *9* (8), 7523−7534.
(84) Cheng, X. Q.; Jiang, X.; Zhang, Y. Q.; Lau, C. H.; Xie, Z. L.; Ng, D.; Smith, S. J. D.; Hill, M. R.; Shao, L. Building Additional Passageways in Polyamide Membranes with Hydrostable Metal Organic Frameworks To Recycle and Remove Organic Solutes from Various Solvents. *ACS Appl. Mater. Interfaces* **2017**, *9* (44), 38877−38886.
(85) Firouzjaei, M. D.; Shamsabadi, A. A.; Aktij, S. A.; Seyedfour, S. F.; Sharifian Gh, M.; Rahimpour, A.; Esfahani, M. R.; Ulbricht, M.; Soroush, M. Exploiting Synergetic Effects of Graphene Oxide and a Silver-Based Metal-Organic Framework To Enhance Antifouling and Anti-Biofouling Properties of Thin-Film Nanocomposite Membranes. *ACS Appl. Mater. Interfaces* **2018**, *10* (49), 42967−42978.
(86) Zirehpour, A.; Rahimpour, A.; Ulbricht, M. Nano-sized metal organic framework to improve the structural properties and desalination performance of thin film composite forward osmosis membrane. *J. Membr. Sci.* **2017**, *531*, 59−67.
(87) Golpour, M.; Pakizeh, M. Preparation and characterization of new PA-MOF/PPSU-GO membrane for the separation of KHI from water. *Chem. Eng. J.* **2018**, *345*, 221−232.
(88) Gong, Y. Q.; Gao, S. J.; Tian, Y. Y.; Zhu, Y. Z.; Fang, W. X.; Wang, Z. G.; Jin, J. Thin-film nanocomposite nanofiltration membrane with an ultrathin polyamide/UIO-66-NH2 active layer for high-performance desalination. *J. Membr. Sci.* **2020**, *600*, 600.
(89) Bagherzadeh, M.; Bayrami, A.; Amini, M. Thin-film nanocomposite forward osmosis membranes modified with Zr-based metal-organic framework to improve desalination performance. *Appl. Organomet. Chem.* **2020**, *34* (2), 5339 DOI: 10.1002/aoc.5339.
(90) Zhang, X.; Zhang, Y. F.; Wang, T. C.; Fan, Z.; Zhang, G. L. A thin film nanocomposite membrane with pre-immobilized UiO-66-NH2 toward enhanced nanofiltration performance. *RSC Adv.* **2019**, *9* (43), 24802−24810.
(91) Zhu, J. Y.; Hou, J. W.; Yuan, S. S.; Zhao, Y.; Li, Y.; Zhang, R. J.; Tian, M. M.; Li, J.; Wang, J.; Van der Bruggen, B. MOF-positioned polyamide membranes with a fishnet-like structure for elevated nanofiltration performance. *J. Mater. Chem. A* **2019**, *7* (27), 16313−16322.
(92) Liu, H. R.; Gao, J.; Liu, G. H.; Zhang, M. Y.; Jiang, Y. J. Enhancing Permeability of Thin Film Nanocomposite Membranes via Covalent Linking of Polyamide with the Incorporated Metal-Organic Frameworks. *Ind. Eng. Chem. Res.* **2019**, *58* (20), 8772−8783.
(93) Wang, L. Y.; Duan, S. X.; Fang, M. Q.; Liu, J.; He, J.; Li, J. D.; Lei, J. D. Surface modification route to prepare novel polyamide@NH2_MIL-88B nanocomposite membranes for water treatment. *RSC Adv.* **2016**, *6* (75), 71250−71261.
(94) Gohain, M. B.; Pawar, R. R.; Karki, S.; Hazarika, A.; Hazarika, S.; Ingole, P. G. Development of thin film nanocomposite membrane incorporated with mesoporous synthetic hectorite and MSH@UiO-66-NH2 nanoparticles for efficient targeted feeds separation, and antibacterial performance. *J. Membr. Sci.* **2020**, *609*, 609.
(95) Van Goethem, C.; Verbeke, R.; Pfanmöller, M.; Koschine, T.; Dickmann, M.; Timpel-Lindner, T.; Egger, W.; Bals, S.; Vankelecom, I. F. J. The role of MOFs in Thin-Film Nanocomposite (TFN) membranes. *J. Membr. Sci.* **2018**, *563*, 938−948.
(96) Beh, J. J.; Ooi, B. S.; Lim, J. K.; Ng, E. P.; Mustapa, H. Development of high water permeability and chemically stable thin film nanocomposite (TFN) forward osmosis (FO) membrane with poly(sodium 4-styrenesulfonate) (PSS)-coated zeolitic imidazolate framework-8 (ZIF-8) for produced water treatment. *Journal of Water Process Engineering* **2020**, *33*, 33.
(97) Zhang, G. H.; Zhang, J.; Lv, P. H.; Sun, J.; Zhao, P. G.; Yang, L. L. Modifying thin film composite membrane with zeolitic imidazolate framework-8@polydopamine for enhanced antifouling property. *Chemosphere* **2020**, *248*, 248.
(98) Li, M. P.; Zhang, X.; Zhang, H.; Liu, W. L.; Huang, Z. H.; Xie, F.; Ma, X. H.; Xu, Z. L. Hydrophilic yolk-shell ZIF-8 modified polyamide thin-film nanocomposite membrane with improved permeability and selectivity. *Sep. Purif. Technol.* **2020**, 247.
(99) Qiu, M.; He, C. J. Efficient removal of heavy metal ions by forward osmosis membrane with a polydopamine modified zeolitic imidazolate framework incorporated selective layer. *J. Hazard. Mater.* **2019**, *367*, 339−347.
(100) Zhu, J. Y.; Qin, L. J.; Uliana, A.; Hou, J. W.; Wang, J.; Zhang, Y. T.; Li, X.; Yuan, S. S.; Li, J.; Tian, M. M.; Lin, J. Y.; Van der Bruggen, B. Elevated Performance of Thin Film Nanocomposite Membranes Enabled by Modified Hydrophilic MOFs for Nanofiltration. *ACS Appl. Mater. Interfaces* **2017**, *9* (2), 1975−1986.
(101) Wang, F. H.; Zheng, T.; Xiong, R. H.; Wang, P. P.; Ma, J. CDs@ZIF-8 Modified Thin Film Polyamide Nanocomposite Membrane for Simultaneous Enhancement of Chlorine-Resistance and Disinfection Byproducts Removal in Drinking Water. *ACS Appl. Mater. Interfaces* **2019**, *11* (36), 33033−33042.
(102) Xu, S. J.; Shen, Q.; Chen, G. E.; Xu, Z. L. Novel beta-CD@ZIF-8 Nanoparticles-Doped Poly(m-phenylene isophthalamide) (PMIA) Thin -Film Nanocomposite (TFN) Membrane for Organic

Solvent Nanofiltration (OSN). *Acs Omega* **2018**, *3* (9), 11770−11787.
(103) Liao, Z. P.; Fang, X. F.; Xie, J.; Li, Q.; Wang, D. P.; Sun, X. Y.; Wang, L. J.; Li, J. S. Hydrophilic Hollow Nanocube-Functionalized Thin Film Nanocomposite Membrane with Enhanced Nanofiltration Performance. *ACS Appl. Mater. Interfaces* **2019**, *11* (5), 5344−5352.
(104) Li, T.; Zhang, W. M.; Zhai, S.; Gao, G. D.; Ding, J.; Zhang, W. B.; Liu, Y.; Zhao, X.; Pan, B. C.; Lv, L. Efficient removal of nickel(II) from high salinity wastewater by a novel PAA/ZIF-8/PVDF hybrid ultrafiltration membrane. *Water Res.* **2018**, *143*, 87−98.
(105) Zhang, R.; Ji, S. L.; Wang, N. X.; Wang, L.; Zhang, G. J.; Li, J. R. Coordination-Driven In Situ Self-Assembly Strategy for the Preparation of Metal-Organic Framework Hybrid Membranes. *Angew. Chem., Int. Ed.* **2014**, *53* (37), 9775−9779.
(106) Lin, Y. Q.; Chen, Y. F.; Wang, R. Thin film nanocomposite hollow fiber membranes incorporated with surface functionalized HKUST-1 for highly-efficient reverses osmosis desalination process. *J. Membr. Sci.* **2019**, *589*, 589.
(107) Bagherzadeh, M.; Bayrami, A.; Amini, M. Enhancing forward osmosis (FO) performance of polyethersulfone/polyamide (PES/PA) thin-film composite membrane via the incorporation of GQDs@UiO-66-NH2 particles. *Journal of Water Process Engineering* **2020**, 33.
(108) Zhao, P. X.; Li, R.; Wu, W. J.; Wang, J.; Liu, J. D.; Zhang, Y. In-situ growth of polyvinylpyrrolidone modified Zr-MOFs thin-film nanocomposite (TFN) for efficient dyes removal. *Composites Part B-Engineering* **2019**, 176.
(109) Guo, X. Y.; Liu, D. H.; Han, T. T.; Huang, H. L.; Yang, Q. Y.; Zhong, C. L. Preparation of Thin Film Nanocomposite Membranes with Surface Modified MOF for High Flux Organic Solvent Nanofiltration. *AIChE J.* **2017**, *63* (4), 1303−1312.
(110) Nasir, A. M.; Goh, P. S.; Ismail, A. F., Chapter 3 - Synthesis route for the fabrication of nanocomposite membranes. In *Nanocomposite Membranes for Water and Gas Separation*; Sadrzadeh, M., Mohammadi, T., Eds.; Elsevier, 2020; pp 69−89.
(111) Mulder, M., Preparation of Synthetic Membranes. In *Basic Principles of Membrane Technology*; Mulder, M., Ed.; Springer Netherlands: Dordrecht, 1991; pp 54−109.
(112) Asad, A.; Sameoto, D.; Sadrzadeh, M., Chapter 1 - Overview of membrane technology. In *Nanocomposite Membranes for Water and Gas Separation*; Sadrzadeh, M., Mohammadi, T., Eds.; Elsevier, 2020; pp 1−28.
(113) Zare, S.; Kargari, A. Membrane properties in membrane distillation. *Emerging Technologies for Sustainable Desalination Handbook* **2018**, 107−156.
(114) Sun, H. Z.; Tang, B. B.; Wu, P. Y. Hydrophilic hollow zeolitic imidazolate framework-8 modified ultrafiltration membranes with significantly enhanced water separation properties. *J. Membr. Sci.* **2018**, *551*, 283−293.
(115) Low, Z. X.; Razmjou, A.; Wang, K.; Gray, S.; Duke, M.; Wang, H. T. Effect of addition of two-dimensional ZIF-L nanoflakes on the properties of polyethersulfone ultrafiltration membrane. *J. Membr. Sci.* **2014**, *460*, 9−17.
(116) Ruan, H. M.; Guo, C. M.; Yu, H. W.; Shen, J. N.; Gao, C. J.; Sotto, A.; Van der Bruggen, B. Fabrication of a MIL-53(Al) Nanocomposite Membrane and Potential Application in Desalination of Dye Solutions. *Ind. Eng. Chem. Res.* **2016**, *55* (46), 12099−12110.
(117) Tan, Y. M.; Sun, Z. Q.; Meng, H.; Han, Y. D.; Wu, J. B.; Xu, J. L.; Xu, Y.; Zhang, X. A new MOFs/polymer hybrid membrane: MIL-68(Al)/PVDF, fabrication and application in high-efficient removal of p-nitrophenol and methylene blue. *Sep. Purif. Technol.* **2019**, *215*, 217−226.
(118) Misdan, N.; Ramlee, N.; Hairom, N. H. H.; Ikhsan, S. N. W.; Yusof, N.; Lau, W. L.; Ismail, A. F.; Nordin, N. CuBTC metal organic framework incorporation for enhancing separation and antifouling properties of nanofiltration membrane. *Chemical Engineering Research & Design* **2019**, *148*, 227−239.
(119) Mazani, M.; Aktij, S. A.; Rahimpour, A.; Kiadeh, N. T. H. Cu-BTC Metal-Organic Framework Modified Membranes for Landfill Leachate Treatment. *Water* **2020**, *12* (1), 91 DOI: 10.3390/w12010091.
(120) Yang, S. J.; Zou, Q. F.; Wang, T. H.; Zhang, L. P. Effects of GO and MOF@GO on the permeation and antifouling properties of cellulose acetate ultrafiltration membrane. *J. Membr. Sci.* **2019**, *569*, 48−59.
(121) Makhetha, T. A.; Moutloali, R. M. Antifouling properties of Cu(tpa)@GO/PES composite membranes and selective dye rejection. *J. Membr. Sci.* **2018**, *554*, 195−210.
(122) Sun, H. Z.; Tang, B. B.; Wu, P. Y. Development of Hybrid Ultrafiltration Membranes with Improved Water Separation Properties Using Modified Superhydrophilic Metal-Organic Framework Nanoparticles. *ACS Appl. Mater. Interfaces* **2017**, *9* (25), 21473−21484.
(123) Ma, J.; Guo, X. Y.; Ying, Y. P.; Liu, D. H.; Zhong, C. L. Composite ultrafiltration membrane tailored by MOF@GO with highly improved water purification performance. *Chem. Eng. J.* **2017**, *313*, 890−898.
(124) Gnanasekaran, G.; Balaguru, S.; Arthanareeswaran, G.; Das, D. B. Removal of hazardous material from wastewater by using metal organic framework (MOF) embedded polymeric membranes. *Sep. Sci. Technol.* **2019**, *54* (3), 434−446.
(125) Xu, W. T.; Zhuang, H. Q.; Xu, Z. H.; Huang, M. L.; Gao, S. C.; Li, Q. B.; Zhang, G. L. Design and Construction of Ag@MOFs Immobilized PVDF Ultrafiltration Membranes with Anti-bacterial and Antifouling Properties. *Advances in Polymer Technology* **2020**, 2020.
(126) Mohammadnezhad, F.; Feyzi, M.; Zinadini, S. A novel Ce-MOF/PES mixed matrix membrane; synthesis, characterization and antifouling evaluation. *J. Ind. Eng. Chem.* **2019**, *71*, 99−111.
(127) Sotto, A.; Orcajo, G.; Arsuaga, J. M.; Calleja, G.; Landaburu-Aguirre, J. Preparation and characterization of MOF-PES ultrafiltration membranes. *J. Appl. Polym. Sci.* **2015**, *132* (21), 41633 DOI: 10.1002/app.41633.
(128) Gholami, F.; Zinadini, S.; Zinatizadeh, A. A.; Abbasi, A. R. TMU-5 metal-organic frameworks (MOFs) as a novel nanofiller for flux increment and fouling mitigation in PES ultrafiltration membrane. *Sep. Purif. Technol.* **2018**, *194*, 272−280.
(129) Huang, A. S.; Liu, Q.; Wang, N. Y.; Zhu, Y. Q.; Caro, J. Bicontinuous Zeolitic Imidazolate Framework ZIF-8@GO Membrane with Enhanced Hydrogen Selectivity. *J. Am. Chem. Soc.* **2014**, *136* (42), 14686−14689.
(130) Zinadini, S.; Zinatizadeh, A. A.; Rahimi, M.; Vatanpour, V.; Zangeneh, H. Preparation of a novel antifouling mixed matrix PES membrane by embedding graphene oxide nanoplates. *J. Membr. Sci.* **2014**, *453*, 292−301.
(131) Yang, S. Y.; Lin, W. N.; Huang, Y. L.; Tien, H. W.; Wang, J. Y.; Ma, C. C. M.; Li, S. M.; Wang, Y. S. Synergetic effects of graphene platelets and carbon nanotubes on the mechanical and thermal properties of epoxy composites. *Carbon* **2011**, *49* (3), 793−803.
(132) Chung, T. S.; Hu, X. D. Effect of air-gap distance on the morphology and thermal properties of polyethersulfone hollow fibers. *J. Appl. Polym. Sci.* **1997**, *66* (6), 1067−1077.
(133) Deshmukh, S. P.; Li, K. Effect of ethanol composition in water coagulation bath on morphology of PVDF hollow fibre membranes. *J. Membr. Sci.* **1998**, *150* (1), 75−85.
(134) Varezhkin, A. V. Wet spinning of asymmetric hollow polysulfone fibres by the double spinning bath method. *Fibre Chem.* **1994**, *25* (6), 458−462.
(135) Prince, J. A.; Bhuvana, S.; Anbharasi, V.; Ayyanar, N.; Boodhoo, K. V. K.; Singh, G. Self-cleaning Metal Organic Framework (MOF) based ultra filtration membranes A solution to bio-fouling in membrane separation processes. *Sci. Rep.* **2014**, 4.
(136) Cheng, D. J.; Zhao, L. H.; Li, N.; Smith, S. J. D.; Wu, D. Y.; Zhang, J. H.; Ng, D.; Wu, C. R.; Martinez, M. R.; Batten, M. P.; Xie, Z. L. Aluminum fumarate MOF/PVDF hollow fiber membrane for enhancement of water flux and thermal efficiency in direct contact membrane distillation. *J. Membr. Sci.* **2019**, *588*, 117204.
(137) Zhao, J.; Luo, G. X.; Wu, J.; Xia, H. S. Preparation of Microporous Silicone Rubber Membrane with Tunable Pore Size via

Solvent Evaporation-Induced Phase Separation. *ACS Appl. Mater. Interfaces* **2013**, *5* (6), 2040−2046.
(138) You, M.; Yin, J.; Sun, R. B.; Cao, X. Z.; Meng, J. Q. Water/salt transport properties of organic/inorganic hybrid films based on cellulose triacetate. *J. Membr. Sci.* **2018**, *563*, 571−583.
(139) Yu, C. X.; Liu, Y. Y.; Zhang, X. Preparation of Cu-BTC/PVDF Hybrid Membranes Using in situ Doping Method and Their Enhanced Dye Adsorption Properties. *Chem. J. Chin. Univ.-Chin.* **2018**, *39* (7), 1384−1391.
(140) Yao, B. J.; Jiang, W. L.; Dong, Y.; Liu, Z. X.; Dong, Y. B. Post-Synthetic Polymerization of UiO-66-NH2 Nanoparticles and Polyurethane Oligomer toward Stand-Alone Membranes for Dye Removal and Separation. *Chem. - Eur. J.* **2016**, *22* (30), 10565−10571.
(141) Liu, T. Y.; Yuan, H. G.; Liu, Y. Y.; Ren, D.; Su, Y. C.; Wang, X. L. Metal-Organic Framework Nanocomposite Thin Films with Interfacial Bindings and Self-Standing Robustness for High Water Flux and Enhanced Ion Selectivity. *ACS Nano* **2018**, *12* (9), 9253−9265.
(142) Ren, Y.; Li, T.; Zhang, W. M.; Wang, S.; Shi, M. Q.; Shan, C.; Zhang, W. B.; Guan, X. H.; Lv, L.; Hua, M.; Pan, B. C. MIL-PVDF blend ultrafiltration membranes with ultrahigh MOF loading for simultaneous adsorption and catalytic oxidation of methylene blue. *J. Hazard. Mater.* **2019**, *365*, 312−321.
(143) Wang, H.; Zhao, S.; Liu, Y.; Yao, R. X.; Wang, X. Q.; Cao, Y. H.; Ma, D.; Zou, M. C.; Cao, A. Y.; Feng, X.; Wang, B. Membrane adsorbers with ultrahigh metal-organic framework loading for high flux separations. *Nat. Commun.* **2019**, *10*, 10.
(144) Gopal, R.; Kaur, S.; Ma, Z. W.; Chan, C.; Ramakrishna, S.; Matsuura, T. Electrospun nanofibrous filtration membrane. *J. Membr. Sci.* **2006**, *281* (1−2), 581−586.
(145) Greiner, A.; Wendorff, J. H. Electrospinning: A fascinating method for the preparation of ultrathin fibres. *Angew. Chem., Int. Ed.* **2007**, *46* (30), 5670−5703.
(146) Bassyouni, M.; Abdel-Aziz, M. H.; Zoromba, M. S.; Abdel-Hamid, S. M. S.; Drioli, E. A review of polymeric nanocomposite membranes for water purification. *J. Ind. Eng. Chem.* **2019**, *73*, 19−46.
(147) Jamshidifard, S.; Koushkbaghi, S.; Hosseini, S.; Rezaei, S.; Karamipour, A.; Rad, A. J.; Irani, M. Incorporation of UiO-66-NH2MOF into the PAN/chitosan nanofibers for adsorption and membrane filtration of Pb(II), Cd(II) and Cr(VI) ions from aqueous solutions. *J. Hazard. Mater.* **2019**, *368*, 10−20.
(148) Yang, F.; Efome, J. E.; Rana, D.; Matsuura, T.; Lan, C. Metal-Organic Frameworks Supported on Nanofiber for Desalination by Direct Contact Membrane Distillation. *ACS Appl. Mater. Interfaces* **2018**, *10* (13), 11251−11260.
(149) Efome, J. E.; Rana, D.; Matsuura, T.; Lan, C. Q. Insight Studies on Metal-Organic Framework Nanofibrous Membrane Adsorption and Activation for Heavy Metal Ions Removal from Aqueous Solution. *ACS Appl. Mater. Interfaces* **2018**, *10* (22), 18619−18629.
(150) Dai, X.; Cao, Y.; Shi, X. W.; Wang, X. L. The PLA/ZIF-8 Nanocomposite Membranes: The Diameter and Surface Roughness Adjustment by ZIF-8 Nanoparticles, High Wettability, Improved Mechanical Property, and Efficient Oil/Water Separation. *Adv. Mater. Interfaces* **2016**, *3* (24), 1600725.
(151) Li, A. W.; Zhou, M. M.; Luo, P. P.; Shang, J. X.; Wang, P. B.; Lyu, L. X. Deposition of MOFs on Polydopamine-Modified Electrospun Polyvinyl Alcohol/Silica Nanofibers Mats for Chloramphenicol Adsorption in Water. *Nano* **2020**, *15* (4), 2050046.
(152) Jin, L.; Ye, J.; Wang, Y.; Qian, X. Y.; Dong, M. D. Electrospinning Synthesis of ZIF-67/PAN Fibrous Membrane with High-capacity Adsorption for Malachite Green. *Fibers Polym.* **2019**, *20* (10), 2070−2077.
(153) Mahmoodi, N. M.; Keshavarzi, S.; Oveisi, M.; Rahimi, S.; Hayati, B. Metal-organic framework (ZIF-8)/inorganic nanofiber (Fe2O3) nanocomposite: Green synthesis and photocatalytic degradation using LED irradiation. *J. Mol. Liq.* **2019**, *291*, 291.
(154) Xu, S.; Ren, L. F.; Zhou, Q.; Bai, H. W.; Li, J.; Shao, J. H. Facile ZIF-8 functionalized hierarchical micronanofiber membrane for high-efficiency separation of water-in-oil emulsions. *J. Appl. Polym. Sci.* **2018**, *135* (27), 46462.
(155) Hong, Y.; Liu, C.; Cao, X.; Chen, Y.; Chen, C.; Chen, Y.; Pan, Z. Process Evaluation of the Metal-Organic Frameworks for the Application of Personal Protective Equipment with Filtration Function. *Polymers* **2018**, *10* (12), 1386.
(156) Shooto, N. D.; Dikio, C. W.; Wankasi, D.; Sikhwivhilu, L. M.; Mtunzi, F. M.; Dikio, E. D. Novel PVA/MOF Nanofibres: Fabrication, Evaluation and Adsorption of Lead Ions from Aqueous Solution. *Nanoscale Res. Lett.* **2016**, *11*, 11.
(157) Wang, C. H.; Wang, H. Y.; Luo, R.; Liu, C.; Li, J. S.; Sun, X. Y.; Shen, J. Y.; Han, W. Q.; Wang, L. J. Metal-organic framework one-dimensional fibers as efficient catalysts for activating peroxymonosulfate. *Chem. Eng. J.* **2017**, *330*, 262−271.
(158) Efome, J. E.; Rana, D.; Matsuura, T.; Lan, C. Q. Metal-organic frameworks supported on nanofibers to remove heavy metals. *J. Mater. Chem. A* **2018**, *6* (10), 4550−4555.
(159) Guo, R. X.; Cai, X. H.; Liu, H. W.; Yang, Z.; Meng, Y. J.; Chen, F. J.; Li, Y. J.; Wang, B. D. In Situ Growth of Metal-Organic Frameworks in Three-Dimensional Aligned Lumen Arrays of Wood for Rapid and Highly Efficient Organic Pollutant Removal. *Environ. Sci. Technol.* **2019**, *53* (5), 2705−2712.
(160) Li, X. Y.; Zhang, H. C.; Wang, P. Y.; Hou, J.; Lu, J.; Easton, C. D.; Zhang, X. W.; Hill, M. R.; Thornton, A. W.; Liu, J. Z.; Freeman, B. D.; Hill, A. J.; Jiang, L.; Wang, H. T. Fast and selective fluoride ion conduction in sub-1-nanometer metal-organic framework channels. *Nat. Commun.* **2019**, *10*, 10.
(161) Sharma, P.; Shahi, V. K. Assembly of MIL-101(Cr)-sulphonated poly(ether sulfone) membrane matrix for selective electrodialytic separation of Pb2+ from mono-/bi-valent ions. *Chem. Eng. J.* **2020**, *382*, 382.
(162) Wang, N. X.; Li, X. T.; Wang, L.; Zhang, L. L.; Zhang, G. J.; Ji, S. L. Nanoconfined Zeolitic Imidazolate Framework Membranes with Composite Layers of Nearly Zero Thickness. *ACS Appl. Mater. Interfaces* **2016**, *8* (34), 21979−21983.
(163) Albuquerque, G. H.; Herman, G. S. Chemically Modulated Microwave-Assisted Synthesis of MOF-74(Ni) and Preparation of Metal-Organic Framework-Matrix Based Membranes for Removal of Metal Ions from Aqueous Media. *Cryst. Growth Des.* **2017**, *17* (1), 156−162.
(164) Chen, Y. F.; Chen, F.; Zhang, S. H.; Cai, Y.; Cao, S. J.; Li, S. Q.; Zhao, W. Q.; Yuan, S.; Feng, X.; Cao, A. Y.; Ma, X. J.; Wang, B. Facile Fabrication of Multifunctional Metal Organic Framework Hollow Tubes To Trap Pollutants. *J. Am. Chem. Soc.* **2017**, *139* (46), 16482−16485.
(165) Lebedev, O. I.; Millange, F.; Serre, C.; Van Tendeloo, G.; Ferey, G. First direct imaging of giant pores of the metal-organic framework MIL-101. *Chem. Mater.* **2005**, *17* (26), 6525−6527.
(166) Rao, A. P.; Joshi, S. V.; Trivedi, J. J.; Devmurari, C. V.; Shah, V. J. Structure-performance correlation of polyamide thin film composite membranes: effect of coating conditions on film formation. *J. Membr. Sci.* **2003**, *211* (1), 13−24.
(167) Tian, M.; Qiu, C. Q.; Liao, Y.; Chou, S. R.; Wang, R. Preparation of polyamide thin film composite forward osmosis membranes using electrospun polyvinylidene fluoride (PVDF) nanofibers as substrates. *Sep. Purif. Technol.* **2013**, *118*, 727−736.
(168) Roh, I. J.; Greenberg, A. R.; Khare, V. P. Synthesis and characterization of interfacially polymerized polyamide thin films. *Desalination* **2006**, *191* (1−3), 279−290.
(169) Shen, L.; Xiong, S.; Wang, Y. Graphene oxide incorporated thin-film composite membranes for forward osmosis applications. *Chem. Eng. Sci.* **2016**, *143*, 194−205.
(170) Zhang, H.; Hou, J.; Hu, Y.; Wang, P.; Ou, R.; Jiang, L.; Liu, J. Z.; Freeman, B. D.; Hill, A. J.; Wang, H. Ultrafast selective transport of alkali metal ions in metal organic frameworks with subnanometer pores. *Science advances* **2018**, *4* (2), No. eaaq0066.
(171) Zhang, H.; Hou, J.; Hu, Y.; Wang, P.; Ou, R.; Jiang, L.; Liu, J. Z.; Freeman, B. D.; Hill, A. J.; Wang, H. Ultrafast selective transport

https://doi.org/10.1021/acs.iecr.1c00543
Ind. Eng. Chem. Res. XXXX, XXX, XXX−XXX

of alkali metal ions in metal organic frameworks with subnanometer pores. *Science Advances* **2018**, *4* (2), eaaq0066.
(172) Echaide-Gorriz, C.; Zapata, J. A.; Etxeberria-Benavides, M.; Tellez, C.; Coronas, J. Polyamide/MOF bilayered thin film composite hollow fiber membranes with tuned MOF thickness for water nanofiltration. *Sep. Purif. Technol.* **2020**, *236*, 236.
(173) Parkerson, Z. J.; Le, T.; Das, P.; Mahmoodi, S. N.; Esfahani, M. R. Cu-MOF-Polydopamine-Incorporated Functionalized Nanofiltration Membranes for Water Treatment: Effect of Surficial Adhesive Modification Techniques. *ACS EST Water* **2021**, *1*, 430.
(174) Seyedpour, S. F.; Arabi Shamsabadi, A.; Khoshhal Salestan, S.; Dadashi Firouzjaei, M.; Sharifian Gh, M.; Rahimpour, A.; Akbari Afkhami, F.; Shirzad Kebria, M. R.; Elliott, M. A.; Tiraferri, A.; Sangermano, M.; Esfahani, M. R.; Soroush, M. Tailoring the Biocidal Activity of Novel Silver-Based Metal Azolate Frameworks. *ACS Sustainable Chem. Eng.* **2020**, *8*, 7588−7599.
(175) Pejman, M.; Firouzjaei, M. D.; Aktij, S. A.; Das, P.; Zolghadr, E.; Jafarian, H.; Shamsabadi, A. A.; Elliott, M.; Esfahani, M. R.; Sangermano, M.; Sadrzadeh, M.; Wujcik, E. K.; Rahimpour, A.; Tiraferri, A. Improved antifouling and antibacterial properties of forward osmosis membranes through surface modification with zwitterions and silver-based metal organic frameworks. *J. Membr. Sci.* **2020**, *611*, 118352.
(176) Li, H.; Zhu, L.; Zhang, J.; Guo, T.; Li, X.; Xing, W.; Xue, Q. High-efficiency separation performance of oil-water emulsions of polyacrylonitrile nanofibrous membrane decorated with metal-organic frameworks. *Appl. Surf. Sci.* **2019**, *476*, 61−69.
(177) Chang, R.; Ma, S.; Guo, X.; Xu, J.; Zhong, C.; Huang, R.; Ma, J. Hierarchically Assembled Graphene Oxide Composite Membrane with Self-Healing and High-Efficiency Water Purification Performance. *ACS Appl. Mater. Interfaces* **2019**, *11*, 46251.
(178) Cao, J.; Su, Y.; Liu, Y.; Guan, J.; He, M.; Zhang, R.; Jiang, Z. Self-assembled MOF membranes with underwater superoleophobicity for oil/water separation. *J. Membr. Sci.* **2018**, *566*, 268−277.
(179) Fang, S.-Y.; Zhang, P.; Gong, J.-L.; Tang, L.; Zeng, G.-M.; Song, B.; Cao, W.-C.; Li, J.; Ye, J. Construction of highly water-stable metal-organic framework UiO-66 thin-film composite membrane for dyes and antibiotics separation. *Chem. Eng. J.* **2020**, *385*, 123400.
(180) Heu, R.; Ateia, M.; Yoshimura, C. Photocatalytic Nanofiltration Membrane Using Zr-MOF/GO Nanocomposite with High-Flux and Anti-Fouling Properties. *Catalysts* **2020**, *10* (6), 711.
(181) Wang, R.; Zhao, X.; Jia, N.; Cheng, L.; Liu, L.; Gao, C. Superwetting Oil/Water Separation Membrane Constructed from In Situ Assembled Metal-Phenolic Networks and Metal-Organic Frameworks. *ACS Appl. Mater. Interfaces* **2020**, *12*, 10000.
(182) Zhang, S.; Liu, Y.; Li, D.; Wang, Q.; Ran, F. Water-soluble MOF nanoparticles modified polyethersulfone membrane for improving flux and molecular retention. *Appl. Surf. Sci.* **2020**, *505*, 144553.
(183) Wang, X.-p.; Hou, J.; Chen, F.-s.; Meng, X.-m. In-situ growth of metal-organic framework film on a polydopamine-modified flexible substrate for antibacterial and forward osmosis membranes. *Sep. Purif. Technol.* **2020**, *236*, 116239.
(184) Li, T.; Ren, Y.; Zhai, S.; Zhang, W.; Zhang, W.; Hua, M.; Lv, L.; Pan, B. Integrating cationic metal-organic frameworks with ultrafiltration membrane for selective removal of perchlorate from Water. *J. Hazard. Mater.* **2020**, *381*, 120961.
(185) Lin, Y.; Wu, H.-C.; Yasui, T.; Yoshioka, T.; Matsuyama, H. Development of an HKUST-1 Nanofiller-Templated Poly(ether sulfone) Mixed Matrix Membrane for a Highly Efficient Ultrafiltration Process. *ACS Appl. Mater. Interfaces* **2019**, *11*, 18782.
(186) Samantaray, P. K.; Madras, G.; Bose, S. Water Remediation Aided by a Graphene-Oxide-Anchored Metal Organic Framework through Pore- and Charge-Based Sieving of Ions. *ACS Sustainable Chem. Eng.* **2019**, *7* (1), 1580−1590.
(187) Shu, L.; Xie, L.-H.; Meng, Y.; Liu, T.; Zhao, C.; Li, J.-R. A thin and high loading two-dimensional MOF nanosheet based mixed-matrix membrane for high permeance nanofiltration. *J. Membr. Sci.* **2020**, *603*, 603.
(188) Shukla, A. K.; Alam, J.; Ali, F. A. A.; Alhoshan, M. A highly permeable zinc-based MOF/polyphenylsulfone composite membrane with elevated antifouling properties. *Chem. Commun. (Cambridge, U. K.)* **2020**, *56* (39), 5231−5234.
(189) Abdi, S.; Nasiri, M. Enhanced Hydrophilicity and Water Flux of Poly(ether sulfone) Membranes in the Presence of Aluminum Fumarate Metal-Organic Framework Nanoparticles: Preparation and Characterization. *ACS Appl. Mater. Interfaces* **2019**, *11*, 15060.
(190) Xiao, S.; Huo, X.; Fan, S.; Zhao, K.; Yu, S.; Tan, X. Design and synthesis of Al-MOF/PPSU mixed matrix membrane with pollution resistance. *Chin. J. Chem. Eng.* **2021**, *29*, 110.
(191) Mansor, E. S.; Jamil, T. S.; Abdallah, H.; Shaban, A. M. Highly thin film nanocomposite membrane based metal organic complexes for brackish water desalination. *J. Environ. Chem. Eng.* **2018**, *6* (4), 5459−5469.
(192) Liu, R.; Sui, Y.; Wang, X. Metal-organic framework-based ultrafiltration membrane separation with capacitive-type for enhanced phosphate removal. *Chem. Eng. J.* **2019**, *371*, 903−913.
(193) Xie, A.; Cui, J.; Yang, J.; Chen, Y.; Lang, J.; Li, C.; Yan, Y.; Dai, J. Graphene oxide/Fe(III)-based metal-organic framework membrane for enhanced water purification based on synergistic separation and photo-Fenton processes. *Appl. Catal., B* **2020**, *264*, 118548.
(194) Samari, M.; Zinadini, S.; Zinatizadeh, A. A.; Jafarzadeh, M.; Gholami, F. Designing of a novel polyethersulfone (PES) ultrafiltration (UF) membrane with thermal stability and high fouling resistance using melamine-modified zirconium-based metal-organic framework (UiO-66-NH2/MOF). *Sep. Purif. Technol.* **2020**, *251*, 117010.
(195) Ghaffour, N.; Missimer, T. M.; Amy, G. L. Technical review and evaluation of the economics of water desalination: Current and future challenges for better water supply sustainability. *Desalination* **2013**, *309* (2013), 197−207.
(196) Buonomenna, M. G. Nano-enhanced reverse osmosis membranes. *Desalination* **2013**, *314*, 73−88.
(197) Akther, N.; Sodiq, A.; Giwa, A.; Daer, S.; Arafat, H. A.; Hasan, S. W. Recent advancements in forward osmosis desalination: A review. *Chem. Eng. J.* **2015**, *281*, 502−522.
(198) Cadotte, J. E. Evolution of composite reverse osmosis membranes. *ACS Symp. Ser.* **1985**, *269*, 273.
(199) Hermans, S.; Bernstein, R.; Volodin, A.; Vankelecom, I. F. J. Study of synthesis parameters and active layer morphology of interfacially polymerized polyamide-polysulfone membranes. *React. Funct. Polym.* **2015**, *86*, 199−208.
(200) Hirose, M.; Ito, H.; Kamiyama, Y. Effect of skin layer surface structures on the flux behaviour of RO membranes. *J. Membr. Sci.* **1996**, *121* (2), 209−215.
(201) Shafiq, M.; Sabir, A.; Islam, A.; Khan, S. M.; Gull, N.; Hussain, S. N.; Butt, M. T. Z. Cellulaose acetate based thin film nanocomposite reverse osmosis membrane incorporated with TiO2 nanoparticles for improved performance. *Carbohydr. Polym.* **2018**, *186*, 367−376.
(202) Lee, H. S.; Im, S. J.; Kim, J. H.; Kim, H. J.; Kim, J. P.; Min, B. R. Polyamide thin-film nanofiltration membranes containing TiO2 nanoparticles. *Desalination* **2008**, *219* (1−3), 48−56.
(203) Yin, J.; Kim, E. S.; Yang, J.; Deng, B. Fabrication of a novel thin-film nanocomposite (TFN) membrane containing MCM-41 silica nanoparticles (NPs) for water purification. *J. Membr. Sci.* **2012**, *423−424*, 238−246.
(204) Kadhom, M.; Yin, J.; Deng, B. A thin film nanocomposite membrane with MCM-41 silica nanoparticles for brackish water purification. *Membranes* **2016**, *6* (4), 50.
(205) Jadav, G. L.; Singh, P. S. Synthesis of novel silica-polyamide nanocomposite membrane with enhanced properties. *J. Membr. Sci.* **2009**, *328* (1−2), 257−267.
(206) Yin, J.; Yang, Y.; Hu, Z.; Deng, B. Attachment of silver nanoparticles (AgNPs) onto thin-film composite (TFC) membranes through covalent bonding to reduce membrane biofouling. *J. Membr. Sci.* **2013**, *441*, 73−82.

https://doi.org/10.1021/acs.iecr.1c00543
Ind. Eng. Chem. Res. XXXX, XXX, XXX−XXX

(207) Lind, M. L.; Eumine Suk, D.; Nguyen, T.-V.; Hoek, E. M. V. Tailoring the structure of thin film nanocomposite membranes to achieve seawater RO membrane performance. *Environ. Sci. Technol.* **2010**, *44* (21), 8230−8235.
(208) Lind, M. L.; Ghosh, A. K.; Jawor, A.; Huang, X.; Hou, W.; Yang, Y.; Hoek, E. M. V. Influence of zeolite crystal size on zeolite-polyamide thin film nanocomposite membranes. *Langmuir* **2009**, *25* (17), 10139−10145.
(209) Bonnett, B. L.; Smith, E.; de la Garza, M.; Cai, M.; Haag, J. V.; Serrano, J. M.; Cornell, H. D.; Gibbons, B.; Martin, S. M.; Morris, A. J. PCN-222 Metal-Organic Framework Nanoparticles with Tunable Pore Size for Nanocomposite Reverse Osmosis Membranes. *ACS Appl. Mater. Interfaces* **2020**, *12*, 15765.
(210) Fujioka, T.; Oshima, N.; Suzuki, R.; Khan, S. J.; Roux, A.; Poussade, Y.; Drewes, J. E.; Nghiem, L. D. Rejection of small and uncharged chemicals of emerging concern by reverse osmosis membranes: The role of free volume space within the active skin layer. *Sep. Purif. Technol.* **2013**, *116*, 426−432.
(211) Geise, G. M.; Park, H. B.; Sagle, A. C.; Freeman, B. D.; McGrath, J. E. Water permeability and water/salt selectivity tradeoff in polymers for desalination. *J. Membr. Sci.* **2011**, *369* (1−2), 130−138.
(212) Kim, S.-J.; Han, D.; Yu, H.-W.; O'Rourke, B. E.; Kobayashi, Y.; Suzuki, R.; Hwang, M.; Kim, I. S. Performance evaluation of polyamide TFC membranes: Effects of free volume properties on boron transport. *Desalination* **2018**, *432*, 104−114.
(213) Li, X.; Chung, T.-S.; Chung, T.-S. Effects of free volume in thin-film composite membranes on osmotic power generation. *AIChE J.* **2013**, *59* (12), 4749−4761.
(214) Abdullah, N.; Yusof, N.; Ismail, A. F.; Lau, W. J. Insights into metal-organic frameworks-integrated membranes for desalination process: A review. *Desalination* **2021**, *500*, 114867.
(215) Lee, T. H.; Roh, J. S.; Yoo, S. Y.; Roh, J. M.; Choi, T. H.; Park, H. B. High-Performance Polyamide Thin-Film Nanocomposite Membranes Containing ZIF-8/CNT Hybrid Nanofillers for Reverse Osmosis Desalination. *Ind. Eng. Chem. Res.* **2020**, *59* (12), 5324−5332.
(216) Yang, W.; Zhu, Y.; Sun, Z.; Gao, C.; Xue, L. Self-Sealed Polyamide (PA)/Zinc Imidazole Framework (ZIF) Thin Film Nanocomposite (TFN) Nanofiltration Membranes with Nanoscale Turing Type Structures. *Adv. Mater. Interfaces* **2019**, *6* (22), 1901482.
(217) Li, P.; Zhang, M.; Zhai, Z.; Wang, M.; Li, P.; Hou, Y.; Jason Niu, Q. Precise assembly of a zeolite imidazolate framework on polypropylene support for the fabrication of thin film nanocomposite reverse osmosis membrane. *J. Membr. Sci.* **2020**, *612*, 118412.
(218) Zhao, D. L.; Yeung, W. S.; Zhao, Q.; Chung, T.-S. Thin-film nanocomposite membranes incorporated with UiO-66-NH2 nanoparticles for brackish water and seawater desalination. *J. Membr. Sci.* **2020**, *604*, 118039.
(219) Wang, J.; Wang, Y.; Zhang, Y.; Uliana, A.; Zhu, J.; Liu, J.; Van der Bruggen, B. Zeolitic Imidazolate Framework/Graphene Oxide Hybrid Nanosheets Functionalized Thin Film Nanocomposite Membrane for Enhanced Antimicrobial Performance. *ACS Appl. Mater. Interfaces* **2016**, *8* (38), 25508−19.
(220) Ma, D.; Han, G.; Peh, S. B.; Chen, S. B. Water-Stable Metal-Organic Framework UiO-66 for Performance Enhancement of Forward Osmosis Membranes. *Ind. Eng. Chem. Res.* **2017**, *56* (44), 12773−12782.
(221) Wang, Y.; Li, X.; Zhao, S.; Fang, Z.; Ng, D.; Xie, C.; Wang, H.; Xie, Z. Thin-Film Composite Membrane with Interlayer Decorated Metal-Organic Framework UiO-66 toward Enhanced Forward Osmosis Performance. *Ind. Eng. Chem. Res.* **2019**, *58* (1), 195−206.
(222) Kim, T.; Choi, M. K.; Ahn, H. S.; Rho, J.; Jeong, H. M.; Kim, K. Fabrication and characterization of zeolitic imidazolate framework-embedded cellulose acetate membranes for osmotically driven membrane process. *Sci. Rep.* **2019**, *9* (1), 5779.
(223) Johnson, N.; Revenga, C.; Echeverria, J. Managing water for people and nature. *Science* **2001**, *292* (5519), 1071−1072.
(224) Fu, F.; Wang, Q. Removal of heavy metal ions from wastewaters: a review. *J. Environ. Manage.* **2011**, *92* (3), 407−418.
(225) Xu, G.-R.; An, Z.-H.; Xu, K.; Liu, Q.; Das, R.; Zhao, H.-L. Metal organic framework (MOF)-based micro/nanoscaled materials for heavy metal ions removal: The cutting-edge study on designs, synthesis, and applications. *Coord. Chem. Rev.* **2021**, *427*, 213554.
(226) Yin, N.; Wang, K.; Wang, L.; Li, Z. Amino-functionalized MOFs combining ceramic membrane ultrafiltration for Pb (II) removal. *Chem. Eng. J.* **2016**, *306*, 619−628.
(227) Xie, Z.; Xu, W.; Cui, X.; Wang, Y. Recent progress in metal-organic frameworks and their derived nanostructures for energy and environmental applications. *ChemSusChem* **2017**, *10* (8), 1645−1663.
(228) Hashem, T.; Ibrahim, A. H.; Wöll, C.; Alkordi, M. H. Grafting zirconium-based metal-organic framework UiO-66-NH2 nanoparticles on cellulose fibers for the removal of Cr (VI) ions and methyl orange from water. *ACS Applied Nano Materials* **2019**, *2* (9), 5804−5808.
(229) Li, Z.; Zhou, G.; Dai, H.; Yang, M.; Fu, Y.; Ying, Y.; Li, Y. Biomineralization-mimetic preparation of hybrid membranes with ultra-high loading of pristine metal-organic frameworks grown on silk nanofibers for hazard collection in water. *J. Mater. Chem. A* **2018**, *6* (8), 3402−3413.
(230) Efome, J. E.; Rana, D.; Matsuura, T.; Lan, C. Q. Effects of operating parameters and coexisting ions on the efficiency of heavy metal ions removal by nano-fibrous metal-organic framework membrane filtration process. *Sci. Total Environ.* **2019**, *674*, 355−362.
(231) Hua, W.; Zhang, T.; Wang, M.; Zhu, Y.; Wang, X. Hierarchically structural PAN/UiO-66-(COOH) 2 nanofibrous membranes for effective recovery of Terbium (III) and Europium (III) ions and their photoluminescence performances. *Chem. Eng. J.* **2019**, *370*, 729−741.
(232) Chen, X.; Chen, D.; Li, N.; Xu, Q.; Li, H.; He, J.; Lu, J. Modified-MOF-808-Loaded Polyacrylonitrile Membrane for Highly Efficient, Simultaneous Emulsion Separation and Heavy Metal Ion Removal. *ACS Appl. Mater. Interfaces* **2020**, *12* (35), 39227−39235.
(233) Jamshidifard, S.; Koushkbaghi, S.; Hosseini, S.; Rezaei, S.; Karamipour, A.; Irani, M. Incorporation of UiO-66-NH2MOF into the PAN/chitosan nanofibers for adsorption and membrane filtration of Pb (II), Cd (II) and Cr (VI) ions from aqueous solutions. *J. Hazard. Mater.* **2019**, *368*, 10−20.
(234) Ahmed, S. A.; Bagchi, D.; Katouah, H. A.; Hasan, M. N.; Altass, H. M.; Pal, S. K. Enhanced water stability and photo-responsivity in metal-organic framework (MOF): a potential tool to combat drug-resistant bacteria. *Sci. Rep.* **2019**, *9* (1), 1−11.
(235) Burtch, N. C.; Jasuja, H.; Walton, K. S. Water Stability and Adsorption in Metal-Organic Frameworks. *Chem. Rev.* **2014**, *114* (20), 10575−10612.
(236) Larsen, T. A.; Hoffmann, S.; Lüthi, C.; Truffer, B.; Maurer, M. Emerging solutions to the water challenges of an urbanizing world. *Science* **2016**, *352* (6288), 928−933.
(237) Mayer, B. K.; Baker, L. A.; Boyer, T. H.; Drechsel, P.; Gifford, M.; Hanjra, M. A.; Parameswaran, P.; Stoltzfus, J.; Westerhoff, P.; Rittmann, B. E. Total Value of Phosphorus Recovery. *Environ. Sci. Technol.* **2016**, *50* (13), 6606−6620.
(238) Van Meter, K. J.; Van Cappellen, P.; Basu, N. B. Legacy nitrogen may prevent achievement of water quality goals in the Gulf of Mexico. *Science* **2018**, *360* (6387), 427−430.
(239) Galloway, J. N.; Winiwarter, W.; Leip, A.; Leach, A. M.; Bleeker, A.; Erisman, J. W. Nitrogen footprints: past, present and future. *Environ. Res. Lett.* **2014**, *9* (11), 115003.
(240) Yan, T.; Ye, Y.; Ma, H.; Zhang, Y.; Guo, W.; Du, B.; Wei, Q.; Wei, D.; Ngo, H. H. A critical review on membrane hybrid system for nutrient recovery from wastewater. *Chem. Eng. J.* **2018**, *348*, 143−156.
(241) Liu, M. J.; Neo, B. S.; Tarpeh, W. A. Building an operational framework for selective nitrogen recovery via electrochemical stripping. *Water Res.* **2020**, *169*, 115226.
(242) Tarpeh, W. A.; Barazesh, J. M.; Cath, T. Y.; Nelson, K. L. Electrochemical Stripping to Recover Nitrogen from Source-Separated Urine. *Environ. Sci. Technol.* **2018**, *52* (3), 1453−1460.

https://doi.org/10.1021/acs.iecr.1c00543
Ind. Eng. Chem. Res. XXXX, XXX, XXX−XXX

(243) Kumar, P.; Bansal, V.; Kim, K.-H.; Kwon, E. E. Metal-organic frameworks (MOFs) as futuristic options for wastewater treatment. *J. Ind. Eng. Chem.* **2018**, *62*, 130−145.
(244) Decoste, J. B.; Denny, J. M. S.; Peterson, G. W.; Mahle, J. J.; Cohen, S. M. Enhanced aging properties of HKUST-1 in hydrophobic mixed-matrix membranes for ammonia adsorption. *Chemical Science* **2016**, *7* (4), 2711−2716.
(245) Khabzina, Y.; Dhainaut, J.; Ahlhelm, M.; Richter, H.-J.; Reinsch, H.; Stock, N.; Farrusseng, D. Synthesis and Shaping Scale-up Study of Functionalized UiO-66 MOF for Ammonia Air Purification Filters. *Ind. Eng. Chem. Res.* **2018**, *57* (24), 8200−8208.
(246) Vikrant, K.; Kumar, V.; Kim, K.-H.; Kukkar, D. Metal-organic frameworks (MOFs): potential and challenges for capture and abatement of ammonia. *J. Mater. Chem. A* **2017**, *5* (44), 22877−22896.
(247) Zhang, X.; Sun, F.; He, J.; Xu, H.; Cui, F.; Wang, W. Robust phosphate capture over inorganic adsorbents derived from lanthanum metal organic frameworks. *Chem. Eng. J.* **2017**, *326*, 1086−1094.
(248) He, J.; Xu, Y.; Wang, W.; Hu, B.; Wang, Z.; Yang, X.; Wang, Y.; Yang, L. Ce(III) nanocomposites by partial thermal decomposition of Ce-MOF for effective phosphate adsorption in a wide pH range. *Chem. Eng. J.* **2020**, *379*, 122431.
(249) Nehra, M.; Dilbaghi, N.; Singhal, N. K.; Hassan, A. A.; Kim, K.-H.; Kumar, S. Metal organic frameworks MIL-100(Fe) as an efficient adsorptive material for phosphate management. *Environ. Res.* **2019**, *169*, 229−236.
(250) Ray, H.; Perreault, F.; Boyer, T. H. Urea recovery from fresh human urine by forward osmosis and membrane distillation (FO-MD). *Environmental Science: Water Research & Technology* **2019**, *5* (11), 1993−2003.
(251) Clark, B.; Tarpeh, W. Selective recovery of ammonia nitrogen from wastewaters with transition metal-loaded polymeric cation exchange adsorbents. *Chem. - Eur. J.* **2020**, *26*, 10099.
(252) Kim, J.; Lee, S.; Yoon, S.; Lee, C. Competitive adsorption of trace organics on membranes and powdered activated carbon in powdered activated carbon-ultrafiltration system. *Water Sci. Technol.* **1996**, *34* (9), 223−229.
(253) Hajibabania, S.; Verliefde, A.; McDonald, J. A.; Khan, S. J.; Le-Clech, P. Fate of trace organic compounds during treatment by nanofiltration. *J. Membr. Sci.* **2011**, *373* (1−2), 130−139.
(254) Tadkaew, N.; Sivakumar, M.; Khan, S. J.; McDonald, J. A.; Nghiem, L. D. Effect of mixed liquor pH on the removal of trace organic contaminants in a membrane bioreactor. *Bioresour. Technol.* **2010**, *101* (5), 1494−1500.
(255) Valcarce, C. O.; Gonzaga, E. W.; Mazyck, D. W. Evaluating the Efficacy of PAC and Water Parameters to Remove Trace Organics. *Journal - American Water Works Association* **2017**, *109*, E50−E60.
(256) Gao, G.; Li, S.; Li, S.; Zhao, L.; Wang, T.; Hou, X. Development and application of vortex-assisted membrane extraction based on metal-organic framework mixed-matrix membrane for the analysis of estrogens in human urine. *Anal. Chim. Acta* **2018**, *1023*, 35−43.
(257) Sun, S.; Huang, L.; Xiao, H.; Shuai, Q.; Hu, S. In situ self-transformation metal into metal-organic framework membrane for solid-phase microextraction of polycyclic aromatic hydrocarbons. *Talanta* **2019**, *202*, 145−151.
(258) Wang, T.; Wang, J.; Zhang, C.; Yang, Z.; Dai, X.; Cheng, M.; Hou, X. Metal-organic framework MIL-101(Cr) as a sorbent of porous membrane-protected micro-solid-phase extraction for the analysis of six phthalate esters from drinking water: a combination of experimental and computational study. *Analyst* **2015**, *140* (15), 5308−5316.
(259) Ragab, D.; Gomaa, H. G.; Sabouni, R.; Salem, M.; Ren, M.; Zhu, J. Micropollutants removal from water using microfiltration membrane modified with ZIF-8 metal organic frameworks (MOFs). *Chem. Eng. J.* **2016**, *300*, 273−279.
(260) Basu, S.; Balakrishnan, M. Polyamide thin film composite membranes containing ZIF-8 for the separation of pharmaceutical compounds from aqueous streams. *Sep. Purif. Technol.* **2017**, *179*, 118−125.
(261) Zhang, C.; Wu, B.-H.; Ma, M.-Q.; Wang, Z.; Xu, Z.-K. Ultrathin metal/covalent-organic framework membranes towards ultimate separation. *Chem. Soc. Rev.* **2019**, *48* (14), 3811−3841.
(262) Li, X.; Liu, Y.; Wang, J.; Gascon, J.; Li, J.; Van der Bruggen, B. Metal-organic frameworks based membranes for liquid separation. *Chem. Soc. Rev.* **2017**, *46* (23), 7124−7144.
(263) Marchetti, P.; Jimenez Solomon, M. F.; Szekely, G.; Livingston, A. G. Molecular Separation with Organic Solvent Nanofiltration: A Critical Review. *Chem. Rev.* **2014**, *114* (21), 10735−10806.
(264) Campbell, J.; Burgal, J. D. S.; Szekely, G.; Davies, R. P.; Braddock, D. C.; Livingston, A. Hybrid polymer/MOF membranes for Organic Solvent Nanofiltration (OSN): Chemical modification and the quest for perfection. *J. Membr. Sci.* **2016**, *503*, 166−176.
(265) Yang, H.; Wang, N.; Wang, L.; Liu, H.-X.; An, Q.-F.; Ji, S. Vacuum-assisted assembly of ZIF-8@GO composite membranes on ceramic tube with enhanced organic solvent nanofiltration performance. *J. Membr. Sci.* **2018**, *545*, 158−166.
(266) Ma, D.; Han, G.; Gao, Z. F.; Chen, S. B. Continuous UiO-66-Type Metal-Organic Framework Thin Film on Polymeric Support for Organic Solvent Nanofiltration. *ACS Appl. Mater. Interfaces* **2019**, *11* (48), 45290−45300.
(267) Chen, K.; Li, P.; Zhang, H.; Sun, H.; Yang, X.; Yao, D.; Pang, X.; Han, X.; Jason Niu, Q. Organic solvent nanofiltration membrane with improved permeability by in-situ growth of metal-organic frameworks interlayer on the surface of polyimide substrate. *Sep. Purif. Technol.* **2020**, *251*, 117387−117387.
(268) Cai, Y.; Shi, D.; Liu, G.; Ying, Y.; Cheng, Y.; Wang, Y.; Chen, D.; Lu, J.; Zhao, D. Polycrystalline zirconium metal-organic framework membranes supported on flexible carbon cloth for organic solvent nanofiltration. *J. Membr. Sci.* **2020**, *615*, 118551−118551.
(269) Basu, S.; Maes, M.; Cano-Odena, A.; Alaerts, L.; De Vos, D. E.; Vankelecom, I. F. J. Solvent resistant nanofiltration (SRNF) membranes based on metal-organic frameworks. *J. Membr. Sci.* **2009**, *344* (1), 190−198.
(270) Campbell, J.; Székely, G.; Davies, R. P.; Braddock, D. C.; Livingston, A. G. Fabrication of hybrid polymer/metal organic framework membranes: mixed matrix membranes versus in situ growth. *J. Mater. Chem. A* **2014**, *2* (24), 9260−9271.
(271) Campbell, J.; Davies, R. P.; Braddock, D. C.; Livingston, A. G. Improving the permeance of hybrid polymer/metal-organic framework (MOF) membranes for organic solvent nanofiltration (OSN) - development of MOF thin films via interfacial synthesis. *J. Mater. Chem. A* **2015**, *3* (18), 9668−9674.
(272) Li, Y.; Wee, L. H.; Volodin, A.; Martens, J. A.; Vankelecom, I. F. J. Polymer supported ZIF-8 membranes prepared via an interfacial synthesis method. *Chem. Commun.* **2015**, *51* (5), 918−920.
(273) Zhu, L.; Yu, H.; Zhang, H.; Shen, J.; Xue, L.; Gao, C.; van der Bruggen, B. Mixed matrix membranes containing MIL-53(Al) for potential application in organic solvent nanofiltration. *RSC Adv.* **2015**, *5* (89), 73068−73076.
(274) Ma, X.; Kumar, P.; Mittal, N.; Khlyustova, A.; Daoutidis, P.; Mkhoyan, K. A.; Tsapatsis, M. Zeolitic imidazolate framework membranes made by ligand-induced permselectivation. *Science* **2018**, *361* (6406), 1008−1011.
(275) Li, W.; Wu, W.; Li, Z.; Shi, J.; Xia, Y. Sol-gel asynchronous crystallization of ultra-selective metal-organic framework membranes for gas separation. *J. Mater. Chem. A* **2018**, *6* (34), 16333−16340.
(276) Shamsaei, E.; Low, Z.-X.; Lin, X.; Mayahi, A.; Liu, H.; Zhang, X.; Zhe Liu, J.; Wang, H. Rapid synthesis of ultrathin, defect-free ZIF-8 membranes via chemical vapour modification of a polymeric support. *Chem. Commun.* **2015**, *51* (57), 11474−11477.
(277) Hu, Y.; Wei, J.; Liang, Y.; Zhang, H.; Zhang, X.; Shen, W.; Wang, H. Zeolitic Imidazolate Framework/Graphene Oxide Hybrid Nanosheets as Seeds for the Growth of Ultrathin Molecular Sieving Membranes. *Angew. Chem., Int. Ed.* **2016**, *55* (6), 2048−2052.

https://doi.org/10.1021/acs.iecr.1c00543
Ind. Eng. Chem. Res. XXXX, XXX, XXX−XXX

(278) Chen, L.; Shi, G.; Shen, J.; Peng, B.; Zhang, B.; Wang, Y.; Bian, F.; Wang, J.; Li, D.; Qian, Z.; Xu, G.; Liu, G.; Zeng, J.; Zhang, L.; Yang, Y.; Zhou, G.; Wu, M.; Jin, W.; Li, J.; Fang, H. Ion sieving in graphene oxide membranes via cationic control of interlayer spacing. *Nature* **2017**, *550* (7676), 380−383.
(279) Wei, W.; Gupta, K. M.; Liu, J.; Jiang, J. Zeolitic Imidazolate Framework Membranes for Organic Solvent Nanofiltration: A Molecular Simulation Exploration. *ACS Appl. Mater. Interfaces* **2018**, *10* (39), 33135−33143.
(280) Li, X.; Mo, Y.; Qing, W.; Shao, S.; Tang, C. Y.; Li, J. Membrane-based technologies for lithium recovery from water lithium resources: A review. *J. Membr. Sci.* **2019**, *591*, 117317.
(281) Razmjou, A.; Asadnia, M.; Hosseini, E.; Habibnejad Korayem, A.; Chen, V. Design principles of ion selective nanostructured membranes for the extraction of lithium ions. *Nat. Commun.* **2019**, *10* (1), 5793.
(282) Jung, M.; Kim, H.; Baek, K.; Kim, K. Synthetic Ion Channel Based on Metal-Organic Polyhedra. *Angew. Chem., Int. Ed.* **2008**, *47* (31), 5755−5757.
(283) Zhang, H.; Hou, X.; Zeng, L.; Yang, F.; Li, L.; Yan, D.; Tian, Y.; Jiang, L. Bioinspired Artificial Single Ion Pump. *J. Am. Chem. Soc.* **2013**, *135* (43), 16102−16110.
(284) Mohammad, M.; Lisiecki, M.; Liang, K.; Razmjou, A.; Chen, V. Metal-Phenolic network and metal-organic framework composite membrane for lithium ion extraction. *Applied Materials Today* **2020**, *21*, 100884.
(285) Guo, Y.; Ying, Y.; Mao, Y.; Peng, X.; Chen, B. Polystyrene Sulfonate Threaded through a Metal-Organic Framework Membrane for Fast and Selective Lithium-Ion Separation. *Angew. Chem., Int. Ed.* **2016**, *55* (48), 15120−15124.
(286) Liang, H.-Q.; Guo, Y.; Peng, X.; Chen, B. Light-gated cation-selective transport in metal-organic framework membranes. *J. Mater. Chem. A* **2020**, *8* (22), 11399−11405.
(287) Agmon, N. The Grotthuss mechanism. *Chem. Phys. Lett.* **1995**, *244* (5), 456−462.
(288) Taylor, J. M.; Dekura, S.; Ikeda, R.; Kitagawa, H. Defect Control To Enhance Proton Conductivity in a Metal-Organic Framework. *Chem. Mater.* **2015**, *27* (7), 2286−2289.
(289) Sadakiyo, M.; Yamada, T.; Honda, K.; Matsui, H.; Kitagawa, H. Control of Crystalline Proton-Conducting Pathways by Water-Induced Transformations of Hydrogen-Bonding Networks in a Metal-Organic Framework. *J. Am. Chem. Soc.* **2014**, *136* (21), 7701−7707.
(290) Sadakiyo, M.; Kasai, H.; Kato, K.; Takata, M.; Yamauchi, M. Design and Synthesis of Hydroxide Ion-Conductive Metal-Organic Frameworks Based on Salt Inclusion. *J. Am. Chem. Soc.* **2014**, *136* (5), 1702−1705.
(291) Pauwels, E.; Declerck, R.; Speybroeck, V. V.; Waroquier, M. Evidence for a Grotthuss-like mechanism in the formation of the rhamnose alkoxy radical based on periodic DFT calculations. *Radiat. Res.* **2008**, *169* (1), 8−18.
(292) Razmjou, A.; Eshaghi, G.; Orooji, Y.; Hosseini, E.; Korayem, A. H.; Mohagheghian, F.; Boroumand, Y.; Noorbakhsh, A.; Asadnia, M.; Chen, V. Lithium ion-selective membrane with 2D subnanometer channels. *Water Res.* **2019**, *159*, 313−323.
(293) Majee, A.; Bier, M.; Podgornik, R. Spontaneous symmetry breaking of charge-regulated surfaces. *Soft Matter* **2018**, *14* (6), 985−991.
(294) Jian, M.; Qiu, R.; Xia, Y.; Lu, J.; Chen, Y.; Gu, Q.; Liu, R.; Hu, C.; Qu, J.; Wang, H.; Zhang, X. Ultrathin water-stable metal-organic framework membranes for ion separation. *Science Advances* **2020**, *6* (23), No. eaay3998.
(295) Ma, Y.; Dong, Z.; You, M.; Zhang, Y.; Feng, X.; Ma, X.; Meng, J. Formation of a thin and continuous MOF membrane with 2-D MOF nanosheets as seeds via layer-by-layer growth. *Chem. Commun.* **2019**, *55* (68), 10146−10149.
(296) Zhang, C.; Mu, Y.; Zhang, W.; Zhao, S.; Wang, Y. PVC-based hybrid membranes containing metal-organic frameworks for Li +/Mg2+ separation. *J. Membr. Sci.* **2020**, *596*, 117724.
(297) Xu, T.; Shehzad, M. A.; Wang, X.; Wu, B.; Ge, L.; Xu, T. Engineering Leaf-Like UiO-66-SO3H Membranes for Selective Transport of Cations. *Nano-Micro Lett.* **2020**, *12* (1), 51.
(298) Cha-Umpong, W.; Hosseini, E.; Razmjou, A.; Zakertabrizi, M.; Korayem, A. H.; Chen, V. New molecular understanding of hydrated ion trapping mechanism during thermally-driven desalination by pervaporation using GO membrane. *J. Membr. Sci.* **2020**, *598*, 117687.
(299) Cha-Umpong, W.; Dong, G.; Razmjou, A.; Chen, V. Effect of oscillating temperature and crystallization on graphene oxide composite pervaporation membrane for inland brine desalination. *J. Membr. Sci.* **2019**, *588*, 117210.
(300) Razmjou, A. The Role of Defects in Li+ Selective Nanostructured Membranes: Comment on "Tunable Nanoscale Interlayer of Graphene with Symmetrical Polyelectrolyte Multilayer Architecture for Lithium Extraction. *Adv. Mater. Interfaces* **2019**, *6* (2), 1801427.
(301) Zhao, Y.; Shi, W.; Van der Bruggen, B.; Gao, C.; Shen, J. Tunable Nanoscale Interlayer of Graphene with Symmetrical Polyelectrolyte Multilayer Architecture for Lithium Extraction. *Adv. Mater. Interfaces* **2018**, *5* (6), 1701449.
(302) Xu, T.; Shehzad, M. A.; Yu, D.; Li, Q.; Wu, B.; Ren, X.; Ge, L.; Xu, T. Highly Cation Permselective Metal-Organic Framework Membranes with Leaf-Like Morphology. *ChemSusChem* **2019**, *12* (12), 2593−2597.
(303) Razmjou, A.; Hosseini, E.; Cha-Umpong, W.; Korayem, A. H.; Asadnia, M.; Moazzam, P.; Orooji, Y.; Karimi-Maleh, H.; Chen, V. Effect of chemistry and geometry of GO nanochannels on the Li ion selectivity and recovery. *Desalination* **2020**, *496*, 114729.
(304) Zhang, H.; Tian, Y.; Jiang, L. Fundamental studies and practical applications of bio-inspired smart solid-state nanopores and nanochannels. *Nano Today* **2016**, *11* (1), 61−81.
(305) Lu, J.; Zhang, H.; Hou, J.; Li, X.; Hu, X.; Hu, Y.; Easton, C. D.; Li, Q.; Sun, C.; Thornton, A. W.; Hill, M. R.; Zhang, X.; Jiang, G.; Liu, J. Z.; Hill, A. J.; Freeman, B. D.; Jiang, L.; Wang, H. Efficient metal ion sieving in rectifying subnanochannels enabled by metal-organic frameworks. *Nat. Mater.* **2020**, *19* (7), 767−774.
(306) Wang, C.; Liu, F.-F.; Tan, Z.; Chen, Y.-M.; Hu, W.-C.; Xia, X.-H. Fabrication of Bio-Inspired 2D MOFs/PAA Hybrid Membrane for Asymmetric Ion Transport. *Adv. Funct. Mater.* **2020**, *30* (9), 1908804.
(307) Legrand, A.; Furukawa, S. A selective ionic rectifier. *Nat. Mater.* **2020**, *19* (7), 701−702.
(308) Sui, X.; Ding, H.; Yuan, Z.; Leong, C. F.; Goh, K.; Li, W.; Yang, N.; D'Alessandro, D. M.; Chen, Y. The roles of metal-organic frameworks in modulating water permeability of graphene oxide-based carbon membranes. *Carbon* **2019**, *148*, 277−289.
(309) Wang, P.; Du, X.; Chen, T.; Hao, X.; Abudula, A.; Tang, K.; Guan, G. A novel electroactive PPy/HKUST-1 composite film-coated electrode for the selective recovery of lithium ions with low concentrations in aqueous solutions. *Electrochim. Acta* **2019**, *306*, 35−44.
(310) Park, S. H.; Lee, S. J. Versatile Amorphous Structures of Phosphonate Metal-Organic Framework/Alginate Composite for Tunable Sieving of Ions. *Adv. Funct. Mater.* **2019**, *29* (42), 1904016.

https://doi.org/10.1021/acs.iecr.1c00543
Ind. Eng. Chem. Res. XXXX, XXX, XXX−XXX